Power Flow Controller Design for Permanent Magnet Synchronous Generator-Based Wind Energy Conversion System Using an Adaptive Neuro-Fuzzy Inference System

Galana Fikadu Tafa

A Thesis Submitted to

Department of Electrical Power and Control Engineering
School of Electrical Engineering and Computing

Presented in Partial Fulfillment of the Requirement for the Degree of Master's in Electrical Power and Control Engineering (Control Engineering)

Office of Graduate Studies
Adama Science and Technology University

September 2022
Adama, Ethiopia

Power Flow Controller Design for Permanent Magnet Synchronous Generator-Based Wind Energy Conversion System Using an Adaptive Neuro-Fuzzy Inference System

Galana Fikadu Tafa

Advisor

Dr. C. S. Reddy (Ph.D.)

A Thesis Submitted to the Department of Electrical Power and Control Engineering

School of Electrical Engineering and Computing

Presented in Partial Fulfillment of the Requirement for the Degree of Master's in Electrical Power and Control Engineering (Control Engineering)

Office of Graduate Studies

Adama Science and Technology University

September 2022

Adama, Ethiopia

DECLARATION

I hereby declare that this Master Thesis entitled “Power Flow Controller Design for Permanent Magnet Synchronous Generator-Based Wind Energy Conversion System Using an Adaptive Neuro-Fuzzy Inference System” is my original work. That is, it has not been submitted for the award of any academic degree, diploma, or certificate in any other university. All sources of materials that are used for this thesis have been duly acknowledged through citation

______________________	______________________	______________________
Name of student	Signature	Date

RECOMMENDATION OF ADVISOR

I, an advisor of this thesis, hereby certify that I have read the revised version of the thesis entitled "Power Flow Controller Design for Permanent Magnet Synchronous Generator-Based Wind Energy Conversion System Using an Adaptive Neuro-Fuzzy Inference System" prepared under my guidance by Galana Fikadu Tafa submitted in partial fulfillment of the requirements for the degree of Master of Science in Electrical Power and Control Engineering. Therefore, I recommend the submission of the revised version of the thesis to the department following the applicable procedures.

Dr. C S Reddy		19-10-2022
Name of Advisor	Signature	Date

APPROVAL PAGE

I, an advisor of the thesis entitled "Power Flow Controller Design for Permanent Magnet Synchronous Generator-Based Wind Energy Conversion System Using an Adaptive Neuro-Fuzzy Inference System" and developed by Galana Fikadu Tafa, hereby certify that the recommendation and suggestions made by the board of examiners are appropriately incorporated into the final version of the thesis.

Dr. C S Reddy		19-10-2022
Name of Advisor	Signature	Date

We, the undersigned, members of the Board of Examiners of the thesis by Galana Fikadu Tafa have read and evaluated the thesis entitled "Power Flow Controller Design for Permanent Magnet Synchronous Generator-Based Wind Energy Conversion System Using an Adaptive Neuro-Fuzzy Inference System" and examined the candidate during the open defense. This is, therefore, to certify that the thesis is accepted for partial fulfillment of the degree of master's in Electrical Power and Control Engineering.

Chairperson	Signature	Date
Internal Examiner	Signature	Date
External Examiner	Signature	Date

Finally, approval and acceptance of the thesis are contingent upon the submission of its final copy to the Office of Postgraduate Studies (OPGS) through the Department Graduate Council (DGC) and School Graduate Committee (SGC).

Department Head	Signature	Date
School Dean	Signature	Date
Office of Postgraduate Studies, Dean	Signature	Date

ACKNOWLEDGEMENT

First and foremost, I would like to thank the almighty God for consistently being my pillar of strength and for giving me the courage for finishing this thesis.

Secondly, I would like to express my sincere gratitude to my thesis advisor Dr. C S Reddy (Ph.D.) for his valuable advice throughout the development of this thesis.

Thirdly, I would like to express my regards and thanks to all department of Electrical Power and Control Engineering of Adama Science and Technology University, and all staff members for all their encouragement and cooperation.

Fourthly, I would like to express my greatest appreciation to my lovely friends, and fellow postgraduates who have helped and given me encouragement throughout my studies.

Finally, and most importantly, I wish to thank and acknowledge all my lovely parents for their support, and continuous encouragement.

With Regards

Galana Fikadu

TABLE OF CONTENTS

CONTENTS **PAGE**

LIST OF TABLES

LIST OF FIGURES

LIST OF ACRONYMS

AC	Alternating Current
ANFIS	Adaptive Neuro-Fuzzy Inference System
ANN	Artificial Neural Network
BOA	Bisector of Area
BTB	Back-to-Back
COG	Centre of Gravity
CCM	Continuous (Current) Conduction Mode
DC	Direct Current
DFIG	Doubly Fed Induction Generator
DQ	Direct-Quadrature
FIS	Fuzzy Inference System
FLC	Fuzzy Logic Controller
FRT	Fault Ride-Through
GSC	Grid Side Converter
GUI	Graphical User Interface
HAWT	Horizontal Axis Wind Turbine
IGBT	Insulated Gate Bipolar Transistor
KVL	Kirchhoff's Voltage Law
LLL	Line to Line to Line
LMI	Linear Matrix Inequality
LM	Leftmost Maximum
MATLAB	MATrix LABoratory
MF	Membership Function
MOM	Mean of Maxima
MOSFET	Metal-Oxide-Semiconductor Field-Effect Transistor
MPPT	Maximum PowerPoint Tracking
MSC	Machine Side Converter
PCC	Phase Common Coupling
PI	Proportional-Integral
PLL	Phase-Locked Loop

PMSG	Permanent Magnet Synchronous Generator
PMSM	Permanent Magnet Synchronous Machine
PWM	Pulse Width Modulation
RM	Rightmost Maximum
RMS	Root Mean Square
RPM	Revolution Per Minute
SCIG	Squirrel Cage Induction Generator
TS	Takagi-Sugeno
TSR	Tip Speed Ratio
VAWT	Vertical Axis Wind Turbine
VCO	Voltage-Controlled Oscillator
VSI	Voltage Source Inverter
VSWT	Variable Speed Wind Turbine
WECS	Wind Energy Conversion System
WRSG	Wound Rotor Synchronous Generator

ABSTRACT

Because of the global energy crisis and environmental pollution problems affecting the world, the need for renewable energy sources is rapidly expanding. Amongst these renewable sources, the penetration of wind power is rising, which presents significant technological challenges for the development of electrical grid networks. For wind energy conversion systems, gearless permanent magnet synchronous generators are becoming more and more popular. The advancement of power electronics in the field of power systems has resulted in the development of new and more efficient power control technology. This thesis uses an Adaptive Neuro-Fuzzy Inference System (ANFIS) to control power flow of a Wind Energy Conversion System (WECS)-based on a Permanent Magnet Synchronous Generator (PMSG). As a benchmark for the performance of the fuzzy system, this includes the simulation and modeling of a wind speed, a wind turbine, a PMSG, an AC-DC uncontrolled rectifier, a boost converter, a DC-AC IGBT-based PWM inverter, a filter, a conventional PI controller, a fuzzy logic controller, and an adaptive neuro-fuzzy inference system controller. The suggested controller uses ANN learning techniques for the issue of tuning a fuzzy logic controller and fine-tuning membership functions. The proposed control algorithms were validated using the simulation results obtained by MATLAB/SIMULINK. The result demonstrates that the proposed controller is highly effective, it has the best dynamic performance, and it is robust to line transmission parameter uncertainties when it is compared with the conventional PI controller and fuzzy logic controller. It is feasible. From the simulations, it can be observed that the overshoot given by the ANFIS controller is reduced to 0.53% from 10.404%, while the regulation time is reduced to 0.00685msec from 0.0585msec, and the settling time is reduced to 0.04248msec from 18.485msec from the PI controllers.

Keywords: *ANFIS, ANN, DC/DC Boost Converter, Permanent Magnet Synchronous Generator, Power Flow Control, Uncontrolled Rectifier, WECS*

CHAPTER ONE

1. INTRODUCTION

1.1 Background

The wind is a clean, environmentally friendly renewable energy source that can help us decrease our dependency on fossil fuels, and it has grown quickly in recent years (Davidson *et* al., 2014; Kumar & Chatterjee, 2016). One of the most affordable ways to produce electricity is through wind energy. It is a renewable technology and has several environmental advantages, including no emissions of carbon dioxide (CO2), sulfur (S), or nitrogen oxides (NO), as well as no waste or leftovers (Maroufi et al., 2020). As a result of these factors, the development of wind energy conversion systems (WECSs) has been increasing steadily. It is one of the cheap and endless alternative energy sources and is now increasingly utilized in electric power systems for sustainable development (Davidson et al., 2014). Among the methods for generating power from renewable energy, wind turbines have proven to be the most developed (Bayhan et al., 2013).

The worldwide installed wind turbine capacity reaches 282, 275 Megawatts (MW) by the end of 2012, whose energy production equals 3% of the global electricity consumption (Apata & Oyedokun, 2020). According to a report by the Global Wind Energy Council and Greenpeace International, global installed wind power reached 496.9 GW at the end of 2016. By 2030, wind power is expected to reach 2110 GW and reach up to 20% of worldwide electricity generation (Shariatpanah et al., 2013). Wind energy conversion systems can convert wind energy to kinetic energy which is brought by wind speed and converted into electrical energy for grid feeding through the generator. Wind speed and turbine blade pitch have an impact on the power output of wind energy conversion systems. With squirrel-cage induction generators, the wind energy conversion systems (WECSs) initially ran at fixed speeds (Miao & Shen, 2013).

Later, doubly fed induction generators (DFIGs) were introduced for variable-speed wind turbines. However, a more recent advance in wind energy conversion systems is the use of permanent magnet synchronous generators (PMSGs). The maximum electricity from the wind may be generated by wind energy systems with variable speeds as compared to those with constant speeds (Miao & Shen, 2013). PMSGs with a high pole number for low speed are also employed to avoid the need for a mechanical gearbox. In comparison to the DFIG, it has several benefits, including higher efficiency, simpler controllability, the absence of reactive magnetizing current, and smaller size (Et. al., Eswaraiah G, 2021; Muhammed & Krishnakumari, 2014). The AC grid must be supplied with the energy generated by wind. In power systems, several power electronic converters are used, and they greatly enhance the power quality before supplying the power to the grid. To ensure that the robustness of voltage and frequency requirements of the AC grid is met, grid-side converters are crucial. In the event of a problem in the PMSG-based WECS, the defect will have an impact on the overall system's performance, resulting in an unstable situation. Without control, the system will not become stable for a long period; but, if adequate control is supplied, the system will become stable rapidly (Et. al., Eswaraiah G, 2021; Muhammed & Krishnakumari, 2014; Sekhar & Babu, 2016).

In this thesis work, a variety of techniques are proposed to control the power flow of wind energy conversion system-based permanent magnet synchronous generators which can name PI, fuzzy logic, and neural network controllers. The thesis regarded the adaptive neuro-fuzzy controller to control the system based on simulations, it is defined that the neuro-fuzzy technology makes better answers to power flow, However, due to their simplicity, the Proportional Integral (PI) controllers are generally used in this, where they give a satisfactory performance under steady-state conditions. But their performance deteriorates under dynamic operating conditions, as it is very difficult to set the optimal gains of PI for rapidly changing operating conditions. Fuzzy Logic Controller (FLC) is chosen also as a controller for this thesis because it has several merits compared to the PI controller. The benefits of an FLC are control simplicity, low cost, and the ability to build without knowing the exact mathematical model of the process. Despite the merits, the lack of a systematic design methodology and the difficulty in predicting the stability and robustness of the controlled system are the limitations. To overcome their drawback of them, this thesis develops an adaptive neuro-fuzzy inference system (ANFIS) controller, where the fuzzy membership functions are continuously tuned using the neuron network methods. The combined capability of a neuro-fuzzy controller is well known, as it reduces the number of fuzzy rules-based and the number of neurons for the fast convergence of controller performance.

1.2 Statement of the Problem

With the fast-growing energy demand, the main supply grid is under pressure, resulting in grid instability. Compared with fossil fuels, a renewable energy source is a better choice to meet load demands. However, because renewable energy sources are placed far from the load, the electricity generated must be transported over long distances before it can be integrated into the main supply grid. Due to these reasons, the instability of the power grid occurs, the stability of the power grid is largely related to faults in a network, such as the tripping of transmission lines, the loss of production capacity (failure of the generator unit), and short circuits amongst of these faults may occur on the system. Because of these faults, many challenges arise, such as power balance failures (active and reactive) and power flow changes. The capacity of the generator in operation may be sufficient, but sudden large voltage drops can occur. Due to the imbalance and redistribution of active and reactive power in the network, the voltage can fluctuate beyond the stable range (Yadav & Upadhayay, 2014). In addition, if the wind turbine generator and main grid control system cannot meet the required voltage level: Steady-state voltage fluctuations, power loss, and damage to electrical equipment connected to the grid can occur. For instance, numerous studies using traditional PI controllers have been conducted; however, in the case of a grid failure, the conventional converter control strategy is harmed, and the wind turbine's ability to ride out failures is also compromised.

A new control method, the design of a power flow control using an adaptive neuro-fuzzy inference system technique for a permanent magnet synchronous generator-based wind energy conversion system, is offered to overcome the aforementioned problems. The performance of both active and reactive power can be controlled and enhanced using this non-linear, adaptive, and reliable control system. Therefore, compared to the traditional PI controller and fuzzy logic controller, this technique effectively improves the dynamic and steady-state performance of the system and allows for quick response in the event of disturbances without the possibility of commutation failures.

1.3 Objectives

1.3.1 General Objective

The main goal of this thesis is to develop and simulate the power flow control using an adaptive neuro-fuzzy inference system for a permanent magnet synchronous generator-based wind energy conversion system.

1.3.2 Specific Objectives

The specific goals of this thesis are:

- To develop the mathematical models of the aerodynamics of the wind turbine system,
- To make the mathematical model of the mass drive train system,
- To model permanent magnet synchronous generator in wind turbine system,
- To design and model a full-scale power electronic converter and test its controllability,
- To design an Adaptive Neuro-Fuzzy Inference System (ANFIS) controller,
- To simulate and investigate an active and reactive power control, and
- To simulate the overall system model using MATLAB/SIMULINK.

1.4 Scope of the Thesis

This thesis will concentrate on the mathematical and simulation design of a permanent magnet synchronous generator-based wind energy conversion system for power flow regulation. The most significant feature of this thesis is that it does not use any physical controllers in hardware implementation and instead operates the full system simulation of the active and reactive power control using a computer-based controller using the MATLAB/SIMULINK software. i.e., the thesis investigation will be limited to software simulation only. Moreover, the study will only focus on the control and analysis of one wind energy conversion system that is rated at 2 MW to be connected to a 25 kV grid. The power converter stations will be connected in a back-to-back converter with passive rectifiers. Finally, the proposed controller's dynamic performance study and comparison with the traditional PI and the fuzzy logic controllers for the active, reactive power, and DC-link voltage control will be carried out.

1.5 Significance of the Thesis

The purpose of this thesis is to present adaptive neuro-fuzzy inference system techniques that can be used to control the power flow of wind energy conversion system-based permanent magnet synchronous generators. Energy waste and air pollution are major issues for the world and the country. As a result, the world is changing its energy usage from non-renewable sources that will be depleted in a few decades to renewable energy sources. The renewable energy source is environmentally friendly. To do this, neuro-fuzzy controllers perform more work than traditional and fuzzy logic controllers because (Shariatpanah et al., 2013):

- ❖ All electrical equipment is prone to failure when exposed to power stability difficulties; nevertheless, regulation of instability is conducted to protect against failure.
- ❖ Improve the current and future power generation and transmission systems.
- ❖ When some parameters change, the control method is universal and can be adapted to a variety of systems, and it is unaffected by variations in grid failures, instability, power imbalance, and external load disturbances.

1.6 Outline of the Thesis

This thesis is organized into five chapters.

Chapter 1: Deals with a brief background study of the thesis, a statement of the problems, objectives, scope, and significance of the thesis.

Chapter 2: Includes a literature review on the background of the wind energy conversion system, wind turbine generators, power converters, proposed controllers, and a review of related works.

Chapter 3: Describes the methodology leading toward the completion of the thesis. This chapter gives a detailed mathematical model of wind energy conversion systems including wind turbine (Aerodynamic) and drive train modeling, permanent magnet synchronous generator model, rectifier model, boost converter model, inverter model, grid filter, model, and grid model. Furthermore, this chapter presents the PI controller, fuzzy logic controller, and adaptive neuro-fuzzy inference system controller design.

Chapter 4: Presents the proposed results and discussions.

Chapter 5: Discusses conclusions and recommendations.

The appendix section covers the parameters used, related MATLAB/SIMULINK, and MATLAB codes.

CHAPTER TWO

2. LITERATURE REVIEW

2.1 Chapter Overview

This chapter highlights the literature cited on the wind energy conversion system, classifications of wind turbines, power operating regions of a wind turbine, wind turbine generators, power converters, power flow control strategies, fuzzy logic controllers, and adaptive neuro-fuzzy inference system controllers, and literature of related works will have discussed.

2.2 Theoretical Background

2.2.1 Overview of Wind Energy Conversion System

The wind energy conversion system consists of that the turbine rotor, gearbox, generator, transformer, and power converter. So that the turbines are consists of the rotor of blades that convert the kinetic energy of the wind energy into mechanical energy, the gearbox/direct drive that increases the speed of the rotor and transmits it into the generator, the generator which converts the mechanical energy into the electrical energy, control system which is used to control the variations and start-up at cut-in speed and make stop at cut-out as per of design requirements and the electronics conditioning that is made up of the electronic devices deals with converting the voltage/current sources from one form to another form. The wind blowing into the turbine is causing it to rotate the rotor blades and it starts to generate electricity. By using the yaw control system used to align the direction of the rotor faces into the wind (Shariatpanah et al., 2013). Most turbines have either two or three blades (Kumar & Chatterjee, 2016).

2.2.1.1 Wind Turbine Components and their functions

The voltage at the generator’s terminal is low so a transformer is used to step up the voltage to the grid voltage level. The transformer could be placed in the nacelle to the minimization of losses or at the bottom of the tower (Sekhar & Babu, 2016). Figure 2.1 shows the major component of a horizontal axis three-bladed wind energy conversion system (Sánchez & Rios, 2016).

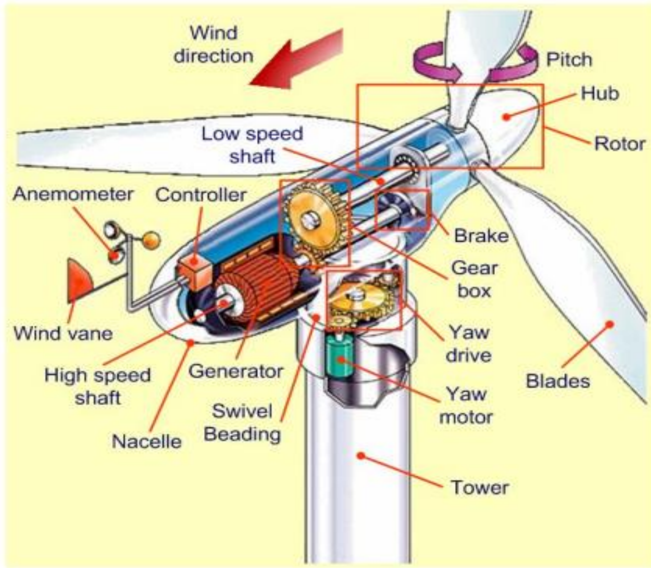

Figure 2. 1 Component of a horizontal axis three-bladed WECS

Other parts of a wind turbine are an anemometer and wind vane which are used for measuring the wind speed and wind direction respectively. To determine whether to start the wind turbine or, if the wind speed is too high, to shut the turbine down because of safety concerns, we must measure the wind speed. Brakes are used to stop the wind turbine to protect it from damage during times of exceptionally high wind and during maintenance. The yaw control mechanism aligns the nacelle with the direction of the wind using the wind direction. According to the design specifications, the controller turns on the machine at the cut-in wind speed, which is typically 3 m/s, and turns it off at the cut-out wind speed, which is typically 25 m/s (Miao & Shen, 2013). To increase the voltage value and decrease the current by avoiding losses in the transport of the current. Wind energy conversion systems (WECS), configurations of wind power generation use either fixed speed or variable speed turbines. According to the speed, wind turbines can categorize into a variable and fixed speeds (Sánchez & Rios, 2016).

Table 2. 1 Comparison between the fixed speed and the variable speed wind turbines

Types of WECSs	**Advantages**	**Disadvantages**
Fixed-speed wind energy conversion system.	❖ Simple and robust construction, ❖ Low maintenance, and ❖ Low cost.	❖ The extracted power is not optimized, less efficient, ❖ Fewer power factors, ❖ Higher stress on turbine and

		❖ Lack of reactive or active power control.
Variable-speed wind energy conversion system.	❖ It can supply power at a constant frequency and voltage even though rotor speed varies. ❖ Independent control of active and reactive power and ❖ High efficiency	❖ It needs complex power electronics converters and ❖ Limited fault control capacity.

2.2.2 Classification of Wind Turbines

Wind turbines are classified into two categories, according to the orientation of the axis of rotation concerning the direction of the wind (Thakur, 2020). These are Horizontal-axis wind turbines (HAWTs) and Vertical-axis wind turbines (VAWTs)

2.2.2.1 Horizontal-axis Wind Turbines

The rotating axis of the rotor shaft is parallel to the ground in horizontal-axis wind turbines. The horizontal axis windmills may come in a variety of designs. Depending on the number of blades, these turbines can be categorized as single-, double-, three-, multi-, and bicycle-bladed. This turbine can be classified as either an up-wind turbine or a down-wind turbine based on the orientation of the blades (Sánchez & Rios, 2016). In the modern era, horizontal axis wind turbines are used in most wind energy conversion systems.

2.2.2.2 Vertical-axis Wind Turbines

The vertical axis wind turbines have the spinning axis of their rotor shaft oriented perpendicular to the ground (Sánchez & Rios, 2016).

Table 2. 2 Comparison between the HAWTs and VAWTs

Types of Wind Turbines	**Advantages**	**Disadvantages**
HAWTs	❖ They have a higher energy conversion efficiency and	❖ High installation and maintenance costs and

	❖ They have features such as blade pitch angle control for power control.	
VAWTs	❖ They have lower installation and maintenance costs and ❖ They are operated independently of the direction of the wind.	❖ They have lower energy conversion efficiency and ❖ They are prone to mechanical vibrations leading to higher fluctuations in torque output.

Horizontal-axis wind turbines were chosen for this thesis because they have more advantages than vertical-axis wind turbines. The wind turbine generator starts to extract maximum power from the wind renewable source energy when the wind speed is equal/exceeds the cut-in wind speed and stops when the wind speed is at/ is approaching the cut-out wind speed (Thakur, 2020).

2.2.3 Overview of the Wind Turbine Generators

In the early wind power development, wind farms were made up of fixed-speed wind turbines (FSWT) and induction generator-based WTs. These wind turbine generators were integrated into the utility grid without converters included. However, the shortcomings of these generators such as low efficiency, limited fault-ride-through ability, and large power fluctuations limited their applications. Several studies in the areas of variable wind speed turbine systems equipped with permanent magnet synchronous generators are given in the literature (Bisoyi, 2013; Bunjongjit & Kumsuwan, 2013; Youssef Errami et al., 2021).

Modern variable speed wind turbine (VSWT) systems are based on doubly fed induction generators (DFIGs) with partially rated power electronic interfaces or permanent magnet synchronous generators (PMSGs) with fully rated electronic interfaces (Sánchez & Rios, 2016; Tripathi et al., 2015).

2.2.3.1 Squirrel-Cage Induction Generator-based Wind Energy Conversion System

In (Cheng & Zhu, 2014) fixed-speed squirrel-cage induction generators were widely employed for large wind turbines in the 1980s, during which most of the technologies of wind turbines were direct coupled generators i.e., the wind turbine generator is directly coupled with the power grid. The rotational speed of the generator is therefore not entirely constant. For a wound rotor induction generator, to produce a magnetic field, it is necessary to provide an extra power supply for the rotor circuit via a slip ring. However, the variation of the rotational speed is generally less than 1% due to the nature of the small slip of induction generators (Jha, 2017), which is a definition as the rate of the differential of the rotation speed of magnetic fields between the synchronous speed and rotation speed, divided by the synchronous speed. Figure 2.2 shows the fixed-speed wind system based on a squirrel-cage induction generator (Cheng & Zhu, 2014).

2.2.3.2 Doubly Fed Induction Generator-based Wind Energy Conversion System

The stator is directly connected to the grid, while the DFIG-based WECS is connected to the grid via a partially rated converter attached to the rotor circuit. To protect the converters, the Crowbar is attached to the rotor-side converter. Wind energy can be sent to the grid by the DFIG at a variety of speeds, from super synchronous to sub-synchronous. The DFIG's variable speed range typically ranges between 30% and 50% of synchronous speed. The back-to-back converter's nominal power is then only around 30% of the wind turbine's rated power (Cheng & Zhu, 2014). By adjusting the rotor-side converter's active power, the generator speed can be adjusted to maximize the amount of wind energy captured. Additionally, the rotor-side converter may manage the reactive power sent to the grid by decoupling active and reactive power (Cheng & Zhu, 2014; Tripathi et al., 2015).

2.2.3.3 Permanent Magnet Synchronous Generator-based Wind Energy Conversion System

The PMSG-based WECS is connected to the grid via a fully rated power electronic converter. The fully rated power converter fully decouples the WT from the grid disturbances thereby allowing full controllability of the system and improved fault-ride-through capability. The PMSG-based WECSs are becoming more popular and more preferred over DFIG-based WECS (Y. S. Kim et al., 2015; Tripathi et al., 2015).

Table 2. 3 Comparisons between the SCIG, DFIG, and PMSG.

Types of Generators	**Advantages**	**Disadvantages**
SCIG	❖ Simple structure, ❖ Low cost, ❖ Easy to maintain and ❖ Simple solution for grid connection.	❖ It does not operate under optimal tip speed ratio with wind speed variation, ❖ Lowest efficiency, ❖ Lowest power factor and

		❖ It requires an extra power supply for excitation.
DFIG	❖ The generator speed can be regulated to optimize the power generated from the wind by controlling the active power of the rotor-side converter and ❖ The reactive power delivered to the grid can also be controlled by the rotor-side converter.	❖ It requires frequent maintenance and may lead to machine failures and electrical losses, because of slip rings and brushes ❖ The FRT capability of the WECS is relatively weak due to the stator of DFIG and the grid is connected directly and ❖ Control methods grid faults are quite complicated.
PMSG	❖ High energy density, ❖ Easy of controllability, ❖ Low maintenance cost, ❖ Improving the efficiency, ❖ Improve fault-ride through capability and ❖ Self-excitation system	❖ Have full-rated power converters, this will cause losses and generate high harmonics and ❖ The permanent magnets run the risk of demagnetization at high temperatures.

In this thesis investigation, a direct-drive PMSG is used to operate the wind energy conversion system. As a result, PMSG modeling and design will be examined in depth.

2.2.4 Overview of Power Converters

Power electronics devices have been applied in WECSs since the 1980s when a thyristor-based soft-starter was applied to a SCIG system that was directly connected to the grid (Blaabjerg et al., 2012). The current surge at startup was controlled by a thyristor-based soft-starter. The ability to manage the WRSG to operate at different speeds was made available in the 1990s with the development of the rotor resistance control technique. The use of the converter-controlled variable resistance has increased the wind turbine's ability to capture energy, even though the speed range is only 10% over the synchronous speed of the generator. For the DFIG systems shown in Figure 2.3, back-to-back converters are frequently employed in CSS, either in reduced power (reduced power means that the power converters only process 30% of the rated power) or Figure 2. shows PMSG systems operating in full power (full power refers to the power converters processing the generator's output power up to its rated power) (Cheng & Zhu, 2014).

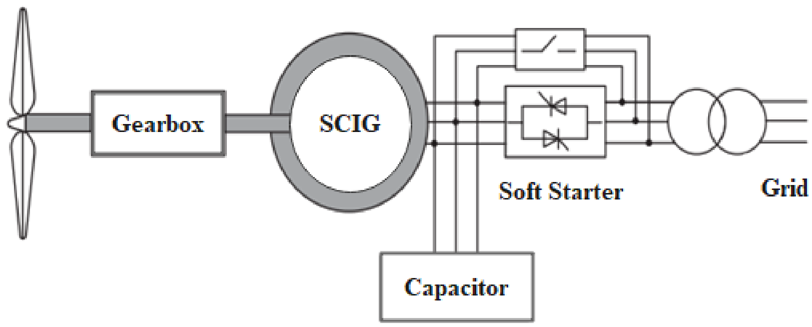

Figure 2. 2 Fixed-speed wind turbine system based on IG.

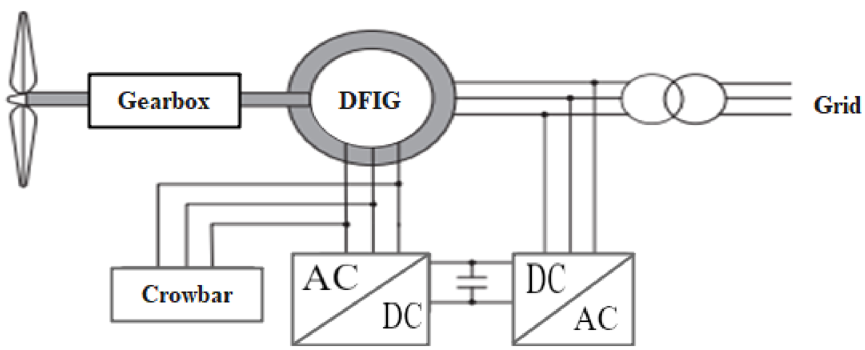

Figure 2. 3 DFIG with partial-scale converters

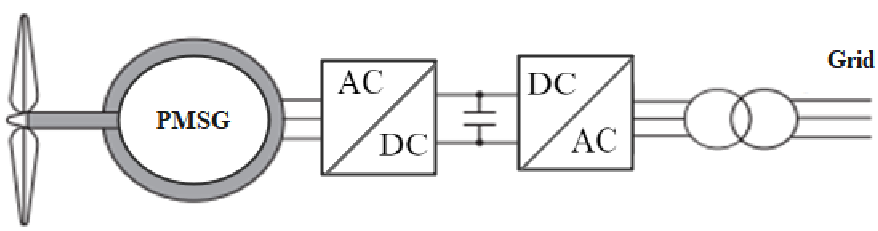

Figure 2. 4 Wind turbine generators with a full-scale power converter

The power converter topologies are classified as direct and indirect based on power conversion strategies. As a result, several arrangements of power converters have been used to perform power conversions (Muhammed & Krishnakumari, 2014).

(a) Direct conversion with single-stage AC/AC conversion which includes cyclo-converters and Matrix Converters etc.

(b) Indirect conversion with two-stage (AC/DC and DC/AC) conversion which includes Voltage Source/Current Source half and full controlled converters with or without DC link, passive controlled converters, etc.

(c) Another indirect conversion uses three-stage (AC/DC, DC/DC, and DC/AC) conversion which includes Voltage Source/Current Source half and full controlled converters with or without DC link, buck, and boost controlled converters, etc.

Switching power loss has a significant impact on power converter efficiency, which can be decreased by using efficient switching techniques and arranging converters optimally (Et. al., Eswaraiah G, 2021). For wind energy systems, power electronics manufacturers have developed several power converter topologies (Blaabjerg et al., 2012).

For this thesis, two-level back-to-back converters with passive rectifiers are chosen among the above power converter topologies. This thesis will discuss why it was chosen through a detailed description of these converters.

2.3 Review of Power Flow Control Strategies

There are two different ways that power can flow: Either from the generator to the grid or from the grid to the generator. So, damage to the generator units, converter, and wind turbine may result from an imbalance in the power between the grid and the generator. Reactive power is unused power, while active power is the power that may be used.

Generally, the control of the power flow approach is observed independently (Maroufi et al., 2020; Noman et al., 2021). A neuro-fuzzy controller is the best choice for controlling the stability and achieving the improved dynamic performance of the power flow controller. Therefore, the study will concentrate on the reactive and active power control of the direct-driven PMSGs of wind turbines.

2.3.1 Active Power Control

In wind turbine direct-driven PMSGs, real and reactive powers are controlled separately, the basis for real power and reactive power-based control approaches (H. W. Kim et al., 2010). And the control system is realized using classical vector control. The dynamic performances of a wind turbine’s direct-driven PMSG can be enhanced using this approach. Otherwise, the dynamic oscillations can be damped through pitch angles or speed controllers. Nevertheless, in all these cases, the responses achieved are slow. This approach can easily be adapted for a wind turbine direct-driven PMSG. Alternatively, the PI controller can be replaced by the fuzzy logic controller to achieve a better dynamic performance in a wind turbine direct-driven PMSG (Chatri & Ouassaid, 2018; Marmouh et al., 2017). This implies that, though they haven't been yet tested, advanced controllers can also be applied to pitch angle controllers for wind turbine direct-driven PMSGs. This thesis attempts to present an adaptive neuro-fuzzy inference system controller for controlling the power flow from a permanent magnet synchronous generator based on wind energy conversion to the grid. Additionally, this proposed technique can be researched to improve dynamic performance in addition to PI controller and fuzzy logic controller-based control strategy.

2.3.2 Reactive Power Control

Few authors explored the effectiveness of reactive power control in enhancing wind turbine dynamic performances. In (Han et al., 2013), a supplementary reactive power controller is used to improve the dynamic performances of a power system. In this thesis, the results illustrate that the dynamic stability problem is controlled. Moreover, (Rodrigues et al., 2013), use a multi-objective genetic algorithm to tune a PI controller that enhances the dynamic stability of a wind turbine's direct-driven PMSG. In (Yadav & Upadhayay, 2014), the reactive power and the DC voltage for the VSI are tightly controlled based on classical control. Alternatively, the PI controller can be replaced by the fuzzy logic controller to achieve a better dynamic performance in a wind turbine direct-driven PMSG (Chatri & Ouassaid, 2018; Marmouh et al., 2017). Usually, reactive power control is implemented in the grid-side converter. Therefore, it is essential to research this strategy for direct-driven PMSGs for wind turbines.

In this thesis, three controllers are shown for comparison purposes to look for enhanced performance and compare the performance of power flow controllers. As a result, the following two sections of this thesis must each be presented as an overview of a fuzzy logic controller and a neuro-fuzzy controller.

2.4 Overview of Fuzzy Logic controller

Fuzzy Logic (FL) is classified in the artificial intelligence category. "Fuzzy Sets" were introduced in 1965 by Lotfi Zadeh from the University of California at Berkeley (Zadeh, 1965). As an extension of the classical control theory. According to him, classical control theory put too much emphasis on precision and therefore could not be a complex system (H. W. Kim et al., 2010; Tiwari & Babu, 2016). FL controllers can interpret data that falls in the gray area much like a human mind can make cognitive decisions when there is no distinct answer. Fuzzy logic is unlike many traditional logic systems in that the reasoning is approximate and not exact. It is this logic approximation also done by humans with commonsense reasoning that makes FL a form of artificial intelligence.

2.5 Overview of Adaptive Neuro-Fuzzy Inference System

2.5.1 Neuro-Fuzzy System

Despite the advantages of fuzzy control, the main limitations are the lack of a systematic design methodology and the difficulty in predicting the stability and robustness of the controlled system. A trial-and-error iterative approach is taken for the controller design due to which we get a sluggish response. Neuro-fuzzy learning incorporates the architecture of a neural network-based fuzzy inference system. A given training data set is partitioned into a set of clusters based on the subtractive clustering method. This is a fast and robust method to generate suitable initial membership functions and rule bases. A fuzzy if is then extracted from each cluster to form a fuzzy rule base from which a fuzzy neural network is designed. Then a hybrid learning algorithm is used to refine the parameters of the fuzzy rule bases.

2.5.2 Adaptive Neuro-Fuzzy Inference System

The Adaptive Neuro-Fuzzy Inference System (ANFIS) is one of the most effective methods for combining neural network systems with fuzzy logic together. To identify and fine-tune the parameters and structure of a fuzzy inference system (FIS), an ANFIS employs neural learning algorithms. Strong generalization abilities, good explanation facilities through fuzzy rules, and ease of integrating both linguistic and numeric knowledge for problem-solving just are a few of the attractive features of an ANFIS. By using the neuro-fuzzy scheme, the fuzzy inference system can be tuned with a neural network algorithm based on some collection of input-output data, which then allows the fuzzy system to learn. Fundamentally, a FIS is used, and it is tuned via a backpropagation method based on a collection of input-output data. FIS can learn because of this. The network structure makes it easier to calculate a FIS parameter's descendent gradient vector (Fang, 2012).

2.5.3 Adaptive Neuro-Fuzzy Inference System Controller

The adaptive neuro-fuzzy inference system uses a feedforward network to search for fuzzy decision rules that perform well in each task. Using a given input/output data set ANFIS creates a fuzzy inference system for which membership function parameters are adjusted using a combination of backpropagation and the least square method. As a result, ANFIS may approximate uncertain and nonlinear systems without the need for pure mathematical models.

2.5.3.1 Structure of Neuro-Fuzzy Controller

The ANFIS's structure is like that of an artificial neural network (Fang, 2012). Consider a scenario where E and CE are the inputs, and f is the output. The following is a possible expression for the first order IF-THEN fuzzy rules:

Rule 1: IF E is A_1 AND CE is B_1, THEN $f_1 = p_1 e + q_1 ce + r$ and

Rule 2: IF E is A_2 AND CE is B_2, THEN $f_2 = p_2 e + q_2 ce + r_2$

Where: A_1, A_2, and B_1, B_2 are the MFs for inputs E and CE respectively. The symbols, $f_1 = p_1 e + q_1 ce + r_1$ and p_2, q_2, r_2 are the associated parameters of the output functions. The five-layered ANFIS architecture is shown in Figure 2.5 (b), and the fuzzy reasoning method for the Sugeno-type fuzzy model to derive output function f from a given input vector [e, ce] is presented in Figure 2.5 (a).

Layer 1: Each node is assigned a fuzzy membership value using membership functions to form a fuzzy set.

$$\begin{aligned} O_{1,i} &= \mu_{A_i}(e) \quad for\, i = 1,2 \\ O_{1,i} &= \mu_{B_{i-2}}(ce) \;\; for\, i = 3,4 \end{aligned} \tag{2.1}$$

Where e, ce is the crisp input to node i, and the membership grades of the membership functions μ_A and μ_B, respectively. Using a generalized bell-shaped MF, the output $O_{1,i}$ can be computed as:

$$O_{1,i} = \mu_{A_i}(e) = \frac{1}{1 + \frac{(e - c_i)^{2b_i}}{a_i}} \tag{2.2}$$

Where: { a_i, b_i, c_i } is the parameter set that changes the shapes of the MF with a maximum equal to 1 and a minimum equal to 0.

Layer 2: In this layer, every node multiplies the input signals, denoted in Figure 2.5(b) as "Π" and represents the rule nodes and the output $O_{2,k}$ that represents the firing strength of a rule and is computed as:

$$O_{2,k} = w_k = \mu_{A_i}(e)\mu_{B_i}(ce) \quad for\;\; i = 1,2 \tag{2.3}$$

Layer 3: This layer consists of the averaging nodes, which are labeled as "N" and composed of the normalized firing strength equal to:

$$O_{3,k} = \bar{w}_i = \frac{w_i}{w_1 + w_2} \quad for\ i = 1,2 \tag{2.4}$$

Layer 4: The node function of this layer is to compute the contribution of each i^{th} rule towards the total output and the function can be defined as:

$$O_{4,i} = \bar{w}_i f_i = w_i(p_i e + q_i ce + r_i) \quad for\ i = 1,2 \tag{2.5}$$

Where: w_i is the output of layer 3 and { p_i, q_i, r_i } is the parameter set.

Layer 5: This layer has a single output node, which computes the overall output of the ANFIS as:

$$O_{5,i} = \sum \bar{w}_i f_i = \frac{\sum w_i f_i}{\sum w_i} \tag{2.6}$$

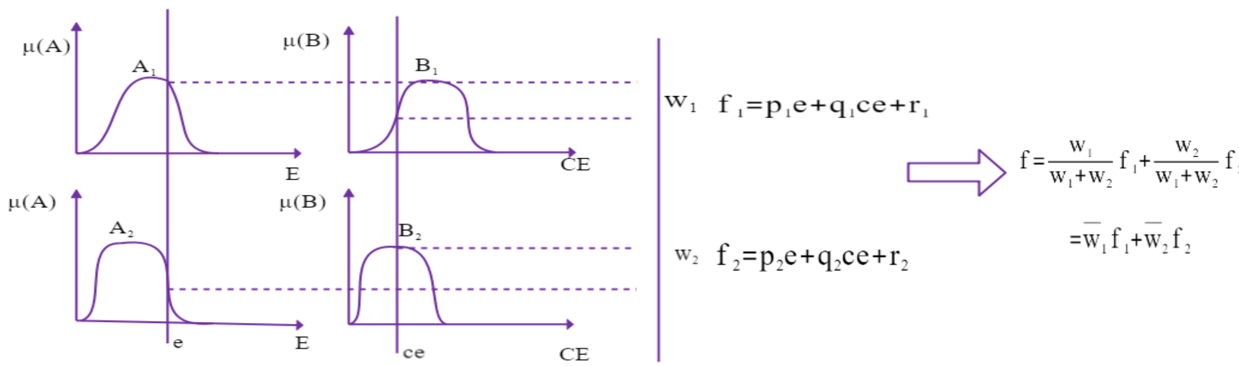

(a)

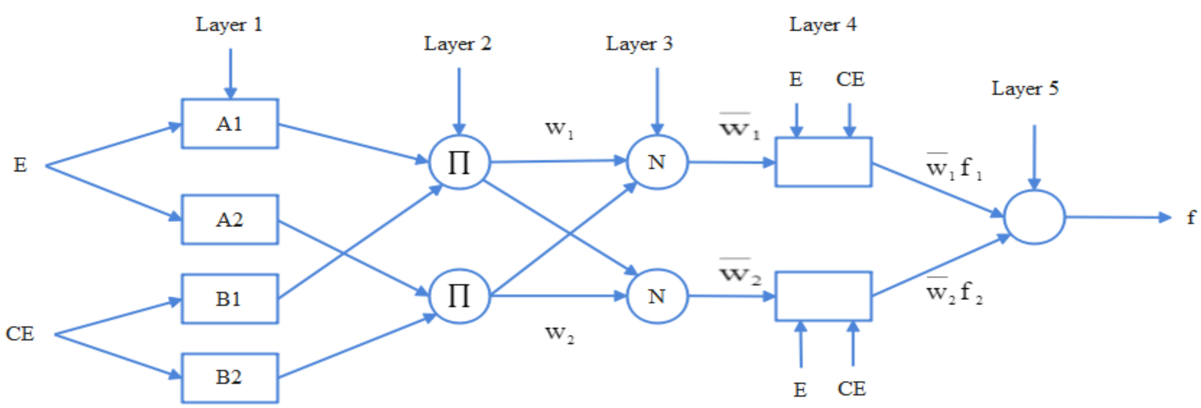

(b)

Figure 2. 5 (a) Fuzzy inference system (b) ANFIS corresponding architecture

The ANFIS is designed by taking error (e) and change in error (ce) as the inputs. The output stabilizing signals are computed using the fuzzy membership functions depending on these variables. The system is simulated and implemented using the ANFIS editor. In a traditional fuzzy approach, the model designer fixes the membership functions and the consequent models with prior knowledge. The components of a fuzzy system (membership and consequent models) can be expressed in a parametric form and the parameters are tuned using neural networks if this set is not available, but a set of input-output data is observed from the process. The fuzzy systems then evolve into neuro-fuzzy systems. While a neural network can learn from training instances and adjust its knowledge, a fuzzy system can only explain the knowledge it encodes and cannot learn from or adapt its knowledge. Neural networks and fuzzy systems complement one other in their strengths and drawbacks. As a result, many researchers are trying to integrate these two schemes to generate hybrid models that can take advantage of the strong points of both.

2.6 Review of Related Work

Numerous studies and publications have been conducted and published on wind energy conversion systems that use a permanent magnet synchronous generator to control power flow. Previous works that are directly or indirectly related to the idea of this thesis work are examined in this section. The works discussed in this section are mainly limited to recently published journal papers (less than 10 years). Even though this work benefited from many materials, due to space constraints, only a few of them are reviewed.

Authors (Shariatpanah et al., 2013) proposed a new model for a permanent magnet synchronous generator-based wind turbine with yaw control. The yaw control strategy is proposed to protect the wind turbine against over speed and excess power. Field oriented control method is applied to the voltage source converters. These controllers independently control reactive and real power. The authors provided a novel model that considered both electrical and mechanical characteristics and was used to assess overall performance. Using a conventional PI controller in MATLAB/SIMULINK, the model demonstrated the efficiency of yaw control. The authors, on the other hand, failed to demonstrate the importance of power electronic converter control and they did not use any optimization technique.

Authors (Bipin Biharee Srivastava, 2014) present that owing to the constant increase in fuel prices, wind energy has attracted increasing interest on a global scale. This author suggests the fuzzy logic controller for maximum power point tracking control to track the wind production system's maximum power. Maximum power is attained by increasing the rotor speed of the wind system, which consists of a wind turbine and a PMSG. The grid-side converter is managed by the voltage source inverter (VSI), which also links the voltage from the DC-link. Regarding providing the best system performance, the suggested technique has a drawback. The control of the reactive and active power without control of the inverter converter is another challenge with this approach. Another main drawback to this system is fuzzy rule expert systems are difficult to acquire knowledge.

Authors (Tiwari & Babu, 2016) proposed a comparative analysis of alternative control algorithms to get the most power out of a wind energy conversion system based on a permanent magnet synchronous generator at varying wind speeds. The WECS is made up of a wind turbine, a PMSG, and a DC-DC converter coupled to a DC load. Maximum Power Point Tracking (MPPT) control methods include the PI control, the Perturb and Observe (P&O) strategy, and the fuzzy logic controller. The criteria considered while assessing the MPPT controller's efficiency are the output DC-link voltage and power across the load. The controllers' overall efficiency was justified by looking at the steady-state voltage and dynamic response of the system at various wind speeds. The control of power flow with voltage change is a challenge with this method.

Author (Vadi, 2020) has proposed a grid-connected wind turbine with a permanent magnet synchronous generator, along with its design and modeling. He created the mathematical model for wind turbines and PMSG. The system is controlled by the control strategy, which is based on a traditional PI controller. By altering the wind speed, pitch angle, load, and inverter output parameters, the dynamic behavior of the wind turbine model may be examined. MATLAB/SIMULINK simulation results are used to test the suggested model. When the system's uncertainties and nonlinearity were not considered, analyzing the outcomes was a good strategy, therefore he did it. But this method is lacking robustness because of the variations in the internal parameters of the machine the system may be affected.

Authors (Hassanzadeh & Hajizadeh, 2017) have offered a grid-connected wind turbine back-to-back converter control to mitigate voltage drops brought by faults. On a fault grid, the effectiveness of back-to-back converter control of a wind turbine system with a permanent magnet synchronous generator is examined. As the maximum tracking active power of the wind turbine system is injected into the grid and the DC-link voltage in the converter is managed, the switching strategy of a grid-side converter is created to improve the voltage drop caused by the failure in the grid. In

MATLAB/SIMULINK, the simulation result is simulated, and the performance of the controller is displayed under both normal and failure conditions. However, this system lacks robustness due to fluctuations in the machine's internal characteristics, and when these variations (faults) occur, the converter controller may damage.

Authors (Marmouh et al., 2017) have put forth a new method for managing a wind energy conversion system that makes use of a permanent magnet synchronous generator to track the maximum amount of power. The MPPT control algorithm is used for the PMSG, whose stator is connected to the grid through a back-to-back converter. To extract the most power from the machine side converter for a wide range of wind speeds, the fuzzy logic controller is used. The grid side converter is managed to give the two converters a stable DC link voltage. The fuzzy logic approaches have also demonstrated increased effectiveness. However, it has a drawback in generating membership functions and rules.

Authors (Chatri & Ouassaid, 2018) have suggested a novel permanent magnet synchronous generator-based fuzzy wind control strategy. To help PMSG states move along their optimal trajectory, the Takagi Sugeno (T-S) fuzzy controller was created. Meanwhile, the parallel distributed compensation approach is used to maximize power production and enhance system performance. The suggested controller's gains are also estimated using the Linear Matrix Inequality approach. Comparisons of simulation results based on T-S fuzzy and PI controllers under sudden changes in wind speed prove that the T-S fuzzy controller guarantees faster response time and lower overshoot. To deal with fuzzy logic controller drawbacks a Takagi-Sugeno fuzzy approach is proposed. The idea of the approach is simple. But these also have drawbacks to the performance analysis. Another drawback of this strategy is reactive and active power and the stable control of the DC link voltage.

Authors (Ali et al., 2015) have suggested that a grid-connected PMSG for WECS be designed to maximize output power and address output control. The real and reactive powers of PMSG are strictly regulated at the needed level to integrate the WECS power into the grid without any issues related to power quality. With the traditional PI controller of the real power, the DC-link voltage is likewise controlled to a certain amount. Using MATLAB/SIMULINK, the performance simulation results are examined. To solve these issues, the adaptive Neuro-fuzzy inference system controller was created. It involves decomposing a nonlinear system's model into several linear subsystems and combining artificial neural networks with fuzzy logic controllers. This indicates that while the neural network control technique has a quick response time, its control performance degrades because of system parameter fluctuation. However, stability and the tracking issue are the main FLC strategy issues. Therefore, combining them is the answer to the issues. The limitation observed here is that they have controlled the machine side only and there was a mismatch between their title and their works. They have not considered and controlled the grid side system.

All the articles mentioned above were proposed by different researchers and are only valid for limited working conditions. Due to significant starting overshoot, sensitivity to controller gains, and sluggish response during rapid disturbances and heavy loading circumstances, these are not valid for a wide range of operating circumstances. The neuro-fuzzy methodologies described in this thesis are the outcome of the combination of an ANN and a fuzzy inference system, which constitute a framework for solving real-world issues. A neuro-fuzzy system is based on a fuzzy system that has been trained using a neural network learning method. While the ability to learn is helpful from the viewpoint of FIS, the construction of a linguistic rule base will be advantageous from the viewpoint of ANN. This method is employed to regulate the reactive, active, and DC link voltages. The simulation findings demonstrate the ANFIS system's improved performance over traditional and fuzzy logic controllers. Fuzzy logic and neural network controllers are used to create the controller performance assessment.

CHAPTER THREE

3. METHODOLOGY AND SYSTEM MODELING

3.1 Introduction

This chapter deals with methods of data collection and analysis, detailed development of all mathematical modeling, and the PI controller, fuzzy logic controller, and proposed controller designs. It mainly consists of the following parts:

Materials used, methods, wind speed model, wind turbine model, drive train model, permanent magnet synchronous generator model, AC-DC converter model, DC-DC boost converter model, DC-AC inverter model, and design of the controllers.

3.1.1 Materials

Software such as MATLAB, Microsoft Office, Mendeley, Wondershare EdrawMax, and Math Type were used in this thesis. MATLAB is a computing software package that includes technical toolboxes and Simulink. The thesis documentation is edited using Microsoft Office. Mendeley is a reference managing and citation tool that can help to store, organize, note, share, and cite references. The circuits, block diagrams, and flow charts in this thesis were created using Wondershare EdrawMax. Math Type is used in Microsoft Office Word and PowerPoint Presentation tools to write mathematical formulas and equations.

3.1.2 Methods

The methods used in this thesis to accomplish the required task are shown as follows:

1. Problem Identification: Describe the problem statement and define the research objectives.

2. Literature Review: The review of the theoretical background of wind energy conversion systems, power converters, types of generators, and the review of related work will be studied. The overview of fuzzy logic and adaptive neuro-fuzzy inference system controllers will be discussed.

3. Data Collection: The data required for the designing of the wind energy conversion system are collected from journals, articles, books, the internet, and so on. Here, from the conventional PI controller, we can take the input data and output data to design the ANFIS controller.

4. Data Analysis: The feasibility of the system will be analyzed from the collected data by using theoretically proved formulas.

5. Design: Finding the appropriate power electronic converters is crucial since there are numerous power converters available in advanced power electronics, including AC-DC, DC-DC, DC-AC, and AC-AC converters. Each converter is also divided into sub-class groups based on its applications. Following that, the overall mathematical designs of the wind energy conversion system have been examined. These designs include an aerodynamic (wind turbine) model, a drive train model, a generator model, a rectifier, a DC-DC boost converter, a PWM inverter model, a filter, and a phase-locked loop.

6. Design and Identify the ANFIS controller training method: After designing all mathematical models of the thesis, develop and design an adaptive neuro-fuzzy inference system controller for improving the performance. Following that, a permanent magnet synchronous generator adaptive model based on ANFIS is created. Since it combines the capacity of fuzzy reasoning in handling the uncertainties system and the capability of artificial neural networks in learning from the processes, the ANFIS architecture has the well-known advantage of modeling a highly non-linear system. An error gradient is tuned using the backpropagation, least-square estimator method, or hybrid. It has two training types which are online and offline training. Offline training is a type of ANFIS Training in which training can take place by taking input and output data gained from traditional PI controllers whereas online training depends on the real data of the system. Then after, the overall systems are simulated including the proposed controller using MATLAB software.

7. Result Analysis: The simulated result in step six is analyzed. This means that may be valid or not if it is a valid result go to a conclusion unless feedback to test the simulation again and again until getting a valid result. And give discussions on the result simulation.

8. Conclusion and recommendations: Finally, the conclusion will be made, and some future work will be recommended.

To attain and obtain the general and specific objectives of this thesis, I should follow the following method and techniques. Figure 3.1 shows the general methodology of the thesis using a flow chart.

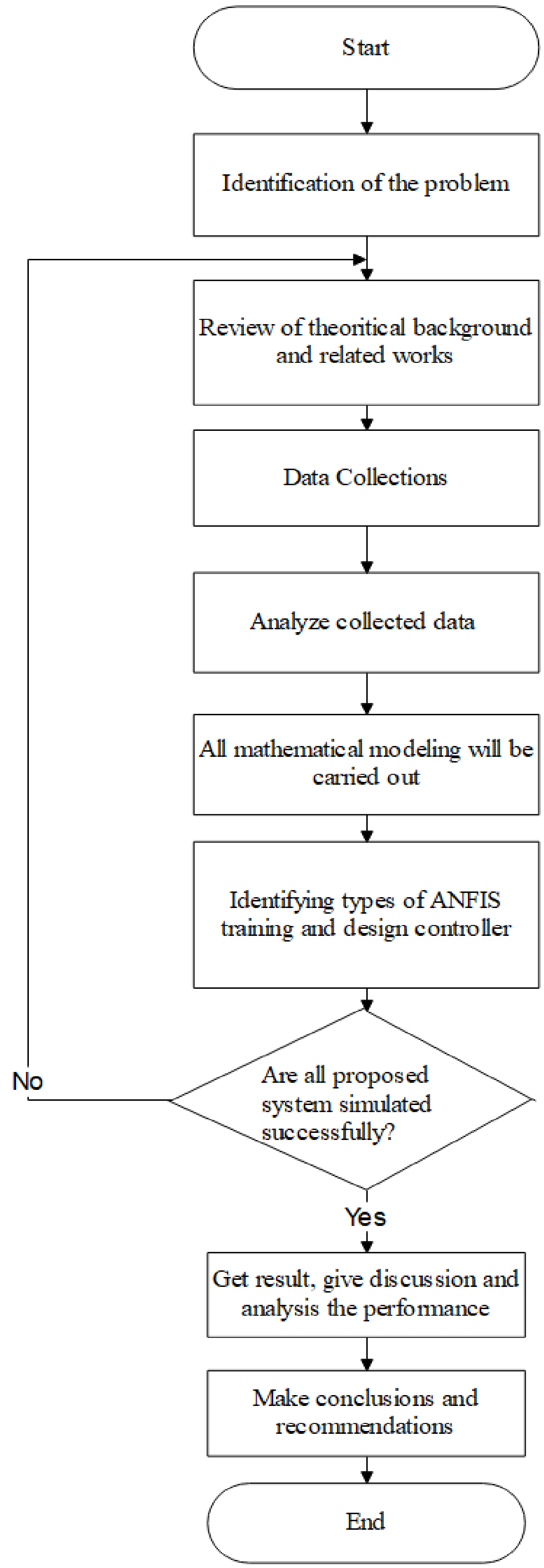

Figure 3. 1 General methodology of thesis in the flow chart

3.2 Dynamic Modeling

Modeling is a basic tool for analysis, such as optimization, design, and control. Dynamic studies must be addressed to incorporate wind power into the power system because wind energy conversion systems differ greatly from conventional generators in nature. Therefore, stability, control systems, and optimization are three different forms of system dynamics analysis that require dynamic modeling. In this thesis, the main components of a permanent magnet synchronous generator-based wind energy conversion system are discussed. The formulation of each component is carried out, which further helps in developing the control techniques for the whole system. Figure 3.2 shows the block diagram permanent magnet synchronous generator-based variable speed wind turbine with fully rated power converters.

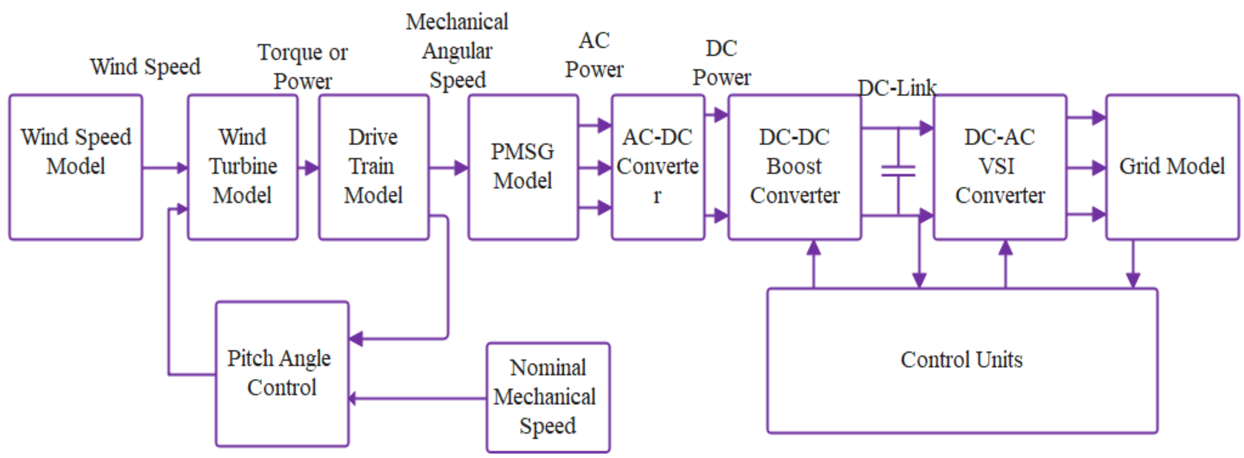

Figure 3. 2 Block diagram of PMSG-based VSWT with a fully rated power converter

3.2.1 Wind Speed Model

Wind speed is a random variable and depends on the climate and geographic location of the wind farm. The instantaneous value of the wind can be modeled by superimposing a constant term, deterministic shape functions of time representing gusts and other wind events, and a noise with an adequate spectrum, the latter representing turbulence (Chong et al., 2021). The wind speed model is composed of four components such as the spatial effect of wind behavior, gust, ramp changes, and background noise that affect the dynamic performances of a wind turbine's direct driven PMSG. The mathematical model of wind speed must first be completed to simulate the actual output characteristics of wind turbines in a simulation without wind.

$$V_{wind} = \overline{V} + V_{wg} + V_{wr} + V_{wn} \tag{3.1}$$

Hence, one of the wind speed models employed in the existing literature considers these components. The basic wind speed is a constant, which equals to mean wind speed while calculating. Thus, the model is given as:

$$\bar{V} = C \tag{3.2}$$

Where C is constant.

Gust represents the sudden change in wind speed. The simulation of the dynamic performances of a wind turbine's direct-driven PMSG can be used for the investigation of the system performances under large disturbances in wind speed. It is given by (Ma et al., 2015):

$$V_{wg} = \begin{cases} 0\,, & for \;\; t < t_{1g} \\ \dfrac{V_{wg\max}}{2}\left[1 - \cos 2\pi(\dfrac{t - t_{1g}}{t_g})\right], & for \;\; t_{1g} < t \le t_{1g} + t_g \\ 0, & for \;\; t > t_{1g} + t_g \end{cases} \tag{3.3}$$

Where V_{wgmax} represents the maximum gust, t_{1g} and t_g are the start and end times of the gusting wind, respectively. The ramp component depicts the gradual change in the character of the wind speed and is given by:

$$V_{wr} = \begin{cases} 0\,, & for \;\; t < t_{1r} \\ V_{wr\max}(\dfrac{t - t_{1r}}{t_{2r} - t_{1r}}) & for \;\; t_{1r} < t \le t_{2r} \\ V_{wr\max} & for \;\; t \le t_{2r} + t_r \\ 0, & for \;\; t > t_{2r} + t_r \end{cases} \tag{3.4}$$

Where:V_{wrmax}, t_{1r}, t_{2r} and t_r are represent the maximum ramp wind speed, starting time, end time of the ramp wind, and duration of ramp change wind speed, respectively.

Fluctuating wind speed (random noise) is aimed at reflecting the stochastic character of wind speed, which can be seen as a turbulent component lasting all the process. The random noise wind is the difference between the combination of wind speed and the mean of wind speed, a gust of wind, and gradient wind, as a result, the time is 0.

$$V_{wn} = \frac{1}{\Delta t}\int_{t_1}^{t_2} V_{wn} dt = 0 \tag{3.5}$$

The noise component can be assumed to be Gaussian noise, having a probability density function given in (3.6) as

$$P(V_{wn}) = \frac{1}{\sigma\sqrt{2\pi}} exp(-\frac{(V_{wn} - \bar{V}_{wn})^2}{2\sigma^2}) \tag{3.6}$$

Where σ is a standard deviation of random noise wind speed, V_{wn} is a random noise wind speed, and $\bar{V}_{wn}$ is a mean of random wind speed. However, in the random noise case, the mean and standard deviations are the average and standard deviations of the random noise wind speed.

In conclusion, the mathematical model for wind speed can be concluded in (3.2), (3.3), (3.4), and (3.5). Figure 3.3 shows the circuit of the wind speed model. A typical component of wind speed is shown in Figure 3.4.

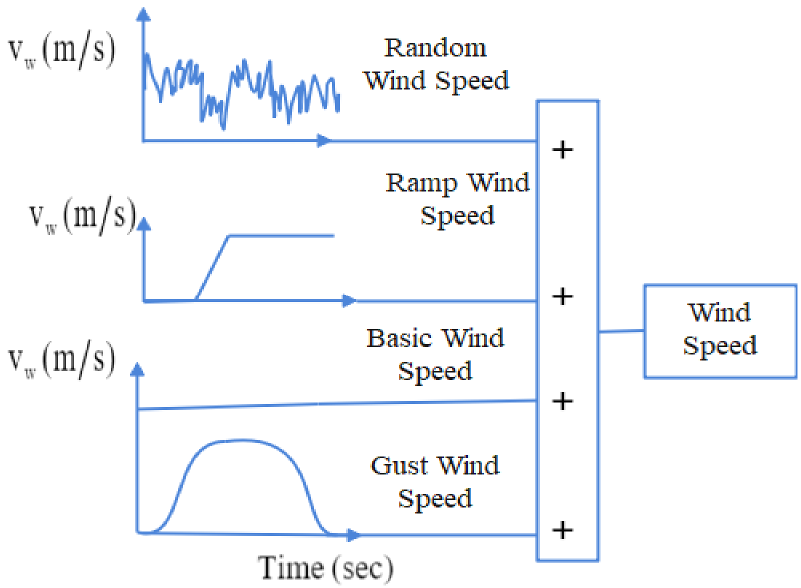

Figure 3. 3 Circuit diagram of wind speed model

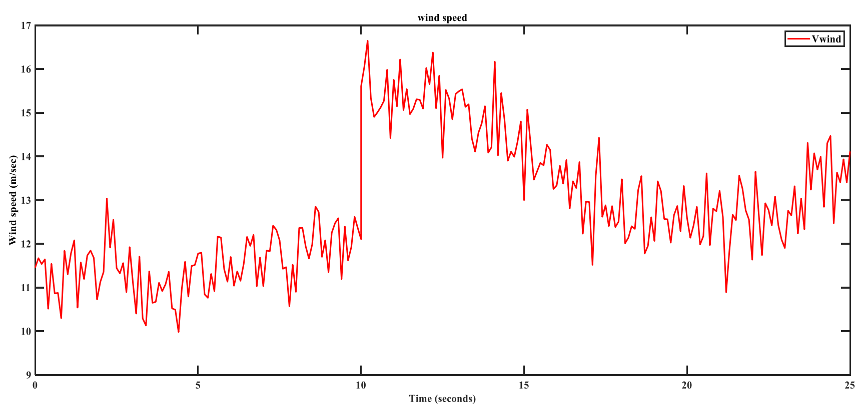

Figure 3. 4 Wind speed variations

3.2.2 Wind Turbine Modeling

The wind stream, which passes over the blades, causes a turning force over a shaft inside the nacelle. The kinetic energy of an air mass of wind with a total mass, m, moving at a wind velocity

V_{wind}, crossing a swept area (A) is given in (3.8) (Hailemariam et al., 2019). This wind speed is shown in (3.1). So that the kinetic energy is

$$K_E = \frac{1}{2} m v_{wind}^2 \tag{3.7}$$

An m dot is the flow rate weight of air particles moving at a wind speed V_{wind} for a period t, where $\dot{m} = \rho A V_{wind} t$, it is substituted in (3.7), and wind power P_{wind} is shown in (3.8)

$$P_{wind} = \frac{E}{t} = \frac{1}{2} \rho A V_{wind}^3 \tag{3.8}$$

Where: ρ is the density of air particles, and A is the swept area equivalent. Since the swept area of the blade is given by ($A = \pi R^2$), again wind power is

$$P_{wind} = \frac{1}{2} \rho \pi R^2 V_{wind}^3 \tag{3.9}$$

Where: P_{wind} is the potentially available power in the wind. From (3.9), as we can see, wind power is proportionally related to the cube of wind speed, which means that even a tiny increase in wind speed will result in a significant rise in wind power. Additionally, as the power is related to the square of the rotor radius of the wind turbine, the power can also be enhanced by making the rotor radius larger. This is the reason behind the increased number of researchers working now on large-scale wind turbine systems (up to 10 MW) (Y Errami et al., 2013).

Moreover, the power expressed in (3.9) can only stand for the maximum wind power, which is available when the wind with speed V_{wind} passes through the swept area of the wind turbine with a radius of R. In 1919, German scientist Albert Betz tried to express the action of the air particles (the wind) passing through wind turbines. According to Betz's theory, the wind's speed falls after interacting with the wind turbine's rotor blades, so even after passing through the blades, the wind still has some kinetic energy. A wind turbine can only recover a small percentage of the energy in the air; in this situation, the power coefficient is said to indicate the wind turbine's conversion efficiency (Y Errami et al., 2013; Hailemariam et al., 2019). Finally, the wind power captured by the blade and converted into mechanical power is calculated as follows (Berhanu et al., 2018)

$$p_m = \frac{1}{2} \rho \pi R^2 v_{wind}^3 C_p \tag{3.10}$$

Where: R is the radius of the wind turbine and the power coefficient C_p is shown in (3.11).

$$C_p = c_1(\frac{c_2}{\lambda_i} - c_3\beta - c_4)\exp(\frac{-c_5}{\lambda_i}) + c_6\lambda \qquad (3.11)$$

The c_1 to c_6 values are depend on the type of wind turbine (Y Errami et al., 2013; Hailemariam et al., 2019; Sánchez & Rios, 2016). In this thesis, the value of $c_1, c_2, c_3, c_4, c_5, and c_6$ are 0.5176, 116, 0.4, 5, 21, and 0.0068, respectively.

$$\frac{1}{\lambda_i} = \frac{1}{\lambda + 0.08\beta} - \frac{0.035}{\beta^3 + 1} \qquad (3.12)$$

A wind turbine characterized by its aerodynamic power is represented in (3.13) where it is dependent on pitch angle and tip speed ratio (Hailemariam et al., 2019; Yadav & Upadhayay, 2014).

$$P_m = \frac{1}{2}\rho\pi R^2 V_{wind}^3 C_p(\lambda, \beta) \qquad (3.13)$$

Where: β is the pitch angle in degrees, and λ is the tip speed ratio.

The tip speed ratio (λ) is given in (3.14) (Berhanu et al., 2018; Hailemariam et al., 2019; Yadav & Upadhayay, 2014).

$$\lambda = \frac{\omega_m R}{V_{wind}} \qquad (3.14)$$

Moreover, from the combination of (3.11), (3.12), and (3.14), the below circuit diagram can be made. Figure 3.5 shows the circuit diagram of Cp, TSR, and the pitch angle of wind turbines.

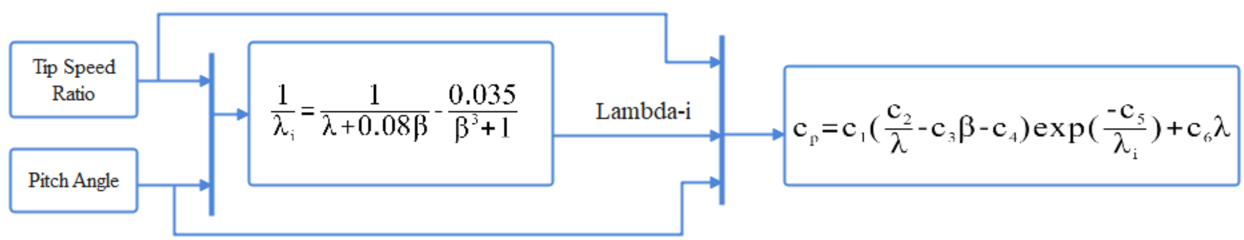

Figure 3. 5 Circuit diagram of Cp, TSR, and the pitch angle of wind turbine

From (3.8), the maximum power is extracted by varying the turbine speed with wind speed in the case of turbine modeling for maximum power tracking. So that it is always on track with the maximum power curve. The optimum power P_{opt} is shown in (3.15) at a pitching angle β =0

$$P_{opt} = \frac{1}{2}\rho\pi R^5 \frac{C_{p\max}}{\lambda_{opt}}(\beta = 0, \lambda_{opt})\omega_m^3 \qquad (3.15)$$

The mechanical torque τ_m can be determined from the optimal power extracted P_{opt} and rotor speed ω_m in (3.16)

$$\tau_m = \frac{P_{opt}}{\omega_m} \tag{3.16}$$

In (3.16) it can be determined that the performance of the wind turbine torque is highly dependent on the wind speed (Tiwari & Babu, 2016). Figure 3.6 shows the overall circuit diagram of wind turbine modeling.

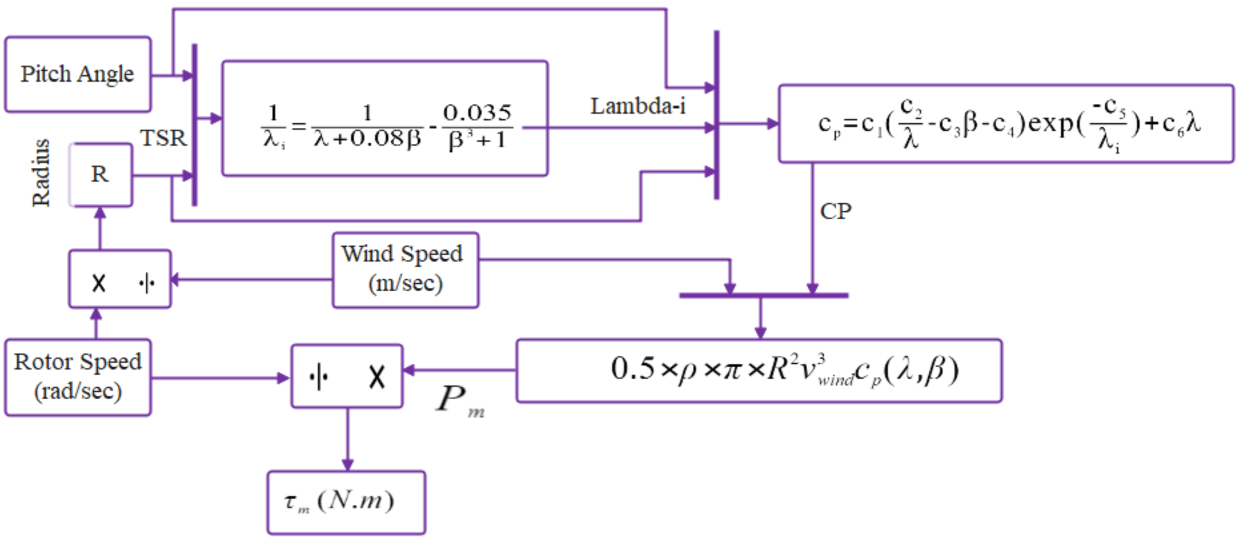

Figure 3. 6 Overall circuit diagram of wind turbine modeling

3.2.3 Mass Drive Train Mathematical Modeling

A drive train is a portion of the wind turbine that transmits torque from the low-speed shaft to the high-speed shaft. The drive train consists of a rotor, a low-speed shaft, a gearbox, a high-speed shaft, and a generator. The drive-train system is modeled as several discrete masses connected by springs and defined by damping and stiffness coefficients. There are four types of drive-train models: Six-mass drive train models, three-mass drive train models, two-mass drive train models, and a single-mass or lumped drive train model are available. The mechanical shaft system of the wind turbine generator can usually be represented either by two masses or by a single mass or lumped parameter (Asri et al., 2015). In this thesis, the turbine rotor is modeled as a lumped mass without consideration of the shaft dynamics. The complexity of the drive train varies depending on the study and interests. Consequently, two-mass or more complex models are needed (Sánchez & Rios, 2016; Tripathi et al., 2015). However, for the sake of time efficiency and acceptable precision, the drive train can be treated as a one-lumped mass model if the study is focused on the integration of a WT into the power utility grids (Bisoyi et al., 2013). Therefore, a lumped-mass drive train is considered in this thesis work, and hence it will be briefly discussed further. Figure 3.7 shows the lumped-mass drive train.

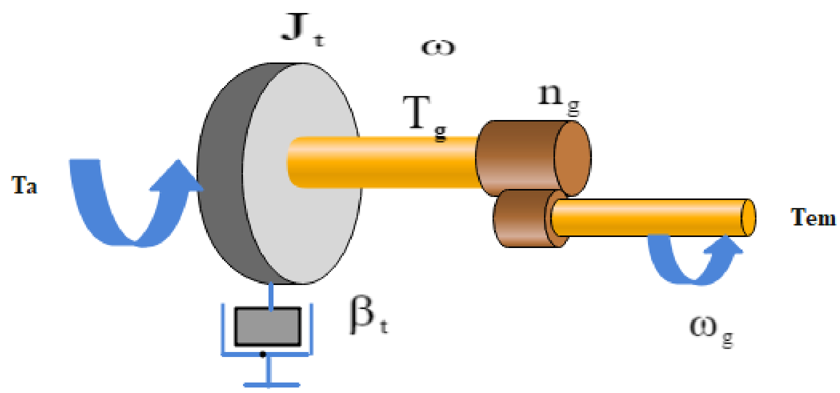

Figure 3. 7 Lumped-mass drive train

The dynamic equation of this model is given by:

$$B_t = B_a + B_g n_g^2 \tag{3.17}$$

Where: B_t is the total damping coefficient, B_a is the low-speed shaft damping, B_g is the high-speed shaft damping coefficient, and n_g is the gear ratio.

The total inertia of the permanent magnet synchronous generator and rotor of the turbine is given in (3.18)

$$J_t = J_{wt} + \frac{J_g}{n_g} \tag{3.18}$$

Where: J_t is the total inertia, J_{wt} and J_g is the rotor wind turbine and the generator inertia, respectively.

The equation motion of the permanent magnet synchronous generator rotor is based on newton's second law of rotation

$$J_t \frac{d\omega_g}{dt} = T_a - B_t \omega_g - T_g \tag{3.19}$$

The mechanical shaft torque T_g can be modeled with the following based on Figure 3.7.

$$\frac{d\omega_g}{dt} = -\frac{B_t}{J_t}\omega_g + \frac{n_g}{J_t}T_a - \frac{n_g^2}{J_t}T_g \tag{3.20}$$

Figure 3.8 shows the circuit diagram of the single mass drive train model.

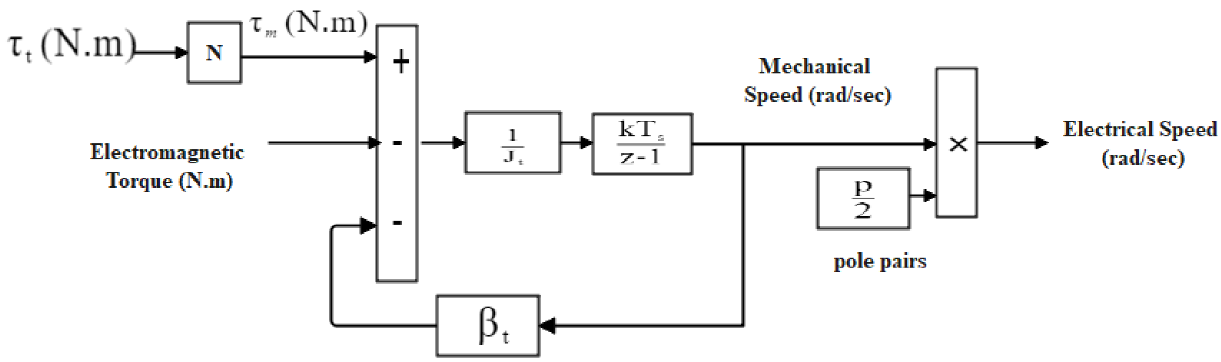

Figure 3. 8 Circuit diagram of a single mass drive train model

Where: J_t is the total inertia mass, ω_g is the angular speed of the wind turbine, B_t is the total damping coefficient, T_g is input mechanical shaft torque delivered to the generator, T_a is wind turbine output torque, T_{em} is electromagnetic torque, and T_m is mechanical driving torque.

The gear ratio connects the mechanical driving torque and the shaft torque. Because a single mass drive train has a gear ratio of one in this thesis, the mechanical driving torque equals the mechanical shaft torque.

3.2.4 Permanent Magnet Synchronous Generator Modeling

Permanent magnet synchronous generators (PMSGs) play a key role in direct-drive wind power generation systems for transforming mechanical power into electrical power.

This section develops the mathematical model of a PMSG and gives the power and torque analysis of PMSGs in both the natural abc three-phase stationary reference frame and the DQ synchronously rotating reference frame.

3.2.4.1 The natural abc 3-phase Stationary Reference Frame of PMSG Modeling

Several crucial presumptions must be established before developing the mathematical model of the PMSG, including the following:

- ❖ The damping effects in the magnets and rotor are negligible.
- ❖ The effects of magnetic saturation are neglected.
- ❖ The hysteresis and eddy current losses are neglected.

Mathematical modeling of the permanent magnet synchronous generator (PMSG) is important for preparing the simulation model of the system.

Dynamic modeling of the permanent magnet synchronous machine is derived from the stator voltage equation of the machine in its natural abc three-phase stationary reference frame (3.21) (Y. Errami et al., 2016; Hailemariam et al., 2019).

$$\begin{bmatrix} v_{as} \\ v_{bs} \\ v_{cs} \end{bmatrix} = \begin{bmatrix} R_s & 0 & 0 \\ 0 & R_s & 0 \\ 0 & 0 & R_s \end{bmatrix} \begin{bmatrix} i_{as} \\ i_{bs} \\ i_{cs} \end{bmatrix} + \frac{d}{dt} \begin{bmatrix} \lambda_{as} \\ \lambda_{bs} \\ \lambda_{cs} \end{bmatrix} \tag{3.21}$$

Where: R_s is the per phase resistance of the stator winding in (Ω), v_{as}, v_{bs}, v_{cs} and i_{as}, i_{bs}, i_{cs} are the instantaneous per phase stator voltages and currents in (V) and (A) and $\lambda_{as}, \lambda_{bs}, \lambda_{cs}$ are the instantaneous flux linkages induced by the three-phase AC currents in (weber).

And the expression for the instantaneous flux linkage is given in (3.22) (Hailemariam et al., 2019).

$$\begin{bmatrix} \lambda_{as} \\ \lambda_{bs} \\ \lambda_{cs} \end{bmatrix} = \begin{bmatrix} L_{aa} & L_{ab} & L_{ac} \\ L_{ba} & L_{bb} & L_{bc} \\ L_{ca} & L_{cb} & L_{cc} \end{bmatrix} \begin{bmatrix} i_{as} \\ i_{bs} \\ i_{cs} \end{bmatrix} + \begin{bmatrix} \psi_m \cos(\theta_r) \\ \psi_m \cos(\theta_r - \frac{2\pi}{3} \\ \psi_m \cos(\theta_r - \frac{4\pi}{3}) \end{bmatrix} \tag{3.22}$$

Where: ψ_m is flux linkages of the rotor caused by a permanent magnet, and L is the inductance of the stator winding. This means $L_{aa}, L_{bb}, and L_{cc}$ are self-inductances of a, b, and c three phases and $L_{ab}, L_{ac}, L_{bc}, L_{ca}, and\ L_{cb}$ are mutual inductance between these phases. All self and mutual inductances are the functions of θ_r . Thus, all the inductances are time-varying parameters.

3.2.4.2 The DQ-axes Synchronously Rotating Reference Frame Modeling of the PMSG

The park's transformation is a mathematical transformation that is used to simplify the analysis of synchronous machine models and was first introduced by R. H. Park in 1929 (Bunjongjit & Kumsuwan, 2013; Hailemariam et al., 2019). In the 3-phase systems like PMSGs, the phase quantities which include stator voltages, stator currents, and flux linkages, are time-varying quantities. The AC quantities are converted into DC quantities that are independent of time by using Park's transformation, which is essentially the projection of the phase quantities onto a rotating two axes reference frame. The abc-dq0 transformation as a matrix in (3.23).

$$\begin{bmatrix} v_{ds} \\ v_{qs} \\ v_{0s} \end{bmatrix} = \sqrt{\frac{2}{3}} \begin{bmatrix} \cos(\theta_r) & \cos(\theta_r - \frac{2\pi}{3}) & \cos(\theta_r - \frac{4\pi}{3}) \\ -\sin(\theta_r) & -\sin(\theta_r - \frac{2\pi}{3}) & -\sin(\theta_r - \frac{4\pi}{3}) \\ \frac{\sqrt{2}}{2} & \frac{\sqrt{2}}{2} & \frac{\sqrt{2}}{2} \end{bmatrix} \begin{bmatrix} v_{as} \\ v_{bs} \\ v_{cs} \end{bmatrix} \quad (3.23)$$

The inverse of Park's transformation is:

$$\begin{bmatrix} v_{as} \\ v_{bs} \\ v_{cs} \end{bmatrix} = \sqrt{\frac{2}{3}} \begin{bmatrix} \cos(\theta_r) & -\sin(\theta_r) & \frac{\sqrt{2}}{2} \\ \cos(\theta_r - \frac{2\pi}{3}) & -\sin(\theta_r - \frac{2\pi}{3}) & \frac{\sqrt{2}}{2} \\ \cos(\theta_r - \frac{4\pi}{3}) & -\sin(\theta_r - \frac{4\pi}{3}) & \frac{\sqrt{2}}{2} \end{bmatrix} \begin{bmatrix} v_{ds} \\ v_{qs} \\ v_{0s} \end{bmatrix} \quad (3.24)$$

Clark transformation is applied in (3.21) and (3.22) to transform the terminal voltage of the machine from its natural three-phase coordinate a-b-c to its equivalent α-β-0 stationary reference frame as shown in (3.25).

$$v^s = Ri^s + L\frac{di^s}{dt} + \psi_m \omega_e \begin{bmatrix} -\sin\theta_r \\ \cos\theta_r \end{bmatrix} \quad (3.25)$$

No zero-sequence voltages and currents exist in a three-phase, three-wire system because in this case, the PMSG, so that v_0 and i_0 can be eliminated from the equation. After, considering that under the balanced conditions the voltage function of the PMSG in the DQ-axes reference frame can be expressed as follows.

Determined the expression for stator terminal voltage of salient pole PMSG with L_d and L_q inductance in the dq0 rotating frame, applied again Park transformation in (3.26).

$$\begin{aligned} v_d &= Ri_d + L_d\frac{di_d}{dt} - L_q i_q \omega_e \\ v_q &= Ri_q + L_q\frac{di_q}{dt} + L_d i_d \omega_e + \psi_m \omega_e \end{aligned} \quad (3.26)$$

Where: v_d and v_q, are the stator voltages in the DQ-axes reference frame i_d and i_q, are the stator currents in the DQ-axes reference frame. Here, L_d and L_q, are the D-axis and Q-axis inductances, and ω_e is the angular speed of the generator, while ψ_m is the maximum flux linkage due to the rotor-mounted PMs. According to expressions (3.26) the equivalent circuits of the PMSG in the DQ-axes reference frame can be drawn as shown in Figure 3.9 and Figure 3.10. Figure 3.11 shows the response of the DQ-axis stator current of PMSG.

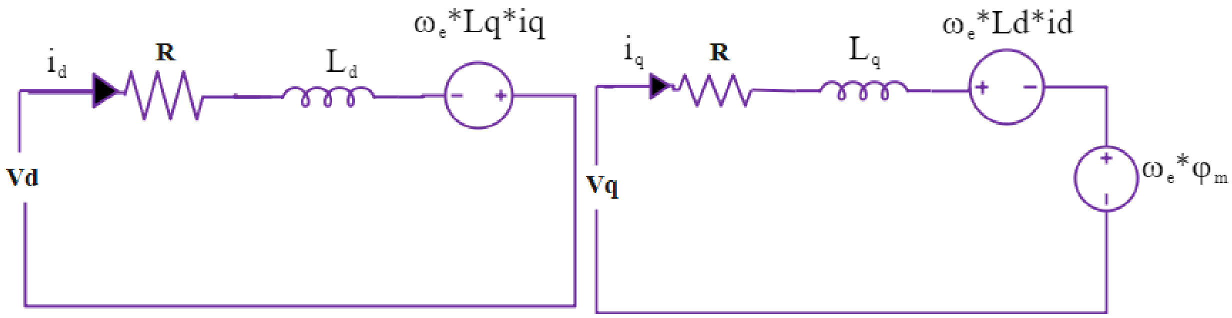

Figure 3. 9 DQ-axis equivalent circuits of a PMSG

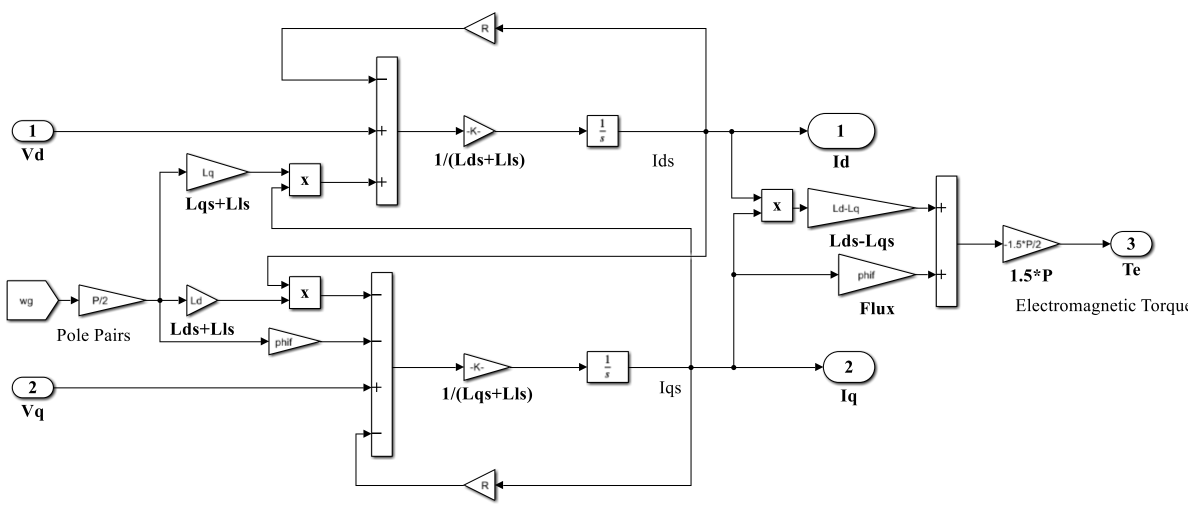

Figure 3. 10 DQ-axis equivalent circuits of a PMSG using MATLAB

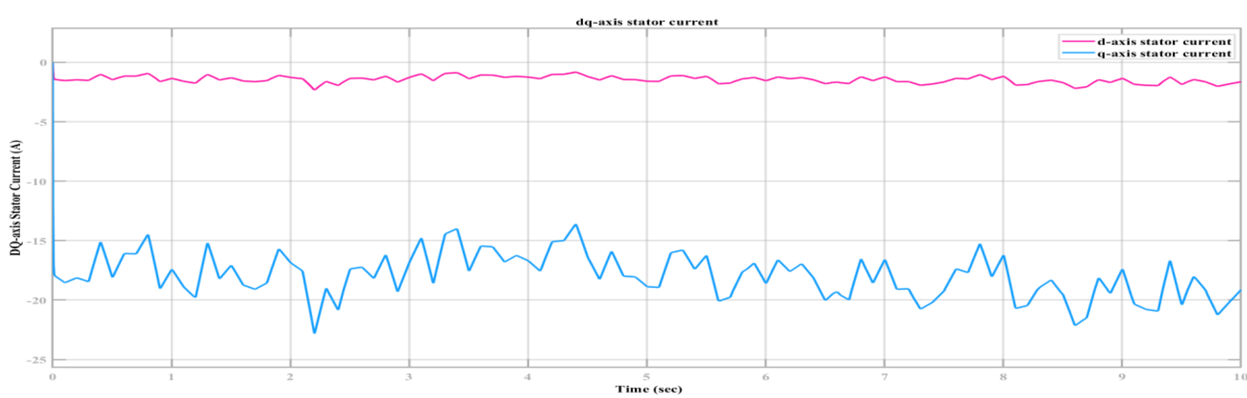

Figure 3. 11 DQ-axes stator currents

For clarity, all PMSM equations are expressed in motor (consumer/load) notation; that is, when the model refers to a generator, a negative current will prevail. A negative current means that at the positive polarity of the terminal of a device, the current is out of that terminal. The simulated graph in Figure 3.11 shows the output direct quadrature stator currents, both are negative, and so this PMSM is the generator. And it shows that power is flowing from the generator to the grid.

3.2.4.3 Power and torque of a PMSG

For any PMSG, the electrical power input can be expressed in the ABC reference frame as follows:

$$P_{abc} = v_a i_a + v_b i_b + v_c i_c \tag{3.27}$$

or in the DQ-axes reference frame as follows:

$$P_{dq} = \frac{3}{2}(v_d i_d + v_q i_q) \tag{3.28}$$

As a part of the input power, in the motoring mode, the active power is the power that is transformed into mechanical power by the machine, which can be represented in (3.29)

$$P_{em} = \frac{3}{2}(e_d i_d + e_q i_q) \tag{3.29}$$

The back emf of the PMSG can be expressed in (3.30)

$$\begin{aligned} e_d &= -\omega_e L_q i_q = -\omega_e \lambda_q \\ e_q &= \omega_e L_d i_d + \omega_e \lambda_r = -\omega_e \lambda_d \end{aligned} \tag{3.30}$$

Where: e_d and e_q are the back emf in the DQ-axes reference frame λ_d and λ_q are the DQ-axes flux linkages. Substituting (3.30) into (3.29), the active power can be obtained in (3.31) and electrical rotating speed (rad/sec) can be re-expressed in (3.31).

$$\begin{aligned} P_{em} &= \frac{3}{2}\omega_e(\lambda_d i_q - \lambda_q i_d) \\ \omega_e &= \frac{p}{2}\omega_g \end{aligned} \tag{3.31}$$

Where, p is the number of poles in the machine, and ω_g the rotor's mechanical rotational speed. Here, the electromagnetic torque developed by a PMSG can be deduced in (3.32) from (3.30) and (3.31).

$$T_e = \frac{P_{em}}{\omega_g} = \frac{3p}{4}(\lambda_d i_q - \lambda_q i_d) = \frac{3p}{4}(\lambda_r i_q + (L_d - L_q) i_q i_d) \tag{3.32}$$

For non-salient pole and low speed, surface mounted PMSGs, $L_d \approx L_q$. As a result, the electromagnetic torque is given in (3.33)

$$T_e = 1.5(\frac{p}{2})\lambda_r i_q \quad (3.33)$$

Where, T_e is the electromagnetic torque of PMSG given in (3.33). Figure 3.12 shows the circuit diagram of the PMSG model.

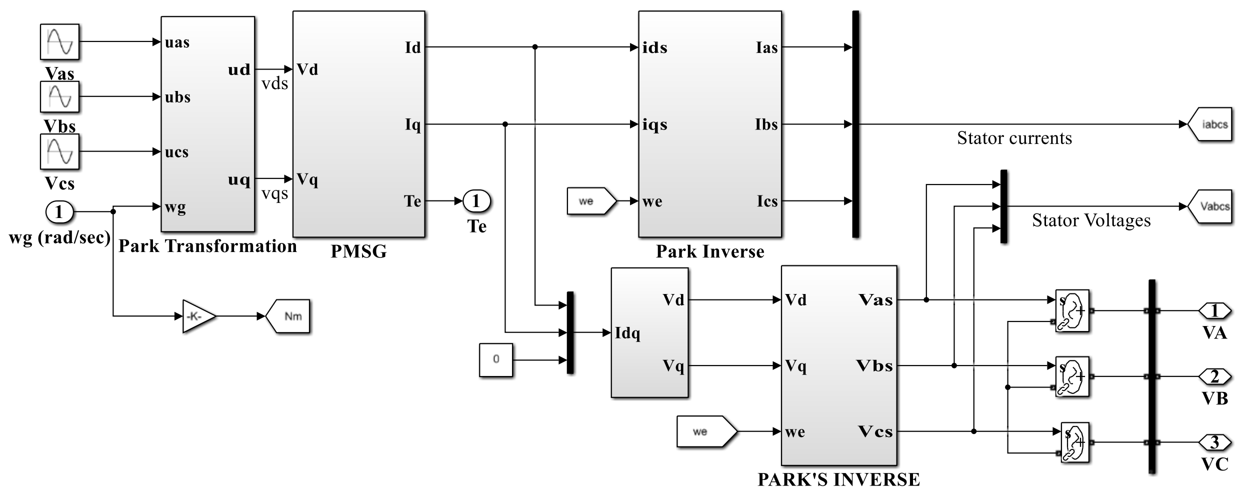

Figure 3. 12 Circuit diagram of permanent magnet synchronous generator model

3.2.5 Power Converters

Power electronics is the application of solid-state electronics to the control and conversion of electric power. The type of input and output power can be used to categorize power conversion systems. Based on their input and output power, three (3) different types of power converters are used in this thesis. These are DC to DC (boost converters), AC to DC (rectifiers), and DC to AC converters (Inverter).

3.2.5.1 AC to DC Converters (Uncontrolled Rectifiers) Modeling

The diode rectifier (uncontrolled rectifier) is used in this work for converting the three-phase output AC voltage at the terminals of the PMSG into a DC voltage. An uncontrolled rectifier gives a fixed DC output voltage for a given AC supply. It is then important to be able to model accurately the behavior of these converters to study their influence on the input currents waveforms and their interactions with the loads (classically inverters and AC-motors) (Hailemariam et al., 2019; Ma et al., 2015). The instantaneous (desired) output voltage of the permanent magnet synchronous generator can be expressed as:

$$v_{an} = v_m \cos(\omega_r t)$$
$$v_{bn} = v_m \cos(\omega_r t - 120^o) \quad (3.34)$$
$$v_{cn} = v_m \cos(\omega_r t + 120^o)$$

Where: v_m is the peak value of phase voltage and $\omega_r t$ is the rotor angular position of PMSG.

The rectified output DC voltage V_{dcrec} from a three-phase diode rectifier is given in (3.35)

$$V_{dcrec} = \frac{1}{\pi/3} \int_{-\pi/6}^{\pi/6} \sqrt{6} V_{L-L} \cos(wt) dwt = \frac{3\sqrt{2}}{\pi} V_{L-L_{rms}} \quad (3.35)$$

Where: V_{L-L} is the value of the line-to-line voltage applied to the rectifier and $V_{L-L_{rms}}$ is the RMS of the line-to-line value of voltage. Inductances Li and L characterize the line and output inductances, respectively. The variable topology approach serves as the foundation for modeling AC-DC converters. The circuit diagram for a three-phase diode rectifier is shown in Figure 3.13.

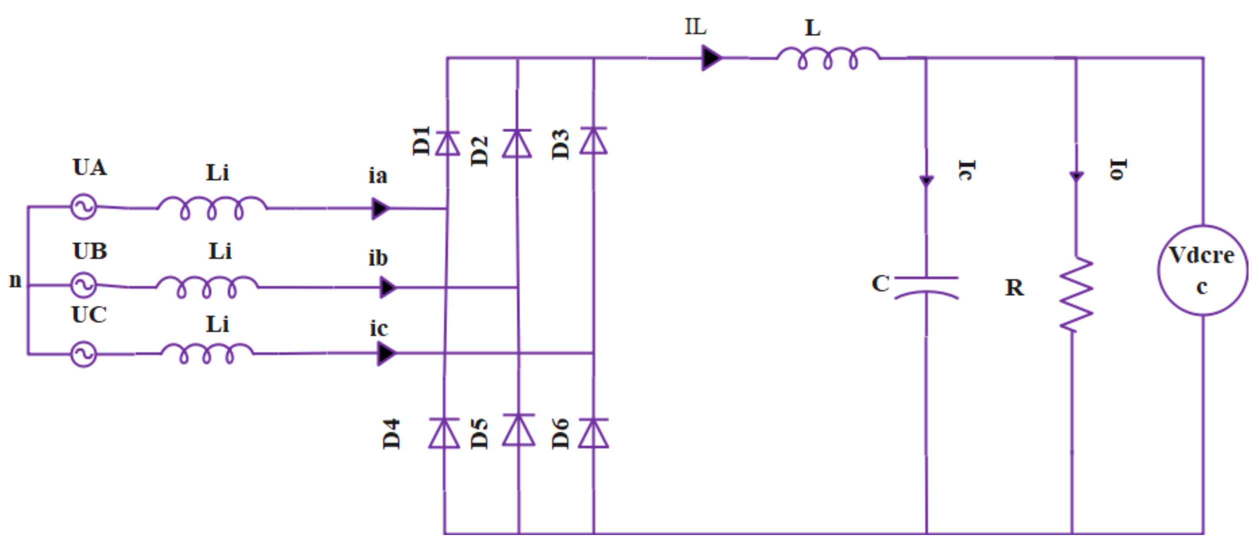

Figure 3. 13 Three-phase AC-DC converters

The rectified output from the diode rectifier is uncontrolled but it does not have any additional losses owing to the switching of any power electronic components. It can, therefore, be assumed that the total power obtained from PMSG is converted from AC to DC if the diode losses are negligible.

Filter design for the 3-phase rectifier.

The inductor value and capacitor value can be gained through the (3.36) and (3.38), respectively.

For 6 pulse rectifiers

$$L = \frac{0.013V_{L-L}(\max)}{2\pi * f * I_{cri}} \tag{3.36}$$

The ripple frequency and cutoff frequency can be expressed as (3.37)

$$f_r = 6f$$

$$\frac{\Delta V_{dcrec}}{\Delta V_r} = \left(\frac{f_c}{f_r}\right)^2 \tag{3.37}$$

$$C = \frac{1}{4\pi^2 f_c^2 L} \tag{3.38}$$

Where: ΔV_{dcrec} is a ripple in the output voltage, ΔV is a ripple in the unfiltered rectified voltage, f_c is cutoff frequency, f_r is ripple frequency, $V_{L-L}(\max)$ is the maximum line to line voltage, f is line frequency in Hz, I_{cri} is up to this current, there will be continuous conductions. As a result of not having pure DC power, there are so many ripples that adding a filter to remove undesirable ripples from the DC power is required.

3.2.5.2 DC-DC Converters Modeling

The DC-DC converters are generally used to obtain an average output voltage above or below the input voltage. In this thesis, the DC-DC converters are used as interfacing units to obtain a matching voltage from both wind systems. Depending on the output voltage level, the three most used topologies are a buck, boost, and buck-boost converters (Y. S. Kim et al., 2015). Amongst of three types of DC-DC converters for this thesis the boost converter is selected.

- ❖ **Boost converter**

The standard unidirectional topology of the DC-DC boost converter (also known as the step-up converter) consists of a switching-mode power device with two energy storage devices (an inductor and a smoothing capacitor) for producing an output DC voltage at a level greater than its input DC voltage.

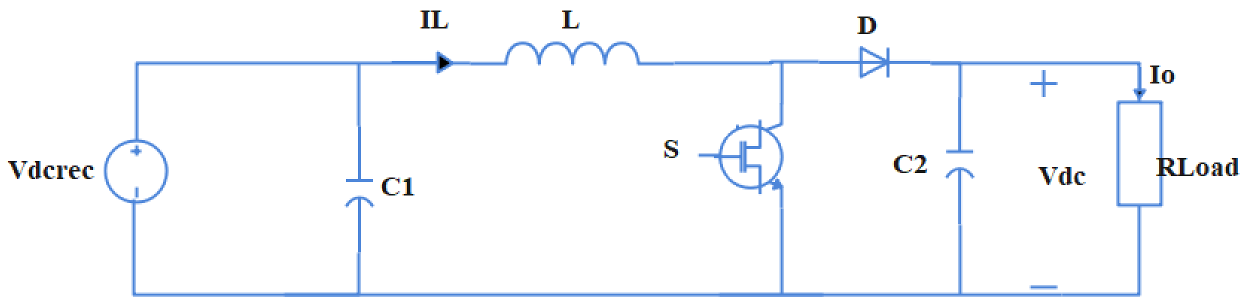

Figure 3. 14 Boost (step-up) converter

This converter serves as a bridge between the full-wave rectifier bridge and the inverter VSI (Hailemariam et al., 2019).

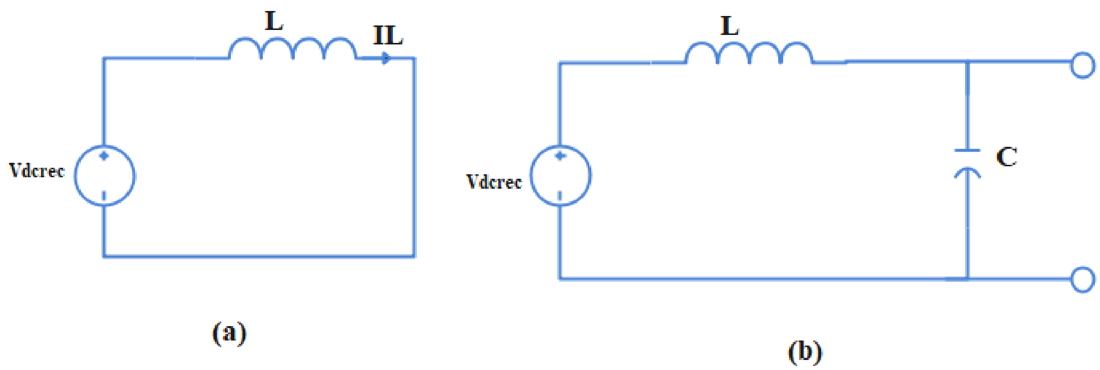

Figure 3. 15 Boost converter when a) switch on, b) switch off

By using pulse-width modulation (PWM) control methods.

The working mode when the switch is closed or switched on is in Figure 3.15 (a). The state equations are

$$\begin{aligned} L\frac{di_L}{dt} &= v_{dcrec} - v_c \\ C\frac{dv_c}{dt} &= i_L - \frac{v_c}{R_L} \end{aligned} \tag{3.39}$$

Where i_L denotes the current of an inductor, which equals to i_{in}, v_c denotes the voltage of the capacitor, which equals to v_{dc}. Let state variable $x_1 = i_L(i_{in}), x_2 = v_c(v_{dc})$, we can rewrite the state equations in state space

$$\begin{bmatrix} \dot{x}_1 \\ \dot{x}_2 \end{bmatrix} = \begin{bmatrix} 0 & 0 \\ 0 & \dfrac{-1}{RC} \end{bmatrix} \begin{bmatrix} x_1 \\ x_2 \end{bmatrix} + \begin{bmatrix} \dfrac{1}{L} \\ 0 \end{bmatrix} v_{dcrec} \quad \text{i.e.,} \quad \dot{x} = A_1 x + B_1 u \tag{3.40}$$

When the switch is open, the simplified circuit is shown in Figure 3.15 (b). The state equations become

$$L\frac{di_L}{dt} = v_{in} - v_c \qquad (3.41)$$
$$C\frac{dv_c}{dt} = i_L - \frac{v_c}{R}$$

In state space representation, the equations are

$$\begin{bmatrix} \dot{x}_1 \\ \dot{x}_2 \end{bmatrix} = \begin{bmatrix} 0 & \frac{-1}{L} \\ \frac{1}{C} & \frac{-1}{RC} \end{bmatrix} \begin{bmatrix} x_1 \\ x_2 \end{bmatrix} + \begin{bmatrix} \frac{1}{L} \\ 0 \end{bmatrix} v_{dcrec},\ \dot{x} = A_2 x + B_2 u \qquad (3.42)$$

Then the average state space model is:

$$\dot{x} = \bar{A}x + \bar{B}u \qquad (3.43)$$

Where: $\bar{A} = A_1 d + A_2(1-d)$ and $\bar{B} = B_1 d + B_2(1-d)$.

Averaging the state space matrix of two different working modes using (3.43), we can get the average model in (3.44)

$$\begin{bmatrix} \dot{x}_1 \\ \dot{x}_2 \end{bmatrix} = \begin{bmatrix} 0 & \frac{-(1-d)}{L} \\ \frac{(1-d)}{C} & \frac{-1}{RC} \end{bmatrix} \begin{bmatrix} x_1 \\ x_2 \end{bmatrix} + \begin{bmatrix} \frac{1}{L} \\ 0 \end{bmatrix} v_{dcrec} \qquad (3.44)$$

In steady-state CCM operation and neglecting parasitic components, the state-space equation that describes the dynamics of the DC-DC boost converter is given by (3.45)

$$\begin{bmatrix} \dot{i}_L \\ \dot{v}_{dc} \end{bmatrix} = \begin{bmatrix} 0 & \frac{-(1-d)}{L} \\ \frac{(1-d)}{C} & \frac{-1}{RC} \end{bmatrix} \begin{bmatrix} i_L \\ v_{dc} \end{bmatrix} + \begin{bmatrix} \frac{1}{L} & 0 \\ 0 & -\frac{1}{C} \end{bmatrix} \begin{bmatrix} v_{dcrec} \\ i_d \end{bmatrix} \qquad (3.45)$$
$$d = \frac{T_{on}}{T_{on} + T_{off}} = \frac{T_{on}}{T}$$

Since, in steady-state conditions, the inductor current variation during both, on and off times of S are essentially equal, there is not a net change of the inductor current from cycle to cycle, and assuming a constant DC output voltage of the boost converter, the steady-state input-to-output voltage conversion relationship of the boost converter is easily derived from (3.45) by setting the inductor current derivative at zero, yielding (3.46)

$$v_{dc} = \frac{v_{dcrec}}{1-d} \tag{3.46}$$

In the same way, the between the average inductor current and the DC-DC converter output current in the CCM can be derived in (3.47)

$$i_{dc} = (1-d)i_L \tag{3.47}$$

So, (3.45) can be re-written as (3.48)

$$\begin{bmatrix} \dot{x}_1 \\ \dot{x}_2 \end{bmatrix} = \begin{bmatrix} 0 & \frac{-(1-d)}{L} \\ \frac{(1-d)}{C} & \frac{-1}{RC} \end{bmatrix} \begin{bmatrix} x_1 \\ x_2 \end{bmatrix} + \begin{bmatrix} \frac{1}{L} & 0 \\ 0 & -\frac{1}{C} \end{bmatrix} [u] \tag{3.48}$$

The boost converter requires a larger inductor (L) and output filter capacitor (C) as compared to the buck converter, but the input current can be kept continuous by properly choosing the inductor and capacitor.

Why DC-DC boost converter is needed, because of two reasons:

First, the PMSGs have low voltages (typically it is about 250V, while the converter needs 575V/690V). So, to step up the output voltage generates through PMSG, a DC-DC boost converter is needed. i.e., 250V to 575V/690V.

Second, the power generates is sensitive to wind speed and load variance. So, to stabilize these varied output currents and voltages again this boost converter is needed. It stabilizes the output voltage and rejects the disturbance from wind speed and external load variations (resistance step). Protect the system from wind speed and external load variations (reverse currents, sudden load variations).

❖ **Calculation of Inductance**

The minimum critical inductance value needed to ensure the converter operates in CCM can be calculated in (3.50) or (3.51). Duty cycle and ripple current input are given in (3.49) for finding the inductance value

$$d = 1 - \frac{v_{dcrec}}{v_{dc}}, \ \Delta i_{in} = \frac{v_{dcrec} * d}{f * L} \tag{3.49}$$

$$L = \frac{v_{dc} - v_{dcrec}}{2P} \frac{v_{dcrec}^2}{v_{dc}} T_s \tag{3.50}$$

$$L = \frac{v_{dcrec} * d}{\Delta i_{in} * f} \tag{3.51}$$

Calculation of Capacitance

For calculating the capacitance value, which is on the side of a low voltage, firstly, define and find the ripple voltage output, and ripple current input in (3.52) and (3.53), respectively.

$$\Delta v_c = \frac{\Delta i_L}{8C_1 * f_s} \tag{3.52}$$

$$\Delta i_L = \frac{v_{dc} - v_{dcrec}}{2L} \frac{v_{dcrec}}{v_{dcrec} * f_s} \tag{3.53}$$

Then,

$$C_1 = \frac{\Delta i_L}{8\Delta v_{dcrec}} \tag{3.54}$$

$$\Delta v_{dc} = \frac{I_{dc}(v_{dc} - v_{dcrec})}{f_s C_2 v_{dc}} \tag{3.55}$$

Hence,

$$C_2 = \frac{I_{dc} * d}{\Delta v_{dc} f_s} \tag{3.56}$$

Calculation of Resistance (load)

$$R_L = \frac{v_{dc}}{I_{dc}} \tag{3.57}$$

Where: Δv_{dc} is output ripple voltage, Δi_L inductor ripple current, P is the maximum power rating, f_s switching frequency, and R_L load resistance.

3.2.5.3 Inverters (DC-AC) modeling

Power electronic converters called inverters are used to convert a DC input voltage to an AC output at a particular frequency. In this thesis, the DC link voltage acquired at the output of a DC-DC converter is converted to a three-phase AC voltage so that it can be fed to an AC load using a three-phase Voltage Source Inverter (VSI). Figure 3.16 shows the schematic diagram of a three-phase voltage source inverter circuit. The switches used are usually Metal-Oxide-Semiconductor Field-Effect Transistors (MOSFETs) or Insulated Gate Bipolar Transistors (IGBTs) and their switching signals are generally obtained using a suitable Pulse-Width Modulation (PWM) technique (Deng et al., 2017)

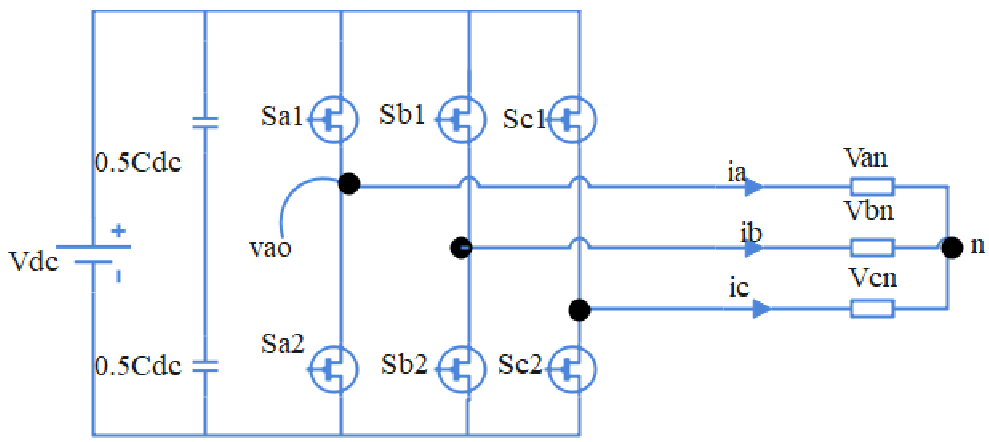

Figure 3. 16 Three-phase inverter

This three-level VSI topology generates a more smoothly sinusoidal output voltage waveform than conventional two-level structures without increasing the switching frequency and effectively doubles the power rating of the VSI for a given semiconductor device. In this way, the harmonic performance of the inverter is improved, also obtaining better efficiency and reliability.

The inverter output voltages are expressed as follows:

$$v_{ao} = \begin{cases} \frac{v_{dc}}{2}, & s_a = 1 \\ -\frac{v_{dc}}{2}, & s_a = 0 \end{cases} \Rightarrow v_{ao} = s_a \frac{v_{dc}}{2}$$
$$v_{bo} = \begin{cases} \frac{v_{dc}}{2}, & s_b = 1 \\ -\frac{v_{dc}}{2}, & s_b = 0 \end{cases} \Rightarrow v_{bo} = s_b \frac{v_{dc}}{2} \quad (3.58)$$
$$v_{co} = \begin{cases} \frac{v_{dc}}{2}, & s_c = 1 \\ -\frac{v_{dc}}{2}, & s_c = 0 \end{cases} \Rightarrow v_{co} = s_c \frac{v_{dc}}{2}$$

Where Sa, Sb, and Sc are the switching states of the upper inverter switches, which are “1” for on-state and “0” for off-state. Vdc is the instantaneous capacitor voltages.

For balanced supply voltages and equal interfacing inductances, the active power filter voltages concerning the neutral point of the supply are defined as the sum of all the voltage between phase and neutral is zero.

$$v_{an} + v_{bn} + v_{cn} = 0 \quad (3.59)$$

$$\begin{cases} v_{oa} + v_{an} = v_{on} \\ v_{ob} + v_{bn} = v_{on} \\ v_{oc} + v_{cn} = v_{on} \end{cases} \Rightarrow \begin{cases} -v_{ao} + v_{an} = v_{on} \\ -v_{bo} + v_{bn} = v_{on} \\ -v_{co} + v_{cn} = v_{on} \end{cases} \tag{3.60}$$

From (3.59) and (3.60), the phase-to-neutral voltages are as follows:

$$\begin{cases} v_{an} = -\frac{1}{3}(v_{ao} + v_{bo} + v_{co}) + v_{ao} \\ v_{bn} = -\frac{1}{3}(v_{ao} + v_{bo} + v_{co}) + v_{bo} \\ v_{cn} = -\frac{1}{3}(v_{ao} + v_{bo} + v_{co}) + v_{co} \end{cases} \Rightarrow \begin{cases} \frac{2}{3}v_{ao} - \frac{1}{3}v_{bo} - \frac{1}{3}v_{co} \\ -\frac{1}{3}v_{ao} + \frac{2}{3}v_{bo} - \frac{1}{3}v_{co} \\ -\frac{1}{3}v_{ao} - \frac{1}{3}v_{bo} + \frac{2}{3}v_{co} \end{cases} \tag{3.61}$$

$$\begin{bmatrix} v_{an} \\ v_{bn} \\ v_{cn} \end{bmatrix} = \begin{bmatrix} \frac{2}{3} & -\frac{1}{3} & -\frac{1}{3} \\ -\frac{1}{3} & \frac{2}{3} & -\frac{1}{3} \\ -\frac{1}{3} & -\frac{1}{3} & \frac{2}{3} \end{bmatrix} \begin{bmatrix} v_{ao} \\ v_{bo} \\ v_{co} \end{bmatrix} \tag{3.62}$$

By substituting (3.58) into (3.62), the phase-to-neutral voltages can be obtained as follows

$$\begin{bmatrix} v_{an} \\ v_{bn} \\ v_{cn} \end{bmatrix} = \begin{bmatrix} \frac{2}{3} & -\frac{1}{3} & -\frac{1}{3} \\ -\frac{1}{3} & \frac{2}{3} & -\frac{1}{3} \\ -\frac{1}{3} & -\frac{1}{3} & \frac{2}{3} \end{bmatrix} \begin{bmatrix} s_a \frac{v_{dc}}{2} \\ s_b \frac{v_{dc}}{2} \\ s_c \frac{v_{dc}}{2} \end{bmatrix} \tag{3.63}$$

$$\begin{bmatrix} v_{an} \\ v_{bn} \\ v_{cn} \end{bmatrix} = \frac{1}{3}\frac{v_{dc}}{2} \begin{bmatrix} 2 & -1 & -1 \\ -\frac{1}{3} & 2 & -1 \\ -1 & -1 & 2 \end{bmatrix} \begin{bmatrix} s_a \\ s_b \\ s_c \end{bmatrix} \tag{3.64}$$

For this thesis, a simplified equivalent VSI, also known as an averaged model, connected to the electrical system is taken into consideration. This model assumes that the VSI is a perfect sinusoidal voltage source operating at the fundamental frequency and that the inverter's operation under balanced conditions is ideal. At the point of common coupling, the net instantaneous output voltages resemble three sinusoidal waveforms that are phase-shifted by 120 degrees from one another. The ideal inverter is shunt-connected to the grid at the phase common coupling through an equivalent inverter inductance (L_s) that accounts for the leakage of the step-up coupling transformer and an equivalent series resistance R_s that represents the transformer winding resistance and conduction losses in VSI semiconductors.

In contrast to the switching losses of the VSI and power losses in the DC capacitors, which are taken into account by a parallel resistance R_p, the equivalent capacitance of the two DC bus capacitors, c_{d1} and c_{d2} is described $c_d = \frac{c_{d1}}{2} = \frac{c_{d2}}{2}$ on the DC side.

By using Kirchhoff's voltage law (KVL), it is possible to immediately determine the state space equation models representing the current exchanged with the utility grid and the instantaneous values of the three-phase output voltages on the ac side of the VSI in (3.65).

$$\begin{bmatrix} v_{inva} \\ v_{invb} \\ v_{invc} \end{bmatrix} - \begin{bmatrix} v_a \\ v_b \\ v_c \end{bmatrix} = (R_s + sL_s) \begin{bmatrix} i_a \\ i_b \\ i_c \end{bmatrix} \quad (3.65)$$

$$R_s = \begin{bmatrix} R_s & 0 & 0 \\ 0 & R_s & 0 \\ 0 & 0 & R_s \end{bmatrix}, and\ L_s = \begin{bmatrix} L_s & M & M \\ M & L_s & M \\ M & M & L_s \end{bmatrix} \quad (3.66)$$

Under the assumption that the system has no zero sequence components, all currents and voltages can be uniquely transformed into the synchronous-rotating orthogonal two-axes reference frame DQ components, instead of its three abc components. Thus, the new coordinate system is defined with the d-axis always aligned with the instantaneous voltage vector, as described in Figure 3.17. By defining the d-axis to be always aligned with the instantaneous voltage vector v, yields v_d equal |v|, while v_q is null. As a result, the instantaneous active power is contributed to by the d-axis current component, whereas the instantaneous reactive power is represented by the q-axis current component. With the help of this process, a simpler and more accurate dynamic model of the inverter may be developed.

By applying Park's transformation state, which is in (3.67) and the (3.65) and (3.66) can be transformed into the synchronous rotating d-q reference frame and is shown in (3.68) for current phase and voltage phases

$$k_s = \frac{2}{3} \begin{bmatrix} \cos(\theta) & \cos(\theta - \frac{2\pi}{3}) & \cos(\theta + \frac{2\pi}{3}) \\ -\sin(\theta) & -\sin(\theta - \frac{2\pi}{3}) & -\sin(\theta + \frac{2\pi}{3}) \\ \frac{1}{2} & \frac{1}{2} & \frac{1}{2} \end{bmatrix} \quad (3.67)$$

With $\theta = \int_0^t \omega(t)dt + \theta(0)$ the angle between the D-axis and the reference phase axis, t is the integration variable, and ω the synchronous angular speed of the network voltage at the fundamental system frequency f (50 Hz).

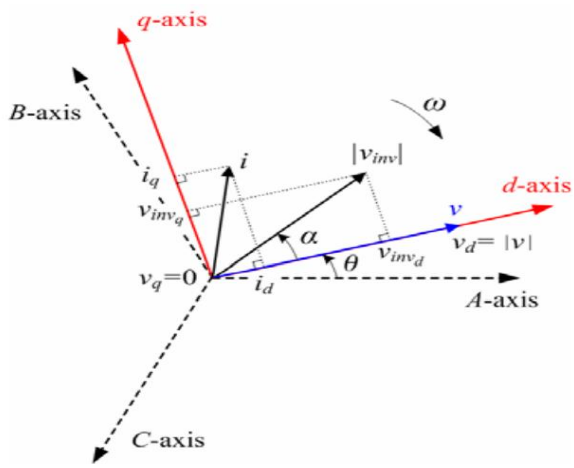

Figure 3. 17 VSI vectors in the synchronous rotating dq reference frame

$$\begin{bmatrix} v_{invd} - v_{d1} \\ v_{invq} - v_{q1} \\ v_{inv0} - v_0 \end{bmatrix} = K_s \begin{bmatrix} v_{inva} \\ v_{invb} \\ v_{invc} \end{bmatrix} - \begin{bmatrix} v_a \\ v_b \\ v_c \end{bmatrix}, \begin{bmatrix} i_d \\ i_q \\ i_0 \end{bmatrix} = K_s \begin{bmatrix} i_a \\ i_b \\ i_c \end{bmatrix} \tag{3.68}$$

Since all currents and voltages have no zero sequence components, by neglecting the zero sequence components from the (3.68) can obtain the (3.69)

$$\begin{bmatrix} v_{invd} - v_{d1} \\ v_{invq} - v_{q1} \end{bmatrix} = (R_f + sL_f) \begin{bmatrix} i_d \\ i_q \end{bmatrix} + L_f \begin{bmatrix} -\omega & 0 \\ 0 & \omega \end{bmatrix} \begin{bmatrix} i_d \\ i_q \end{bmatrix} \tag{3.69}$$

$$R_f = \begin{bmatrix} R_s & 0 \\ 0 & R_s \end{bmatrix}, L_f = \begin{bmatrix} L_f & 0 \\ 0 & L_f \end{bmatrix} \Rightarrow \begin{bmatrix} L_s - M & 0 \\ 0 & L_s - M \end{bmatrix} \tag{3.70}$$

It should be observed that when the VSI transformers are magnetically symmetric, the coupling of phases through the term M in the matrix in (3.70), was eliminated in the DQ reference frame. This synchronous-rotating system's phase decoupling allows for a more simplified control system design (Noman et al., 2021; Yüksel et al., 2013). By rewriting (3.69) can be obtained (3.71)

$$\begin{aligned} L_f \frac{di_d}{dt} &= -R_f i_d + \omega L_f i_q + v_{invd} - |v| \\ L_f \frac{di_q}{dt} &= -R_f i_q - \omega L_f i_d + v_{invq} \end{aligned} \tag{3.71}$$

Where: L_f and R_f are the inductance of filter inductor and resistance of filter resistor, v_{invq} and v_{invd} are the inverted d-axis and q-axis voltage components, respectively.

The relationship between the DC-side voltage v_{dc} and the generated AC side voltage v_{invd} can be represented through the average switching function matrix in the DQ-reference frame s_{dq} of the VSI inverter given in (3.72). This relation assumes that the DC capacitors' voltages are balanced and equal to $\frac{v_{dc}}{2}$.

$$\begin{bmatrix} v_{invd} \\ v_{invq} \end{bmatrix} = s_{dq} v_{dc} \tag{3.72}$$

and the average switching function matrix in dq coordinates is represented as

$$s_{dq} = \begin{bmatrix} s_d \\ s_q \end{bmatrix} = \frac{1}{2} ma \begin{bmatrix} \sin(\alpha) \\ \cos(\alpha) \end{bmatrix} \tag{3.73}$$

Where: m is the modulation index of the voltage source inverter $m \in [0,1]$, α is the phase-shift of the inverter output voltage from the reference position, and a is the turns ratio of the step-up $\Delta - Y$ coupling transformer, $a = \frac{\sqrt{3}n_2}{\sqrt{2}n_1}$.

A power balance must exist between the inverter's input and output because of the immediate relationship between the AC power exchanged by the inverter and the DC-link power (Berhanu et al., 2018). This will ensure that the AC power is equal to the sum of the DC resistance R_p power, representing losses (IGBTs switching and DC capacitors), and the rate of charging of the DC equivalent capacitor c_d (neglecting the wind generator action)

$$\begin{aligned} P_{ac} &= P_{dc} \\ \frac{3}{2}(v_{invd} i_d + v_{invq} i_q) &= -\frac{c_d v_{dc}}{2} \frac{dv_{dc}}{dt} - \frac{v_{dc}^2}{R_p} \end{aligned} \tag{3.75}$$

In general, starting from (3.66) up to (3.75) are done for inverters, that is modeling static inverters by using a synchronous-rotating orthogonal DQ-axes reference frame offers higher accuracy than employing stationary coordinates. Moreover, this operation permits designing a simpler control system than using abc or α-β.

It can be summarized in the state-space representation as described in (3.76)

$$\frac{di_d}{dt} = -\frac{R_f}{L_f} i_d + \omega i_q + \frac{s_d}{2L_f} v_{dc} - \frac{|v|}{L_f}$$
$$\frac{di_q}{dt} = -\omega i_d - \frac{R_f}{L_f} i_q + \frac{s_q}{2L_f} v_{dc} \tag{3.76}$$
$$\frac{dv_{dc}}{dt} = -\frac{3s_d}{2c_d} i_d - \frac{3s_q}{2c_d} i_q - \frac{2}{R_p c_d} v_{dc}$$

As it was described, the d-axis was defined as always aligned with the instantaneous voltage vector v, then v_d, results in a steady-state equal to $|v|$, while $v_q$is null. In addition to the VSI converter model, a grid filter model is required. Obtaining pure alternating current power is difficult. A modeling filter is so necessary.

3.2.6 Grid Filter Model

The grid-connected inverters' control method has a significant impact on renewable energy sources. The grid filter modeling is crucial for understanding the grid-side operation performance of the grid-connected wind turbine generator. IGBT and Gate Turn-off Thyristor (GTO) are fully regulated power electronic devices that are modulated by high-frequency PWM.

This filter aims to decrease the current and voltage harmonics produced by the converter's switching (Berhanu et al., 2018). Due to the consistently huge changes in voltage and current.

By inducing high-order harmonic flow current into the power grid, some presence of vagrant parameters produced harmonic pollution. It is impossible to obtain pure or smooth AC power from an inverter output; the harmonics produced by the power electronic converters are the reason we were unable to obtain pure AC power. This problem will raise the question of why a filter is required. A filter is required to solve this problem (Giallanza et al., 2017). The grid connected to the inverter is where an inductor filter is most frequently used. The inductance needs to be raised to reduce the current ripple. Although the LC filter's structure and parameters are simple, the network impedance unpredictability causes the filtering effect to be poor. LCL filters had a naturally high cut-off frequency and good low-frequency penetration. LCL filter is now widely used in inverters. However, the parameter and control resonance are the problems. The LCL filter was chosen for this thesis because it offers several advantages over the other filters. The structure of the LCL filter is shown in Figure 3.18, and the single-phase LCL filter circuit diagram can be shown in Figure 3.19.

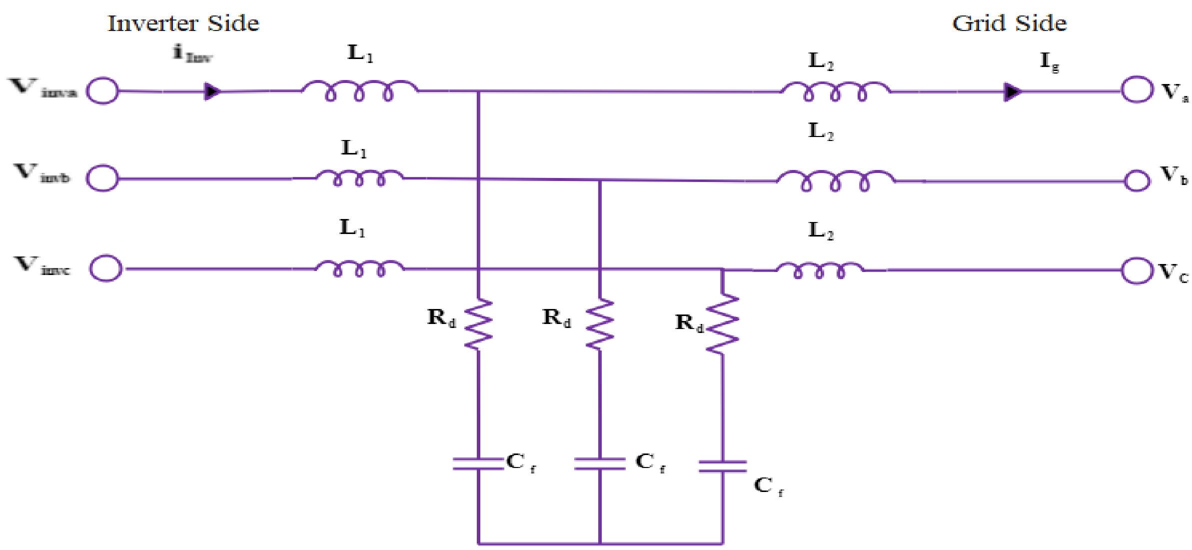

Figure 3. 18 Structure of LCL filter

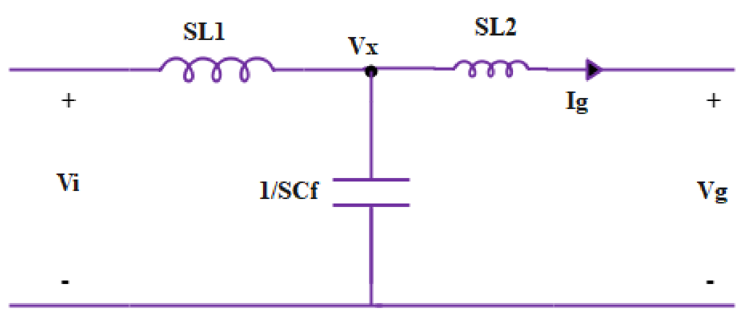

Figure 3. 19 Single-phase LCL filter

By applying Kirchhoff's voltage law (KVL) in Figure 3.19, you can obtain the following (3.77) and (3.78)

$$\frac{v_i - v_x}{sL_1} = I_g + \frac{v_x}{1/sC_f} \tag{3.77}$$

$$v_x = I_g sL_2 \tag{3.78}$$

Rearranging and substituting (3.78) into (3.77), it can be expressed by following transfer functions (3.79)

$$\frac{I_g(s)}{v_i(s)} = \frac{1}{s^3 L_1 L_2 C_f + s(L_1 + L_2)} \tag{3.79}$$

Let, $L = L_1 + L_2$ and $L_p = \frac{L_1 L_2}{L_1 + L_2}$ so that substituting into (3.79), the following (3.80) is obtained

$$\frac{I_g(s)}{v_i(s)} = \frac{1}{sL(1+s^2C_fL_p)} \tag{3.80}$$

3.2.6.1 Filter Design

Current ripple, switching frequency, and resonant frequency are elements that must be considered when designing LCL filters. The capacitor's interaction with the grid may resonate due to the reactive power requirements. For passive or active dampening, a series resistor is added to the capacitor. We can use the following procedures to design the grid filter: Choosing switching and resonant frequencies, find the filter's capacitance value:

The choice of the capacitor is mostly determined by the reactive power the capacitor provides at the fundamental frequency. Reactive power is chosen during design as 15% of the rated power is provided by (3.82).

$$Q = \frac{v_g^2}{1/2\pi fC_f} \tag{3.81}$$

Where: $2\pi f C_f v_g^2 = 15\%$ of rated power (Prated)

$$C_f = \frac{0.15P_{rated}}{6\pi f v_g^2} \tag{3.82}$$

Finding the value of the inductance: To get the value of inductance, substituting the resonant and switching frequency into (3.77), we can obtain (3.83) and (3.84).

Where: $\omega_{res} = \frac{1}{\sqrt{C_f L_P}}$ and $s = j\omega_{sw}$ resonant frequency and switching frequency, respectively.

$$\frac{I_g(j\omega_{sw})}{v_i(j\omega_{sw})} = \frac{1}{j\omega_{sw}L(1+\frac{(j\omega_{sw})^2}{\omega_{res}^2})} \tag{3.83}$$

From this, possible to get the inductance value of the filter so that it is shown below on (3.84)

$$L = \left| \frac{1}{\omega_{sw}\frac{I_g(\omega_{sw})}{v_i(\omega_{sw})}(1-\frac{(\omega_{sw})^2}{\omega_{res}^2})} \right| \tag{3.84}$$

Thus, $I_g(\omega_{sw})$ is equal to 0.3% of grid current I_g and $v_i(\omega_{sw})$ is equal to 0.9 times v_g. Due to the LCL filter having resonance, some order harmonic current that comes from the grid-connected inverters may increase frequently. For this case, adding the damping resistance into the filter to suppress the resonances. Generally, it is a resistor.

This damping resistance is expressed by (3.85)

$$R_d = \frac{1}{(3\omega_{res} C_f)} \tag{3.85}$$

So, differential equations of the grid-connected to LCL the filter in the DQ rotating reference frame can be written as (3.86), (3.87), and (3.88) by adding damping resistance on the circuit series with capacitance of the filter to suppress the resonances

$$\begin{aligned} L_1 \frac{di_d}{dt} &= v_{invd} - v_{d1} - R_d i_d + L_1 \omega i_q + R_d i_{d1} \\ L_1 \frac{di_q}{dt} &= v_{invq} - v_{q1} - R_d i_q - L_1 \omega i_d + R_d i_{q1} \end{aligned} \tag{3.86}$$

$$\begin{aligned} L_2 \frac{di_{d1}}{dt} &= v_{d1} - v_{d2} - R_d i_{d1} + L_2 \omega i_{q1} + R_d i_d \\ L_2 \frac{di_{q1}}{dt} &= v_{q1} - v_{q2} - R_d i_{d1} - L_2 \omega i_{d1} + R_d i_q \end{aligned} \tag{3.87}$$

$$\begin{aligned} C_f \frac{dv_{d1}}{dt} &= i_d - i_{d1} + \omega C_f v_{q1} \\ C_f \frac{dv_{q1}}{dt} &= i_q - i_{q1} - \omega C_f v_{d1} \end{aligned} \tag{3.88}$$

Where: v_{invd} and v_{invq} is inverted D-axis and Q-axis voltage components, i_d and i_q is inverted D-axis and Q-axis current components, $L_1$and $L_2$is inverter side and grid side inductance, C_f is filter capacitor, ω is the angular frequency of the filter, v_{d2} and v_{q2} is D-axis and Q-axis voltage components, $i_{d1}$and i_{q1} is D-axis and Q-axis current components, and $R_d$is damping resistance.

Next to this grid filter model, the model of the phase-locked loop and the design of its controller is needed. Unless voltage on the q-axis is not zero. For this reason, to obtain synchronized voltage, you should have to design the controller for the PLL.

3.2.7 Phase Locked Loop (PLL) Model

A Phase Locked Loop (PLL) is used for synchronizing through the phase θ_s, the pulses generated for the 3-ϕ inverter. The block diagram of PLL can be shown in Figure 3.20.

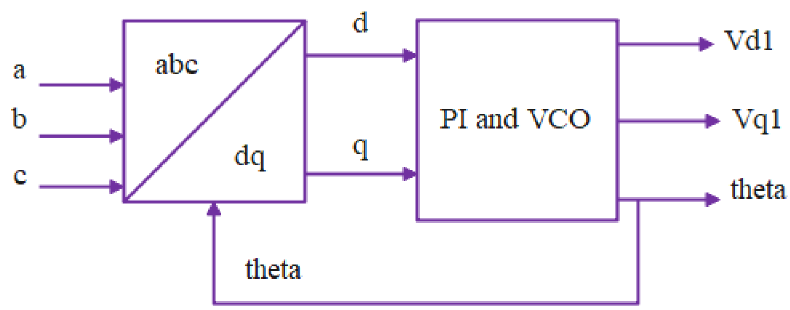

Figure 3. 20 Phase Locked Loop (PLL) block diagram

It consists of a proportional-integral (PI) controller and a voltage-controlled oscillator (VCO). The following are the primary elements of a PLL:

A voltage-controlled oscillator generates the output signal, whose frequency varies around a central frequency depending on the output of the loop filter after a phase detector generates an error signal by comparing the input signal with the output signal. A loop filter then removes unwanted harmonics terms from the error signal. The Phase Locked Loop is configured to synchronize the d-axis of the rotation reference frame with phase A. Thus, the voltage vector Phase Common Coupling (PCC) is θ_s= 0. Input signals for PLL are DQ components of the PCC voltage. The PI controller is used to obtain $v_q = 0$ and the output angle theta. The PLL output is the angle used to obtain the transformation of DQ the PCC voltage v_d and v_q. When it becomes zero, the D-axis voltage has reached its maximum phase voltage value. Figure 3.21 shows the circuit diagram of a DQ-PLL.

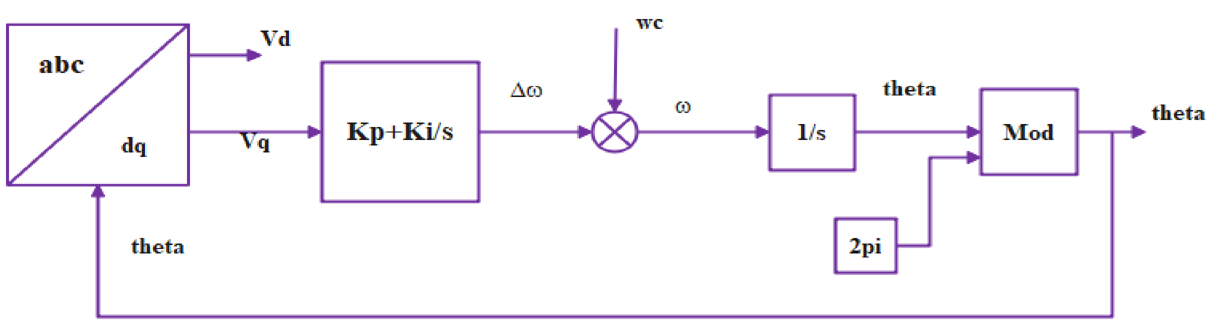

Figure 3. 21 Structure of a DQ-PLL

The AC voltage vector's positive sequence components, as measured at the inverter's PCC, are used to generate the phase signal. The q-axis component will be driven to zero by the controller. Synchronizing the phase with the phase voltage's peaks. The PI controller is the one that is used. The actuation signal, which is the controller's output, is added to the center frequency. The output of the sum is the angular frequency in radians and is integrated to obtain the angle θ_s. The output of the integrator and the constant 2π is passed to a modulo operation. The output of the mod block properly wraps the angle θ_s and gains it between 0 and 2π. Figure 3.22 (a) shows the phase angle tracked by the PLL. Figure 3.22 (b) shows the synchronized DQ-axis voltage through the PLL.

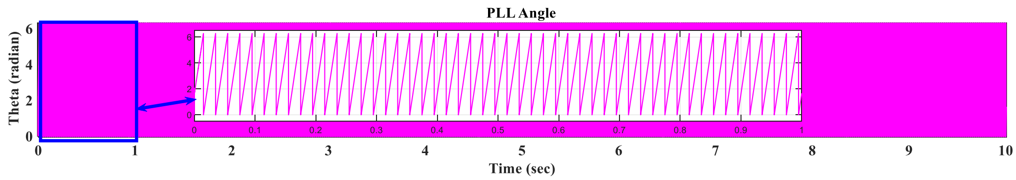

(a)

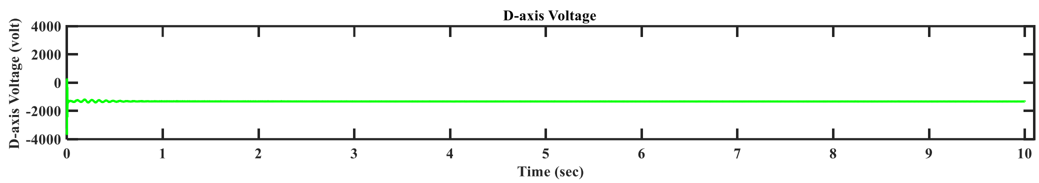

(b)

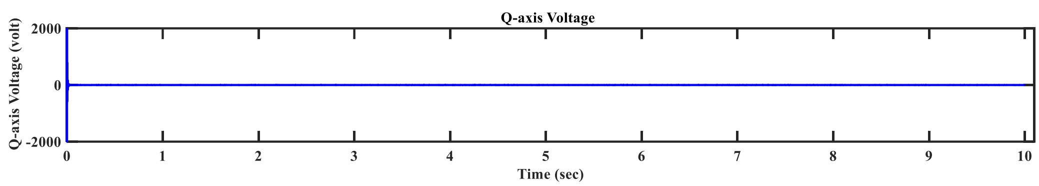

(c)

Figure 3. 22 (a) Phase angle tracked by PLL (b) Synchronized D axes voltage (c) Synchronized Q axes voltage

3.2.8 DC-Link Model

The DC side of the back-to-back converter is commonly called the DC link. It stores a certain amount of energy in the capacitors. Power flow through a DC link from the permanent magnet synchronous generator to the power grid is shown in Figure 3.23. Where: C_{vdc} is the capacitance of the DC link capacitor, P_s and P_m are by the active powers from the stator of PMSG and the machine side converter, respectively. P_{dc}, P_g, and P_f are the active power flow into the DC-link capacitor, the grid side converter, and the filter respectively. The active power transferred from the PMSG to the grid can be described as follows, assuming that the power losses in the MSC, the GSC, the filter, and the transformer can be neglected:

$$P_s = \frac{3}{2}(-v_{ds}i_{ds} - v_{qs}i_{qs}) = P_m$$
$$P_{dc} = v_{dc}i_{dc} = v_{dc} * c_{vdc}\frac{dv_{dc}}{dt} = P_m - P_g \tag{3.89}$$
$$P_g = P_f = P_{out}$$
$$P_g = \frac{3}{2}(v_{d1}i_d + v_{q1}i_q)$$

So, in a PMSG wind turbine integrated into a grid, the real power flow through the converters and DC link is balanced. Neglecting losses, the net real power can be given as:

$$P_s + P_{dc} + P_g \tag{3.90}$$

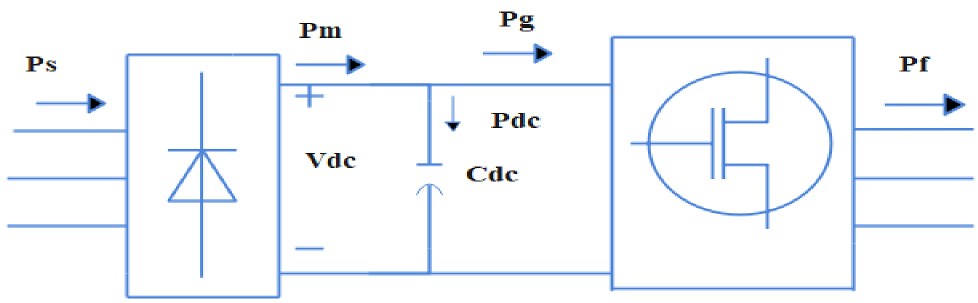

Figure 3. 23 DC bus power flow

Finally, the model of the DC-link can be given as follows:

$$c_{vdc}\frac{dv_{dc}}{dt} = \frac{3}{2}(\frac{v_{d1}}{v_{dc}}i_d + \frac{v_{q1}}{v_{dc}}i_q) - i_{dc} \tag{3.91}$$

Where: v_{dc} and i_{dc} are the DC bus voltage and the DC bus current, respectively, i_d and $i_q$are the D-axis current and Q-axis current of the inverters, respectively, v_{d1} and v_{q1} are the D-axis output voltage and Q-axis output voltage of grid filters respectively. The Q-axis output voltage of the grid is null, which is gained by the PLL.

The coupling transformer and transmission line that connects the PMSG wind energy conversion system to the grid. Figure 3.24 shows the coupling transformer, transmission line, and grid single-line diagram. Where x_T and $x_L$are the transformer and transmission line reactance, respectively. The respective resistances are neglected. v_{dq2} is the grid voltage. The terminal voltage of the filter is considered as the reference, and δ is the angle of the grid voltage from v_{dq1}.

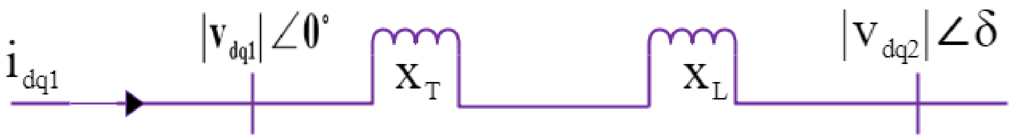

Figure 3. 24 One-phase line diagrams of the grid, the transmission line, and the transformer.

You can describe the current flowing from the wind turbine to the grid as,

$$i_{dq1} = \frac{|v_{dq1}|\sin 0 - |v_{dq2}|\sin\delta}{x_T + x_L} + j\frac{|v_{dq1}|\cos 0 - |v_{dq2}|\cos\delta}{x_T + x_L} \tag{3.92}$$

For the unity power factor, the current and the terminal voltage of the filter are in phase. As a result, the current's real and imaginary components can be represented as

$$\begin{aligned} i_{d1} &= \frac{-|v_{dq2}|\sin\delta}{x_T + x_L} \\ i_{dq1} &= \frac{-|v_{dq1}| + |v_{dq2}|\cos\delta}{x_T + x_L} \end{aligned} \tag{3.93}$$

3.2.9 Power Flow Control

Power flow control is the ability to change the way that power flow through the grid by actuating line switching hardware or by controlling high voltage devices connected in series or shunt with transmission lines. Power flow control can regulate the flow of both active and reactive power. To regulate both, it is critical to first assess the controllability of power converters and then select the right power converters. This means that electricity flows bidirectionally, from the grid to the generator or from the generator to the grid. Therefore, using the grid synchronous voltage orientation technique, (3.94) and (3.95) show that the d-axis current component of the voltage source inverter contributes to the instantaneous active power p and the q-axis current component represents the instantaneous reactive power q (3.96) and (3.97). To achieve a decoupled active and reactive power control, it is important to provide a decoupled control mechanism (Berhanu et al., 2018; Chai et al., 2021).

$$p = \frac{3}{2}\left(v_{d1}i_d + v_{q1}i_q\right) = \frac{3}{2}|v|\,i_d \tag{3.94}$$

$$q = \frac{3}{2}\left(v_{q1}i_d - v_{d1}i_q\right) = -\frac{3}{2}|v|\,i_q \tag{3.95}$$

Therefore, according to (3.71), (3.94), and (3.95), p and q are defined as the control variables, then, the power control model can be expressed as follow

$$\frac{3}{2}v_{d1} * v_{invd} = R_f p + L_1 \frac{dp}{dt} - \omega L_1 q + \frac{3}{2}v_{d1}^2 \quad (3.96)$$

$$\frac{3}{2}v_{d1} * v_{invq} = R_f q + L_1 \frac{dq}{dt} + \omega L_1 p \quad (3.97)$$

Thus, to provide decoupled control of active power and reactive power, the output power from the grid side converter in the synchronous reference frame could be formulated as

$$\frac{3}{2}v_{d1} * v_{invd} = p_0 - \omega L_1 q + \frac{3}{2}v_{d1}^2 \quad (3.98)$$

$$\frac{3}{2}v_{d1} * v_{invq} = p_o + \omega * L_1 p \quad (3.99)$$

The p_0 and q_0 is given in (3.100) and (3.101), respectively

$$R_f p + L_1 \frac{dp}{dt} = p_0 \quad (3.100)$$

$$R_f q + L_1 \frac{dq}{dt} = q_0 \quad (3.101)$$

Where p is the rated active power, q is the rated reactive power, v_{d1} is the d-component output voltage of the filter, v_{invd} is the d-axis inverter voltage, v_{invq} is the q-axis inverter voltage, R_f damping resistance of the filter, and L_1 is the inductor filter inside of the inverter.

A control system for power flow and DC link voltage can be constructed using the modeled filter as a framework. First of all, before we go to designing the controller, the things we need to do to test its controllability and stability. In the design of the control system these are required.

3.3 Controllability

A control system's ability to be controlled is a key component of many control issues, including stabilizing unstable systems through feedback and achieving optimal control. The capacity to move a system through the complete configuration space using only a limited number of permitted actions is generally referred to as controllability.

3.3.1 Controllability Test

To check and test the system controllability, finding the equation matrix is one criterion. Therefore, obtaining the state space representation matrix is the problem for determining whether the system is controllable or not. Find the system's determinants based on the state space variables matrix. The system is controllable if it has a full row rank and a non-zero determinant, and if it does, it will have linearly independent columns. If the columns are linearly independent, each of the states is reachable by providing the system with the appropriate inputs through the variable. The state matrix or the pair (A, B) state is controllable if and only if the n × nm state controllability matrix $U_c = [B{:}\,AB{:}\,A^2B{:}\ldots{:}\,A^{n-1}B]$ has rank n, i.e., full row rank.

3.3.1.1 DC-DC Boost Converter Controllability Test

To test the controllability of the DC-DC boost converter, in the first stage, getting the matrix equation is much more necessary. After that, in the given state space (3.48) put the constant values for all variables and get (3.102).

$$\begin{bmatrix} \dot{x}_1 \\ \dot{x}_2 \end{bmatrix} = \begin{bmatrix} 0 & -0.072 \\ 95.61 & -548.23 \end{bmatrix} \begin{bmatrix} x_1 \\ x_2 \end{bmatrix} + \begin{bmatrix} 0.132 & 0 \\ 0 & -175.44 \end{bmatrix} [u] \tag{3.102}$$

Where: $\bar{A} = \begin{bmatrix} 0 & -0.072 \\ 95.61 & -13.4953 \end{bmatrix}, \bar{B} = \begin{bmatrix} 0.132 & 0 \\ 0 & -175.44 \end{bmatrix}$

$$\dot{x} = \bar{A}x + \bar{B}u \tag{3.103}$$

The controllable matrix can be obtained in (3.104) $U_c = \left[\bar{B} : \bar{A}\bar{B} \right]$.

$$U_c = 1.0e+03 * \begin{bmatrix} 0.0001 & 0 & 0 & 0.0013 \\ 0 & -0.0175 & 0.0013 & 2.3676 \end{bmatrix} \tag{3.104}$$

From this, it concluded, that the controllable matrix has rank 2 and it has a determinant of 6.8531, because of this the system is controllable. And, the matrix has a determinant positive singular value, so the system is controllable and stable. The rank of the controllable matrix must match the number of rows in matrix A to determine if the system is controllable or not, and the determinant must not be singular or zero. The system is controllable since it fully satisfies the controllability test's criteria.

3.3.1.2 Inverter Converter Controllability Test

To test the controllability of the DC-AC converter, in the first stage you can get the controllable matrix and check the conditions of the controllable test. The state space representation of the DC-AC converter was given in (3.76), from this can find the state space representation matrix of the given equation, finally, the state space matrix can be obtained in (3.105).

$$\begin{bmatrix} \dot{i}_d \\ \dot{i}_q \\ \dot{v}_{dc} \end{bmatrix} = \begin{bmatrix} \frac{R_f}{L_f} & \omega & \frac{s_d}{2L_f} \\ -\omega & -\frac{R_f}{L_f} & \frac{s_q}{2L_f} \\ -\frac{3s_d}{2c_d} & -\frac{3s_q}{2c_d} & -\frac{2}{R_p c_d} \end{bmatrix} \begin{bmatrix} i_d \\ i_q \\ v_{dc} \end{bmatrix} - \begin{bmatrix} \frac{|v|}{L_f} \\ 0 \\ 0 \end{bmatrix} \tag{3.105}$$

To achieve the controllable matrix, substitute the constant values into the above state matrix and you will get the state variables A and B on (3.106) after that use the formula which is given in (3.107), and you can get the controllable matrix

$$A = 1.0e + 04 * \begin{bmatrix} -1.003 & 0.0314 & 0.1977 \\ -0.0314 & -1.003 & 0.0437 \\ -0.0449 & -0.0099 & -0.1258 \end{bmatrix}, B = 1.0e4 \begin{bmatrix} 1.3197 \\ 0 \\ 0 \end{bmatrix} \tag{3.106}$$

$$U_c = \left[A : AB : A^2 B \right] \tag{3.107}$$

The below matrix is the controllable matrix, which is obtained after substituting the constant values in (3.106).

$$U_c = 1.0e + 12 * \begin{bmatrix} 0.0000 & -0.0001 & 1.3146 \\ 0 & 0.0000 & 0.0806 \\ 0 & -0.0000 & 0.0674 \end{bmatrix} \tag{3.108}$$

So, by applying the conditions of controllable criteria, this state matrix model has rank 3 and it has a determinant of 2.6213e+21. Then, the rank is equal to the number of row matrix A and the controllable matrix has the determinant non-singular or non-zero. Because all conditions of controllability were full filled, the DC-AC converter is controllable.

3.4 Stability

Stability is one of the control system properties like controllability and observability. As the controllability of the system is tested, the system must be a bounded output with a bounded input. Due to this, the control system's stability is determined by its capability of providing a bounded output in response to a bounded input. To explain it more precisely, we can say that stability enables the system to reach a steady state and maintain it for that specific input even when the system's parameters change.

3.4.1 Stability Test

Before testing the stability of the system, based on the equilibrium states of the system, this thesis can be determined the types of stability. The capacity of a power system's interconnected PMSG to remain synchronized when subjected to small disturbances is referred to as small signal stability. Variations in load and generations are good examples. So, testing the stability of the system is mandatory. The linear time-invariant is given by (3.109)

$$\begin{aligned} \dot{x}(t) &= Ax(t) + Bu(t) \\ y(t) &= Cx(t) + Dx(t) \end{aligned} \qquad 3.109)$$

3.4.1.1 Eigenvalues Stability Analysis

Furthermore, to analyze, the equilibrium states of the converter system only having a matrix is enough using the eigenvalues of stability analysis. So, the equilibrium state $\tilde{x}$ =0 of (3.110) is

$$\dot{x}(t) = Ax(t) \;\; x(0) = x_0 \qquad (3.110)$$

Stable if and only if all eigenvalues of A have a non-positive real part and the geometric multiplicity of any eigenvalue with zero real part equals the associated algebraic multiplicity. $\text{Re}(\lambda) = 0$, $\text{Re}(\lambda) > 0$, and (globally) asymptotically stable if and only if every eigenvalue of A has a strictly negative real part. If A matrix has strictly negative real-part eigenvalues, then it must be a non-zero/non-singular determinant. Find the characteristics equations of the system when

$$Ax = 0 \qquad (3.112)$$

From (3.118), the eigenvector is expressed as

$$Ax = \lambda x \qquad (3.113)$$

Where: x is an eigenvector, λ is the eigenvalues, and A is the state matrix of the system.
So, from above (3.113), we can get the characteristics equation

$$(A - \lambda I) = 0 \qquad (3.114)$$

$$Det(A - \lambda I) = 0 \qquad (3.115)$$

Because A is a matrix but x is not a matrix so for subtracting from each other identity matrix is multiplied x and subtracted from the A matrix.
This leads to the complex eigenvalues λ of A in the form

$$\lambda = \sigma \pm j\omega \qquad (3.116)$$

The real part represents the damping of the corresponding mode, and the imaginary part represents the frequency (f) of the oscillation given by

$$f = \frac{\omega}{2\pi} \qquad (3.117)$$

The damping ratio of this frequency is given by

$$\xi = \frac{-\sigma}{\sqrt{\sigma^2 + \omega^2}} \qquad (3.118)$$

The parameters ξ and ω in above are used for the stability prediction in this thesis. The following cases are generated:

Case 1: When the system has strictly negative real-part eigenvalues then corresponding to an asymptotically stable system.

Case 2: When it has non-repeated eigenvalues on the imaginary axis since the geometric and algebraic multiplicities are each one, the system is stable.

Case 3: When it has one or more eigenvalues with a positive real part, the system is unstable.

Asymptotic stability is a fundamental property of the system, it is only dependent on matrix A and not on other matrices of B, C, or D.

Suppose that using (3.115), find the eigenvalues and test the stability of the system. In this thesis, to test the stability of the system, we can only focus on the matrix given in (3.102) and (3.105) for the DC-DC boost converter and the DC-AC converter (inverter), respectively.

Firstly, starts with the stability test of a DC-DC boost converter

$$\begin{bmatrix} 0 & -0.072 \\ 95.61 & -13.4953 \end{bmatrix} - \begin{bmatrix} \lambda & 0 \\ 0 & \lambda \end{bmatrix} \tag{3.119}$$

The characteristic polynomial is $\lambda^2 + 13.4953\lambda + 6.8531 = (\lambda + 0.529)(\lambda + 12.97)$ from which the eigenvalues are $\lambda_{1,2} = -0.5285, -12.97$ each of which is real and negative. This system is asymptotically stable and bounded-input, bounded-output stable using eigenvalues stability analysis.

Secondly, testing the stability of a DC-AC converter is observed as the following

$$1.0e+04 * \begin{bmatrix} -1.0030 & 0.0314 & 0.1977 \\ -0.0314 & -1.0030 & 0.0437 \\ -0.0449 & -0.0099 & -0.1258 \end{bmatrix} - \begin{bmatrix} \lambda & 0 & 0 \\ 0 & \lambda & 0 \\ 0 & 0 & \lambda \end{bmatrix} \tag{3.120}$$

The characteristic polynomial is $\lambda^3 + 1370\lambda^2 + 10^8\lambda + 1.37 * 10^{11} = (\lambda + 1370)(\lambda^2 + 10^8)$ from which the eigenvalues are $\lambda_{1,2,3} = -1370, -9980 \pm 312i$ all the eigenvalues are real and negative. It is asymptotically stable, and this system is bounded-input, bounded-output stable means when a constant voltage is applied, the output of DC bus voltage will increase linearly with bound in a steady state of the system.

3.4.1.2 Lyapunov Stability Analysis

Using Lyapunov stability analysis also will get the same results as the eigenvalues stability analysis. The Russian mathematician A.M. Lyapunov (1857-1918) observed that conclusions regarding the stability of the equilibrium state can be drawn from a more general class of energy-like functions. He discovered that the equilibrium state $\tilde{x} = 0$ is stable if the partial derivatives of x ($\dot{v}(x)$) are negative semi-definite; that is, $\dot{v}(x) \leq 0$ for all x and asymptotically stable if $\dot{v}(x)$ is negative definite; that is, $\dot{v}(x) < 0$ for all x=0.

In general, the Lyapunov matrix equation effectively represents $\frac{(n^2+n)}{2}$ equations in as many unknowns because P, Q, and $A^T P + PA$ are each symmetric. For simplicity Q=I so that,

$$A^T P + PA = -Q \tag{3.121}$$

Has a unique positive-definite solution P using Sylvester's criterion to test stability, it is shown in **Appendix B.1** by m-files. The results are 1.0217 and 1.8704 for boost converters, 0.6241*10^-4, 3.1338*10^-9, and 1.9325*10^-8 for inverters. All determinant of P is positive-definite, so the system is asymptotically stable using the Lyapunov stability analysis.

In conclusion, the full-rated power converters' controllability and stability are verified using controllability techniques and stability techniques, respectively. In this thesis, the system's stability is tested using two different forms of stability analysis approaches. Specifically, Lyapunov stability analysis and eigenvalue stability analysis.

3.4.2 Control System Performance Measure

The performance indices are designed to offer a framework for comparing various types of control and solution. The design of the power circuit and control is mostly determined by meeting these performance indices. The response up to the settling time is known as transient response and the response after the settling time is known as steady state response. In this section, we can examine how to increase performance by specifying the requirements.

Delay time is the time required for the response to reach half of its final value from the zero instant. By using linear approximation, you can get the delay time (t_d) as

$$t_d = \frac{1 + 0.7\xi}{\omega_n} \tag{3.122}$$

Rise time is the amount of time it takes for a plant's output to first rise 0% to 100% of the desired level. This is applicable for under-damped systems.

$$t_r = \frac{\pi - \theta}{\omega_d} \quad (3.123)$$

Where ω_d (damping frequency) is equal to $\omega_n \sqrt{1-\xi^2}$ and θ is shift angle.

We can conclude that the rise time and damped frequency are inversely proportional to each other.

Overshoot measures the difference between the peak level and steady state, normalized against the steady state. Mathematically, we can write it as

$$M_p = c(t_p) - c(\infty) \quad (3.124)$$

Then, maximum overshoot can be calculated by

$$\%M_p = \frac{M_p}{c(\infty)} \times 100\%$$
$$\%M_p = \left(e^{-\left(\frac{\xi\pi}{\sqrt{1-\xi^2}}\right)} \right) \times 100\% \quad (3.125)$$

From the Equation, we can conclude that percentage of peak overshoot will decrease if the damping ratio increases.

The amount of time it takes for the system to reach its steady state and stay with the specified tolerance band is known as the **settling time**.

In general, the tolerance bands are 2% and 5%. The settling time of the 5% tolerance band is

$$t_s = \frac{3}{\xi\omega_n} = 3\tau \quad (3.126)$$

Both settling time and time constant are inversely proportional to damping ratio. Both the settling time and time constant are independent of the system gain. Means that even the system gain changes, the settling time and time constant will never change. As a result, the following indices relate to time response and requirements:

- ❖ Settling time ≤ 3 sec
- ❖ Overshoot $\leq 10\%$
- ❖ Rise time ≤ 0.5 sec

These indices must be fulfilled to obtain the desired dynamic responses. After we know and test the controllability and the performance indices. Next to these all, the controller designs of the proposed controller, PI, and FLC can be designed.

3.5 Controller Design

3.5.1 Proportional-Integral Controller Design

3.5.1.1 PI Parameters

Two major categories can be used to study PI controllers. Regarding how it controls the entire system, each controller has unique characteristics. Adjustments in proportional control are made based on the present difference between the desired and actual power and voltage. Adjustments in an integral control are based on the most recent errors.

3.5.1.2 Tuning PI parameters

There are many tuning methods, but the most common methods are as follows:

- Manual tuning method,
- Ziegler-Nicholas tuning method,
- Cohen-Coon tuning method, and
- PI tuning software methods (ex. MATLAB).

PI controllers are usually tuned using hand-tuning or Ziegler-Nicholas methods and software tuning. Hand tuning or Ziegler Nichols is generally used by experienced control engineers based on the rules. But these rules are not always valid. For instance, if an integrator exists in the plant, then increasing proportional gain results in a more stable control. This thesis used the hand (manual) tuning methods and obtain the values of the proportional and integral gain for all systems. The coefficients of PI controllers (PI1 to PI4) for DC link voltage, current, active power, and reactive power controllers were obtained on the trial-and-error approach. A lot of values were investigated for different system conditions and finally, the values shown in Table A.3.4 are selected as the best values.

The mathematical model of continuous-time linear proportional-integral (PI) controller in position form is described as

$$u(t) = k_p e(t) + k_i \int_0^t e(t)dt \tag{3.127}$$

The corresponding discrete-time position form is described as

$$u(k) = k_p e(k) + k_i \sum_{i=0}^{k} e(i) \tag{3.128}$$

Where $k_p$and k_i are the proportional gain and integral gain coefficients of the PI controller, respectively.

As a result, p_0 and q_0 can be expressed by defining the power feedback loops by using PI controller gains as follows:

$$p_0 = k_p(p_{ref} - p) + k_i \int (p_{ref} - p)dt \tag{3.129}$$

$$q_0 = k_p(q_{ref} - q) + k_i \int (q_{ref} - q)dt \tag{3.130}$$

Where p_{ref} and q_{ref} are rated active power and reactive power respectively.

The rated active power is used to maintain a constant output voltage and rated reactive power is determined by the power factor.

3.5.1.2.1 DC-Link Voltage Control

The proposed controller's purpose is to regulate the DC link voltage to achieve stability when the wind speed changes (Pandya, 2020). Figure 3.25 shows the DC link voltage control using the PI controller.

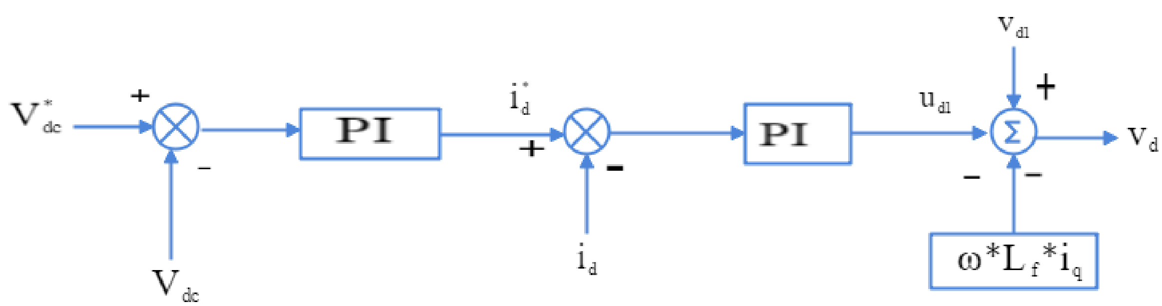

Figure 3. 25 DC bus voltage control

3.5.1.2.2 Active and Reactive Power Control

On the other hand, the active and reactive powers of the grids are expressed as (3.94) and (3.95), respectively, for synchronizing the AC power produced by the wind energy conversion system with the power grid. Direct grid current and quadrature grid current components, respectively, govern the active and reactive powers (Pandya, 2020). Figures 3.26 and 3.27 show the PI controller is used to control the active power flow and reactive power flow, respectively.

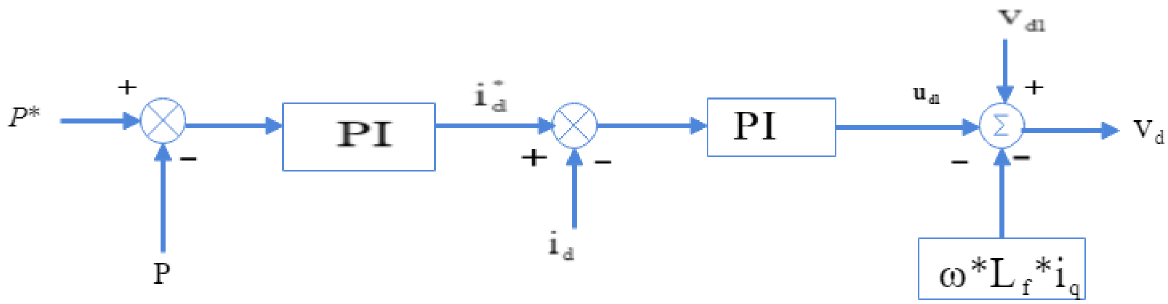

Figure 3. 26 Active power control

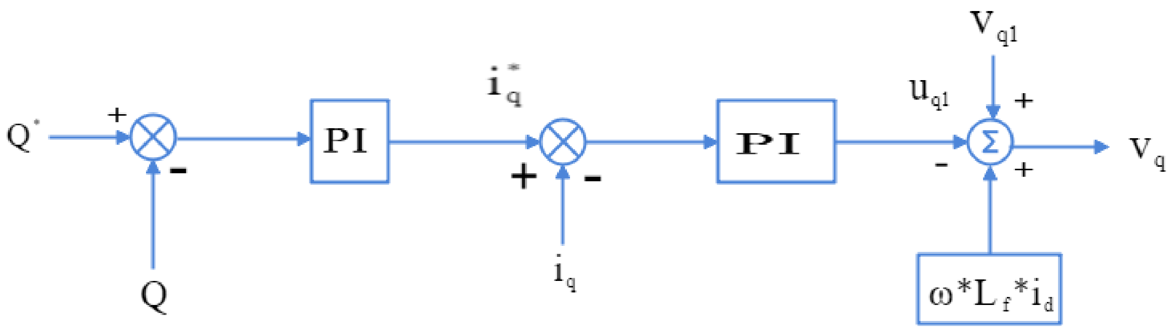

Figure 3. 27 Reactive power control

Because the system input is unstable, the fixed PI controller isn't always the best option. As a result, a new controller is designed to replace the fuzzy logic controller. This has drawbacks as well. The adaptive neuro-fuzzy inference system controller can replace both the PI and fuzzy logic controllers in this thesis.

3.5.2 Fuzzy Logic Controller Design

A formal methodology for representing, manipulating, and implementing a human's heuristic knowledge of how to control a system is provided by fuzzy control. For designing a fuzzy control system:

1. Choosing the fuzzy controller inputs and outputs
2. Deciding whether post-processing is required for the outputs or just preprocessing for the controller inputs.
3. Creating each of the fuzzy logic controller's four individual parts.

Moreover, most often the designer settles on an inference mechanism and may use this for many applications. Additionally, the designer often chooses an inference method and may employ it for a variety of processes. Therefore, the rule-base is the primary component of the fuzzy controller on which we concentrate during design. The rule base is created with a human expert "in the loop" in mind. As a result, the data that we input into the rules in the rule-base could originate from a real human expert who has spent a lot of time figuring out how to manage the process. In other circumstances, where there is no such human expert, the control engineer will only study the dynamics of the plant (perhaps via modeling and simulation) and record a set of logical control rules. The fuzzy controller is made up of four primary parts: The knowledge of how to best manage the system is stored in the "rule-base" as a set of rules. The inference mechanism determines what input to give the plant after determining which control rules are applicable now. Defuzzification transforms the inference mechanism's conclusions into plant inputs, while fuzzification just alters the inputs so that they may be read and compared to the rules in the rule-base.

3.5.2.1 Developing Fuzzy Expert System

Defining linguistic variables and specifying the problem is the first step to making the Mamdani controller.

1. **variables and their representations**

According to Zadeh, a linguistic variable is a variable whose values are words or sentences in a language, whether it be natural or artificial. The three key linguistic variables are as follows:

1. Error (E)
2. Change in Error (CE)
3. Change in Output

In fuzzy logic, some of the typical linguistic terms used are shown in Table 3.1

Table 3. 1 Meaning of typical linguistic terms in fuzzy logic

Linguistic Term	Meaning
PB	Positive Big
PS	Positive Small
Z	Zero
NS	Negative Small
NB	Negative Big

2. **fuzzification**

The fuzzy set of error “E” input contains five triangular memberships, the fuzzy set of the change error “CE” input contains five triangular memberships, and the fuzzy set of the output “Idc” contains five triangular memberships. The error and deviation of error between the reference DC-bus voltage and measured DC bus voltage input to the fuzzy logic controller one (FLC_1) and normalized to [-1, 1], and the output signal DC (I_{dc}) is normalized to [-1, 1]. The error and deviation of error between the reference active power and measured active power are inputs to the fuzzy logic controller one (FLC_2) and normalized to [-1, 1], and the output signal (I_{dref}) is normalized to [-1, 1]. The error and deviation of error between the reference reactive power and measured reactive power are inputs to the fuzzy logic controller one (FLC_3) and normalized to [-1, 1], and the output signal (I_{qref}) is normalized to [-1, 1].

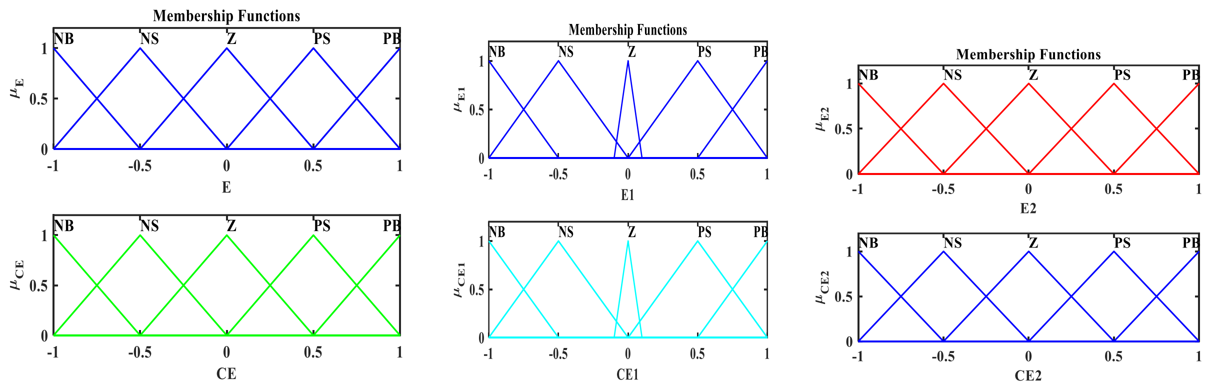

(a) (b) (c)

Figure 3. 28 (a) Membership function for error and change in error in DC-link voltage (b) Membership function for error and change in error in active power (c) Membership for error and change in error in reactive power

Figure 3.28 (a) shows the membership functions for error and change in DC link voltage, (b) shows the membership functions for error and derivative of the active power, and (c) shows the membership functions for error and change in the error of the reactive power. The shape of the membership function and the universe of discourse for each function are found by trial-and-error after many simulations were done. The fuzzy inputs membership functions used are triangular types.

3. control base rule

A fuzzy rule may contain fuzzy variables and fuzzy subsets characterized by a membership function, but they can be presented in different formats. In this system, the rules are presented to the controller in a format like the one below. End-user in a format like the one below,

1. If an error is NB and the change in error is NB, then Δu is NB
2. If an error is NS and the change in error is NS, then Δu is NB
3. If an error is Z and the change in error is Z, then Δu is Z

4. If an error is PS and the change in error is PS, then Δu is PB
5. If an error is PB and the change in error is PB, then Δu is PB, and ….

The knowledge base defining the rules for the desired relationship between the input and output is presented in Table 3.2.

Table 3. 2 Rule base for five membership functions

E \ CE	**NB**	**NS**	**Z**	**PS**	**PB**
NB	NB	NB	NB	NS	Z
NS	NB	NB	NS	Z	PS
Z	NB	NS	Z	PS	PB
PS	NS	Z	PS	PB	PB
PB	Z	PS	PB	PB	PB

4. defuzzification

Defuzzification is the process of converting a fuzzified output into a single crisp value regarding a fuzzy set, as can be seen from the current literature. The defuzzified output value in FLC represents the process control action that must be executed. Among the recognized techniques for defuzzification, in this thesis, the Bisector of Area (BOA) method was applied. The place under the curve where the areas on both sides are equal may be determined using this method. The action that divides the area into two regions with the same area is generated by the BOA. Consequently, the BOA's formula is provided by

$$\int_{\alpha}^{x_o} \mu_A(x)dx = \int_{x_0}^{\beta} \mu_A(x)dx \tag{3.131}$$

Where $\alpha = min\{x|x \in X\}$and $\beta = max\{x|x \in X\}$, and $\mu_A(x)$ is membership of x in the fuzzy set A and x_o denotes the defuzzified value which can be obtained through the BOA.

The outputs defuzzification membership function is shown in Figure 3.29 (a) and (b).

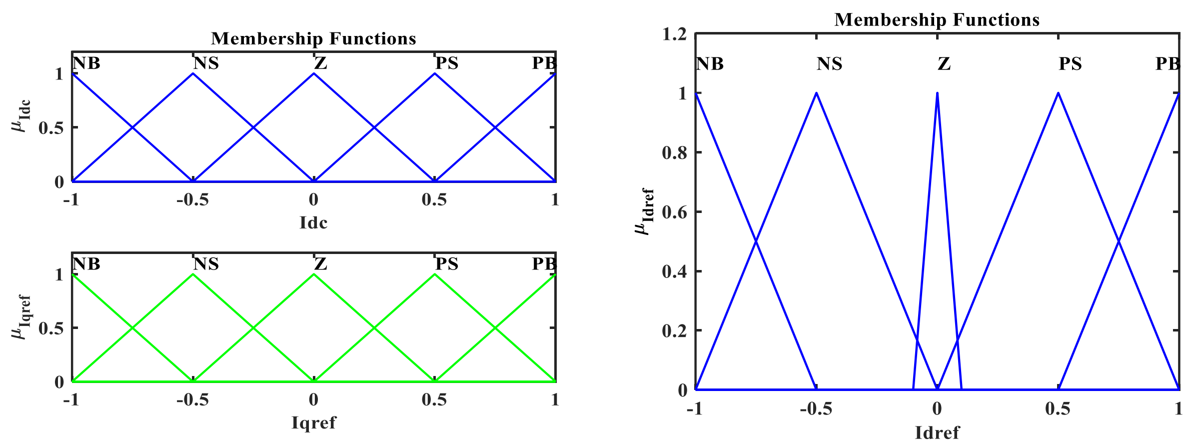

(a) (b)

Figure 3. 29 (a) Output membership function for change in Idc and Iqref and (b) Output membership function for change in Idref

Figure 3.30 and Figure 3.31 Shows the SIMULINK model for DC link voltage control and power flow control of WECS using FLC, respectively.

In the above expressions and Figure 4.29, we obtained the defuzzified (crisp values) outputs of the given fuzzy set, which were converted from this set using the defuzzification technique known as the Bisector of Area (BOA). Conclude that the value of Negative Big is $-0.952 \approx -1$, Negative Small is -0.5, Zero is 0, Positive Small is 0.5, and Positive Big is $0.952 \approx 1$.

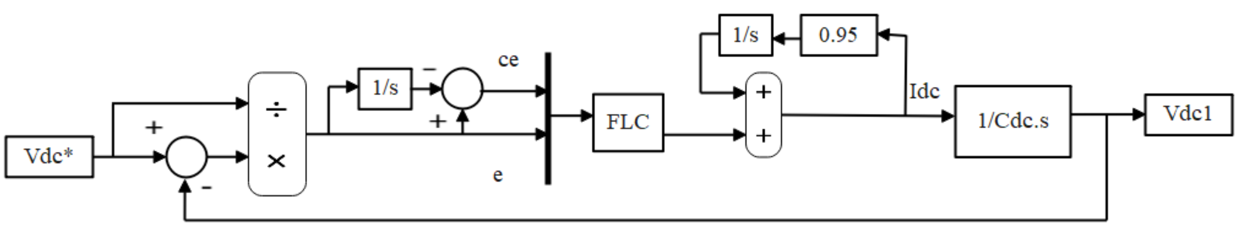

Figure 3. 30 SIMULINK model for DC bus voltage control of WECS using FLC

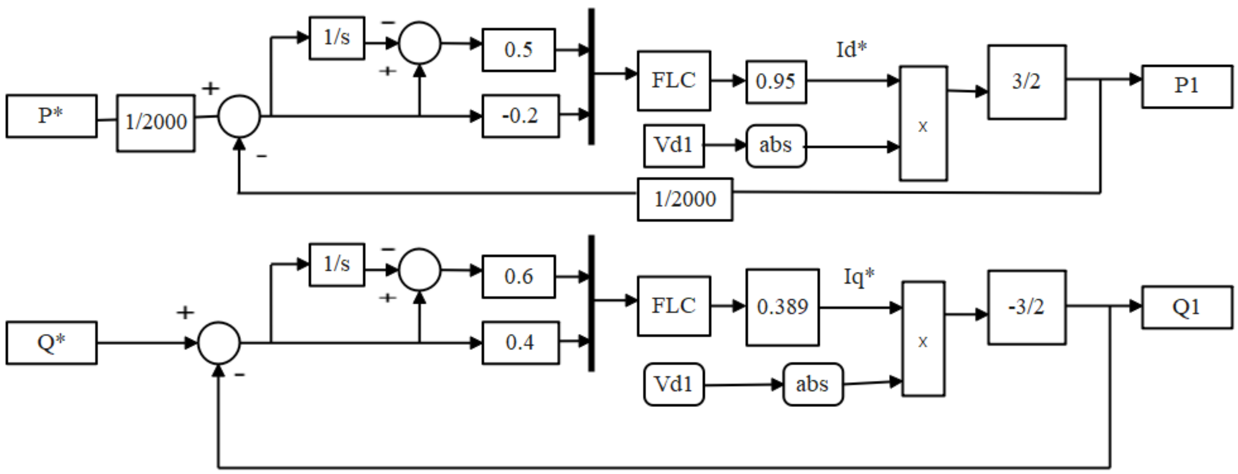

Figure 3. 31 SIMULINK model for power flow control of WECS using FLC

The adaptive neuro-fuzzy inference system controller may then be designed and interpreted into simulations in the following section of this thesis to observe the results by comparing the designed PI controllers and fuzzy logic controllers.

3.5.3 Adaptive Neuro-Fuzzy Inference Controller Design

The membership function parameters of single-output, Sugeno-type fuzzy inference systems are determined by ANFIS using a hybrid learning technique. To find fuzzy decision rules that work well for each task, the ANFIS employs a feedforward network. ANFIS develops a fuzzy inference system from a given input/output data set by adjusting the membership function parameters through a hybrid method. The two components of the ANFIS design estimator are construction and training. The parameters of the structure are chosen in the construction phase. These are the kind and quantity of MF inputs, as well as the kind of MF outputs. Effective input space partition is crucial since it can reduce the number of rules and speed up both learning and application processes. Output MFs may take the form of a constant or a linear formula.

The estimator rule base is constructed when the number and type of input MFs have been described. Since using expert knowledge is not standardized, automatic rule development is typically preferred. As a result, rule bases for estimators have automatically been created given the number of inputs and MFs. The learning algorithm and training parameters are selected following the construction of the ANFIS structure. So, in this thesis, a hybrid learning algorithm is used. The algorithm has the following parameters: epoch size, error tolerance, initial step size, step size reduction rate, and step size increase rate. Epoch size is the size at which the full data set is presented. A trial-and-error method is employed because there is no precise method in the literature for determining the optimum of these parameters. Either the ANFIS editor GUI or the command line can be used to generate an ANFIS model. As previously indicated, an ANFIS controller needs to be fed by inputs and outputs that are optimized for good performance.

Numerous techniques have been developed to accomplish this purpose. The goal of this thesis is to develop a proportional Integral-based (composed technique) ANFIS method, which consists of the following five steps:

1. Assuming a specific transfer function, we control it using a PI controller with the best P and I parameters. The optimal P and I parameters for this controller should allow for effective process control.
2. The output of the PI controller should be communicated to the workspace in MATLAB program at some points in this method's development. For more precision, it's ideal to have a few extra points.
3. An expert operator should now modify and optimize these points in the areas where the PI controller is not acting properly.
4. After the points have been updated, we train the ANFIS inputs and outputs using these modified points in this step of the approach. The third step's output is the input, and the inputs are the error and its deviation.
5. Use the new ANFIS controller to manage the transfer function in this stage. The ANFIS controller contains certain fuzzy rules and memberships with unique inputs and outputs after the processes. Unknown non-linear process plants may also use this.

The first step to achieving good performance is to control the process using a PI controller. After that, with the composing method, we can have the ANFIS control that unknown process much better.

3.5.3.1 Adaptive Neuro-fuzzy Inference System Editor

The data set and train anfis were loaded for DC link voltage control, active power control, and reactive power control, respectively, from the ANFIS editor, illustrated in Figures 3.32-3.34 GUIs using anfisedit. There were used three (3) ANFIS controllers. Data can be generated for the input and output of each of these controllers. The first controller used output data (DC current) and input data (error and change in error). For the active power control, data inputs (error 1 and change in error 1), output data (d-axis current), and data points (error 2, change in error 2, and q-axis current) are then employed for reactive power control. As a result, Table 3.3 can show the data points and data sets of these controllers. A major problem to face while designing a fuzzy rule procedure is its optimization as no systematic tools are available, neither to complete a stability analysis nor to perform a parametric optimization. So, for this reason the ANFIS is proposed.

Table 3. 3 Input data and output data

Controllers	**Data Inputs**						**Data Outputs**		
	E	CE	E1	CE1	E2	CE2	Idc	Id	Iq
DC-link Voltage Control	10k	10k					10k		
Active power control			10k	10k				10k	
Reactive power control					2k	2k			2k

Based on the generated data neuro-fuzzy semiautomatic procedure is developed and used to optimize the fuzzy adaptive laws using suitable sets of given data. As an example, for the active power control, when the ANFIS editor GUI is opened using anfisedit("active_power_control"), a FIS structure that is stored as a file called active_power_control is used to implement ANFIS. ANFIS model structure DC link voltage control, active power control, and reactive power control is shown in Figure 3.35. FIS anfisedit(active_power_control) operates in the same manner for a FIS structure active_power_control that is saved as a variable in the MATLAB workspace. The above data sets are the data which are obtained from workspace, data generated on this workspace are not only the above one, but I used some of it. Because the remaining data is mostly equal and redundancy data. There is a menu bar on the ANFIS editor GUI that you can use to access associated GUI tools, save, open systems, and other functions.

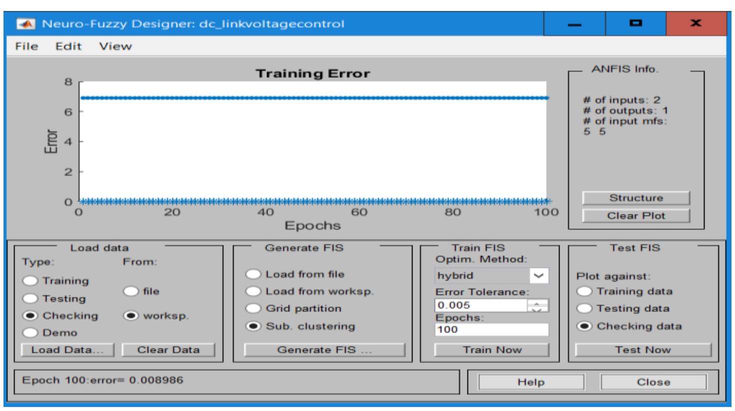

Figure 3. 32 ANFIS editor for DC-link voltage control

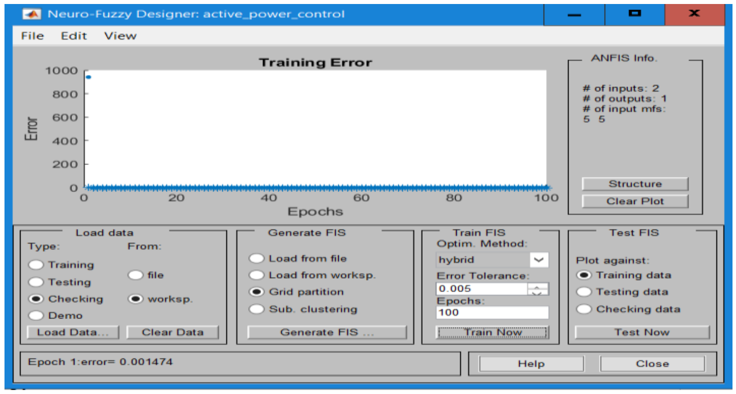

Figure 3. 33 ANFIS editor active power control

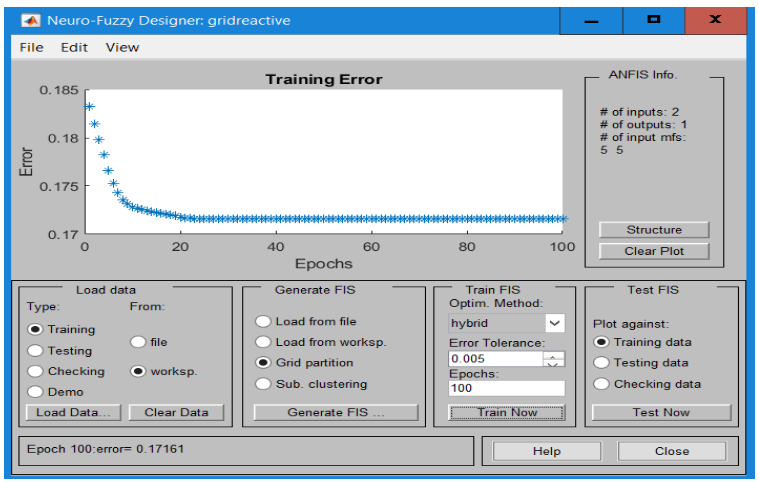

Figure 3. 34 ANFIS editor for reactive power control

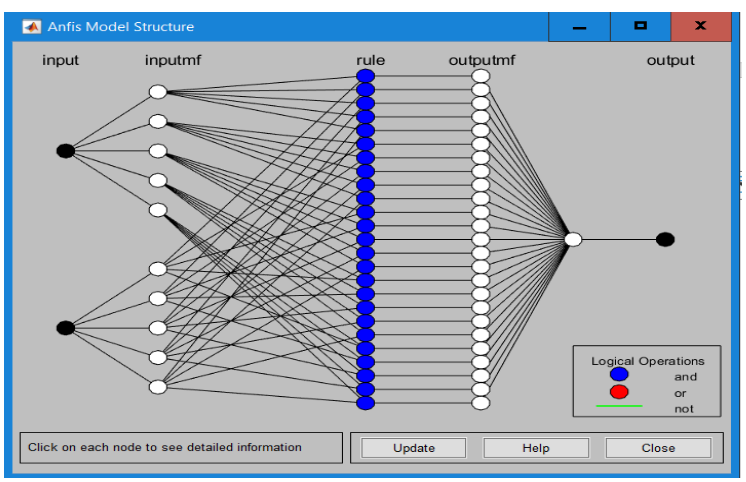

Figure 3. 35 ANFIS model structure

3.5.3.2 Flow chart for ANFIS Training Process

There are two methods of ANFIS training. Those are offline and online training methods. The ANFIS training offline methodology using ANFIS GUI in MATLAB fuzzy logic Toolbox is summarized in Figure 3.36. Obtaining a training data set of input/output data pairs is the first step in the process. The premise parameters for the membership functions are determined using the training data set. The difference between the actual and desired output is measured against a threshold value. The least-squares method is used to find the resulting parameters. Then, an error is found for every data pair. If this error is larger than the threshold value, then the premise parameters are updated using the gradient descent method (backpropagation). The process is terminated when the error becomes less than the threshold value. Then the checking data set is used to compare the model with the actual system. Figure 3.37 and Figure 3.38 shows the SIMULINK model for DC link voltage control and power flow control of WECS using ANFIS, respectively.

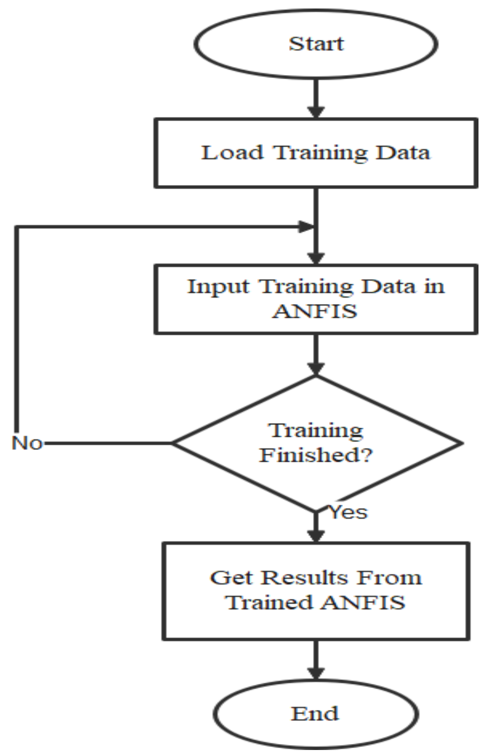

Figure 3. 36 ANFIS training process

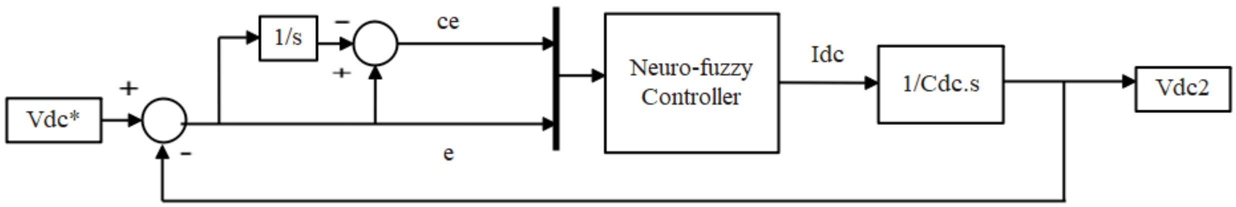

Figure 3. 37 SIMULINK model for DC-link voltage control of WECS using ANFIS

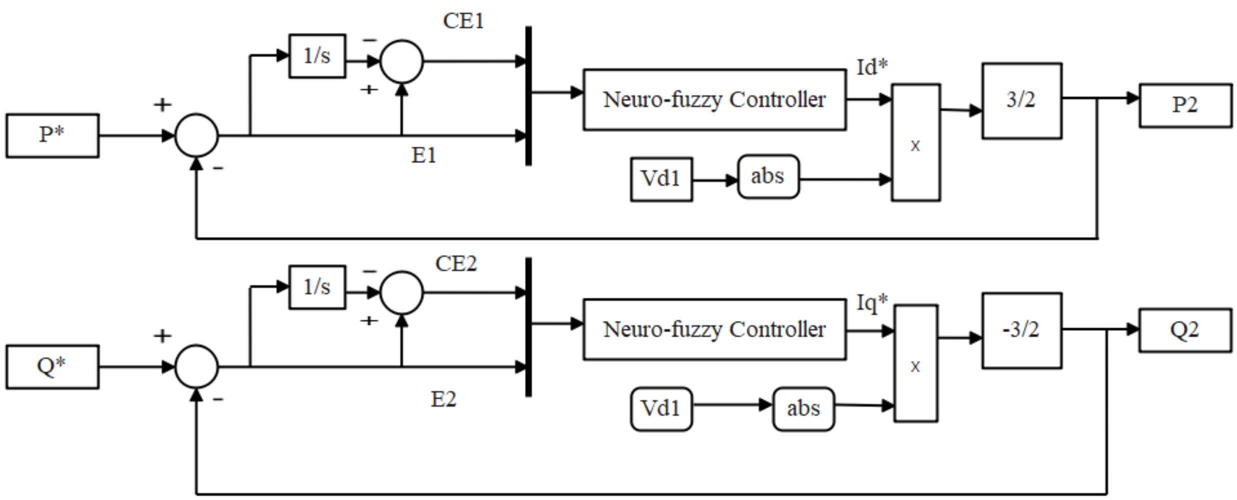

Figure 3. 38 SIMULINK model for power control of WECS using ANFIS

3.6 Simulink Model of WECS for Power Flow Control

The overall SIMULINK model of the wind energy system and its control system is shown in Figure B.1. The simulation model is developed based on a permanent magnet synchronous generator (PMSG), DC-DC boost converter, DC-AC inverter, and filter. The parameters of the wind turbines, lumped mass drive system, PMSG, AC-DC uncontrolled rectifier, DC-DC boost converter, DC-AC inverter, and grid filter are in Appendix A. The power converters and the controllers with DC-link voltage and power flow control algorithm are included in the model. The load is set to be an equivalent resistor of 113 ohms and the chosen simulation type in Simulink is set as a discrete type with a sample time of 2e-6 sec. VA, VB, and VC are the 3-phase output ports connected to an uncontrolled rectifier. The ports related to torque are not on the same base. The rated power of a wind turbine is 2 MW and the rated angular speed of PMSG is 152.89 rad/sec.

CHAPTER FOUR

4. SIMULATION RESULTS AND DISCUSSIONS

4.1 Simulation Results

This thesis studied the different methods for DC bus voltage control and power flow control of wind energy conversion systems based on PMSG. To validate the control strategies as described above, MATLAB simulations were carried out on a wind energy conversion system whose parameters are given in chapter 3, section 2, and Appendix A. Figure 4.2 shows the response of stator voltages and stator currents with variable wind speed. This thesis more focuses on the simulation results of variable speed wind turbines with PMSG which are interconnected with the grid through fully rated power converters for the control of power flow and DC link voltage. Figure 4.3 shows the response of pitch angle control, variable wind speed, power performance coefficient, and tip speed ratio. The response of electromagnetic torque, mechanical angular speed in (rad/sec), and mechanical angular in (rpm) are shown in Figure 4.4. Figure 4.5 shows the response of wind turbine rotor speed and maximum power extracted from the wind turbine. The response of wind turbines and mechanical torque is shown in Figure 4.6. Figure 4.7 shows the response of DQ-axis current control and voltage control using PI controllers. The response of DC link voltage with the PI controller, fuzzy logic controller, and neuro-fuzzy controller is illustrated in Figure 4.11. Figure 4.12 illustrate the response of the active power with the PI, fuzzy logic, and neuro-fuzzy controllers. The response of reactive power with PI, fuzzy logic, and neuro-fuzzy controllers are shown in Figure 4.13. The three controllers can be used to control DC link voltage, active power, and reactive power from which the ANFIS controller performs slightly better than the other controllers.

4.1.1 Simulation Result for Machine Side Converters

When the wind speed is 12m/s (rated wind speed), the simulation result is shown in Figure 4.1. From simulations, can be observed the voltages and currents are not varied because of wind turbine used here is a fixed-speed wind turbine. In this type of wind turbine, it is not possible to extract maximum power tracking. Figure 4.1 (a) and (b) show the response of stator voltages and stator currents, respectively. The constant voltages and currents are obtained.

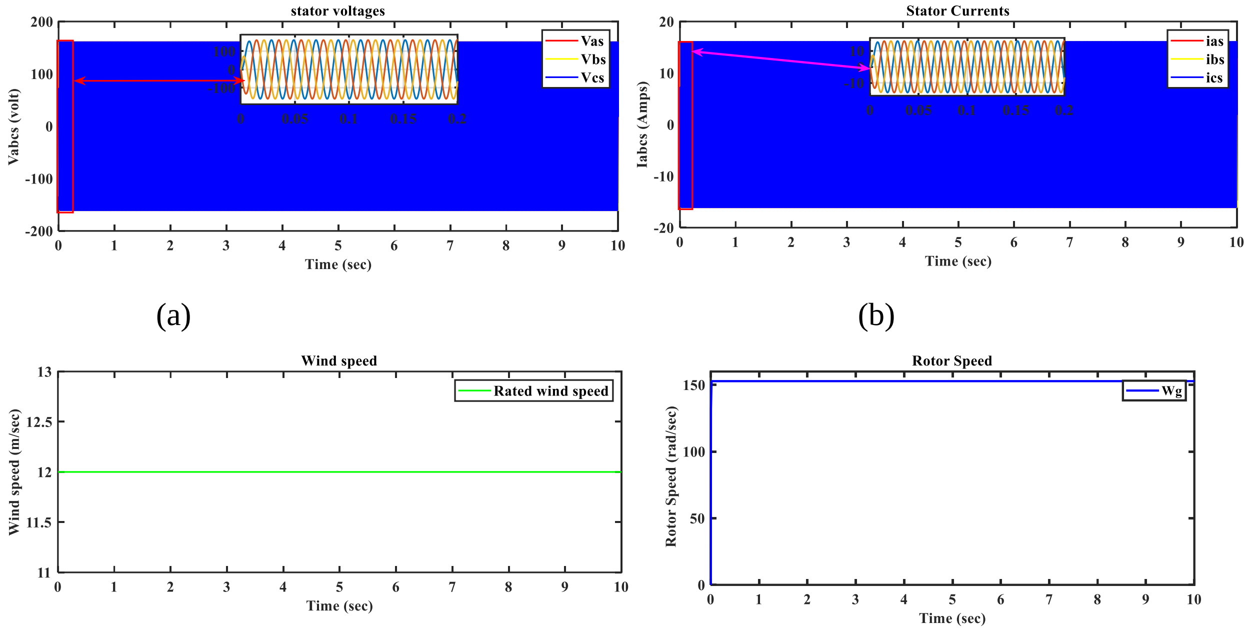

(c) (d)

Figure 4. 1 (a) Stator voltages (b) stator currents (c) fixed wind speed and (d) rotor speed

The stator voltages and currents can be changed with variable wind speeds in Figure 4.2 (a) and (b). When the wind speed slows, so do the voltages and currents. As the current and voltage fall, so does the power generate.

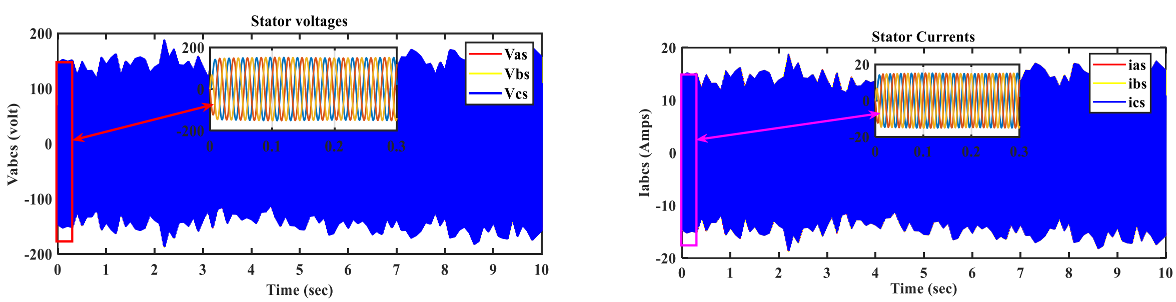

(a) (b)

Figure 4. 2 (a) Stator voltages (b) Stator currents

The mechanical rated rotational speed is shown in Figure 4.1 (d) from the simulation result, the generator operates under a constant rotation speed of 152.89 rad/sec.

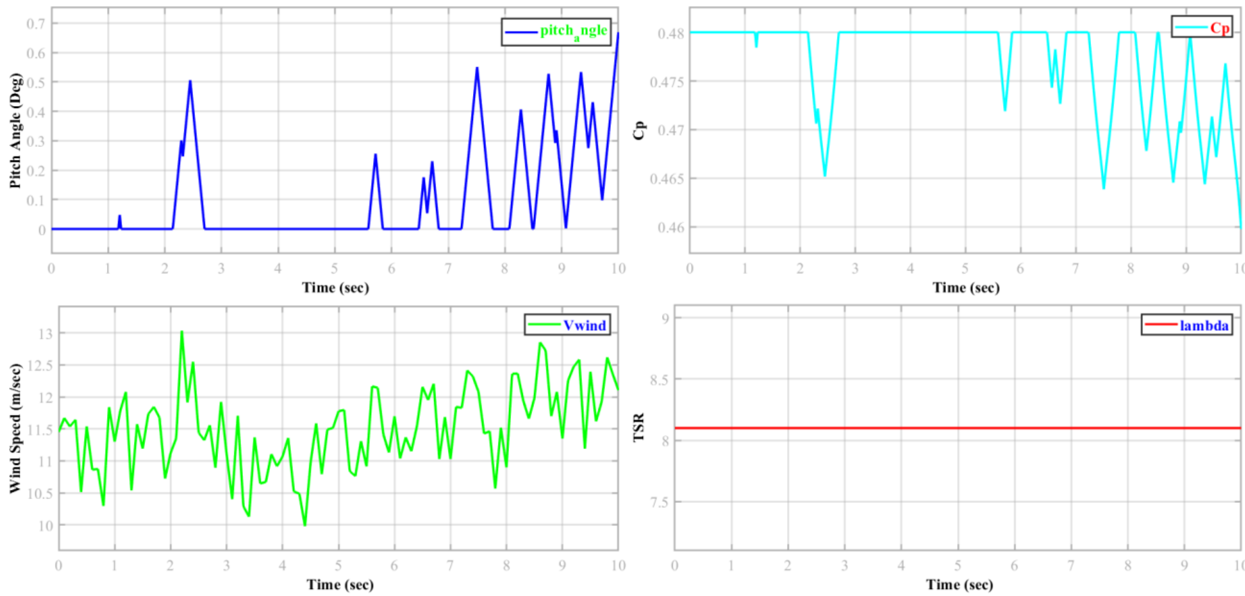

Figure 4. 3 Pitch angle, wind speed, cp, and tip speed ratio

The power coefficient of this wind turbine is shown in Figure 4.3 to be maintained at the optimum value of 0.48 whenever the wind speed is less than the rated speed and equal to the rated speed, but it decreases if the wind speed is higher than the rated speed. Additionally, the wind turbine's pitch angle is maintained at 0 degrees unless the wind speed exceeds the rated wind speed, in which case it will vary. Then, whenever the wind speed varies, the tip speed ratio can be maintained at the optimum value of 8.1.

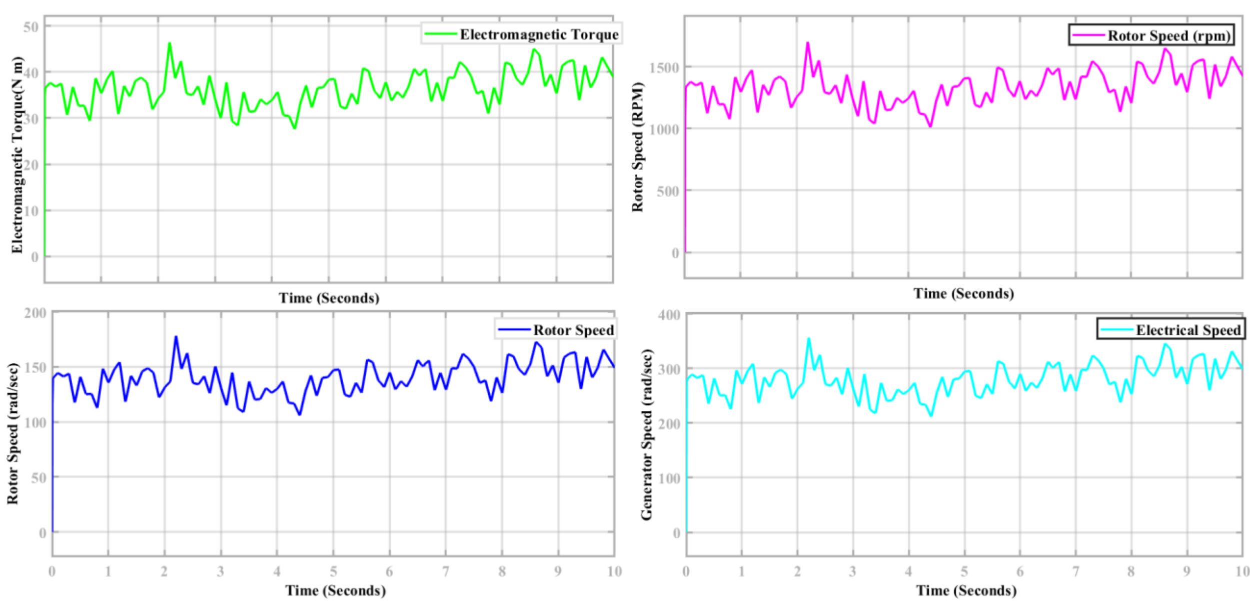

Figure 4. 4 Electrical torque, rotor speed (rpm), rotor speed (rad/sec), and electrical speed (rad/sec).

In Figure 4.4, variations in wind speed can change the electromagnetic torque and mechanical angular speed by up to 40 Nm and 152.89 rad/sec, respectively. This thesis has 4 number of pole pairs because of this the electrical speed can be twice of mechanical angular speed. The maximum power extracted from the wind turbine can be adjusted in Figure 4.5 as the wind speed changes. Since the PMSG's input might be either angular speed or torque, Figure 4.6 demonstrated that there is no input voltage to the device. The generators' job is to transform mechanical energy into electrical energy. This simulation's results show this. With varying wind speeds beyond their rated value, mechanical torque and wind turbine torque can also vary.

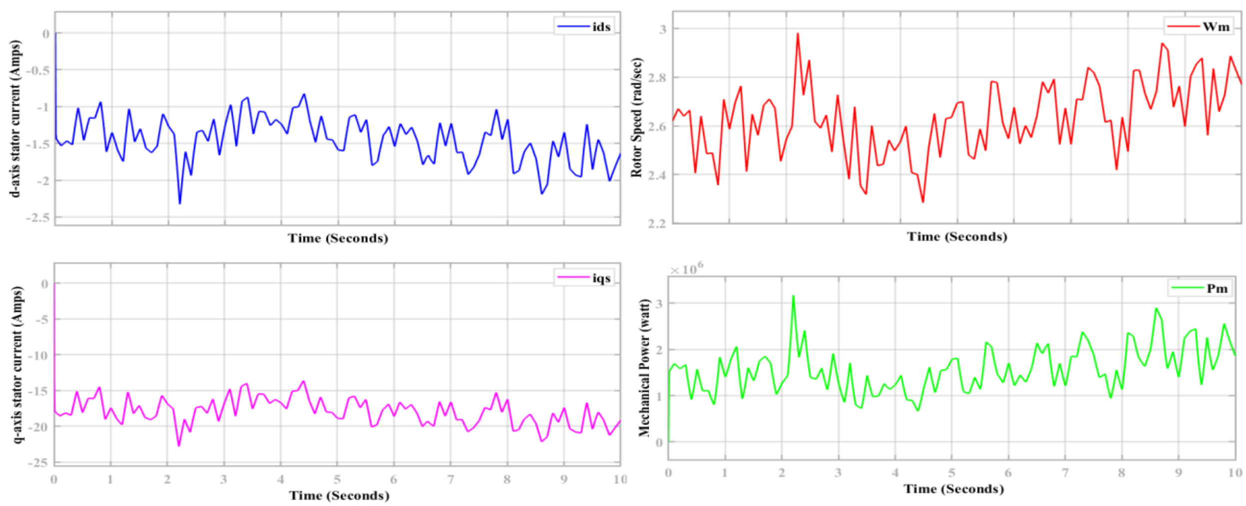

Figure 4. 5 D-axis stator current, rotor speed of wind turbine, Q-axis stator current, and maximum power

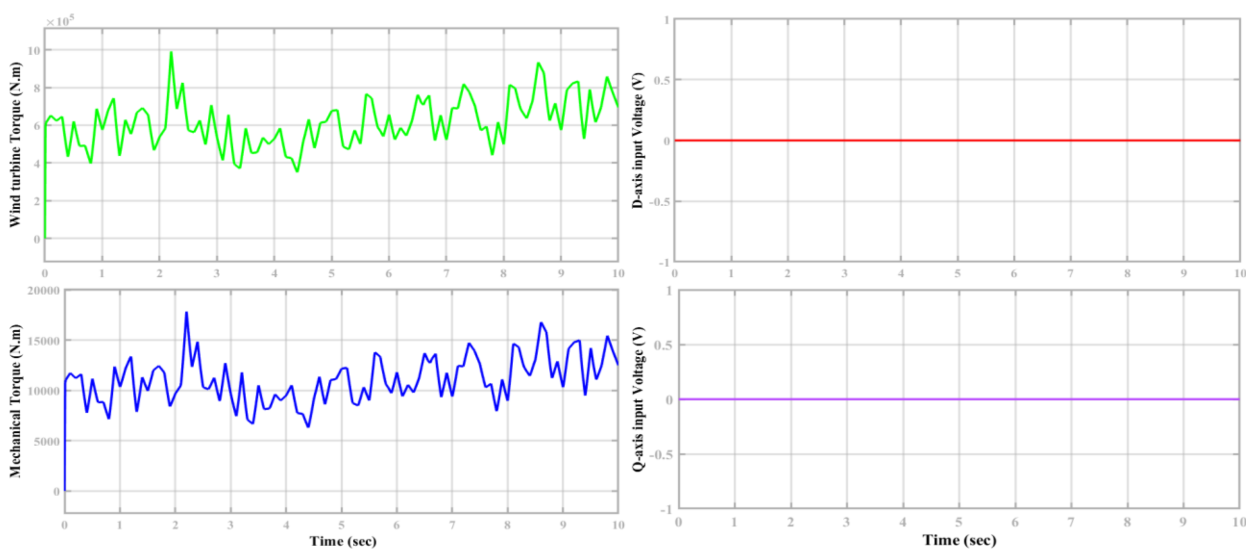

Figure 4. 6 Wind turbine torque, mechanical torque, and DQ-axis input voltages of generator

4.1.2 Simulations and Performance measures for Current and Voltage Control in Inverter Side with PI Controller

Due to the variable output voltage of the rectifier caused by fluctuations in wind speed, boost converter control is required. Boost converters are made to raise the voltage value. Both the D-axis current and the Q-axis current in Figure 4.7 are controllable. This allows for the reliable regulation of the D-axis current. It has been seen that initially, it oscillates between -1000 and 1500 A, but after 1 second it moves to 1000 A and reaches a steady condition. The q-axis current also initially displays values between -500 and 2000; however, after a period, starting at 1 second, it goes to zero, however it is not quite zero (it is near to zero). The PI controller controls the current along the D and Q axes. The reduced settling time, quick time, small overshoot, and zero steady-state error, 10.211msec, 7.676msec, 3.352%, and 0 are obtained, respectively for D-axis current control. And for Q-axis current control 16.707msec, 13.018msec, and 12.276%, settling time, rise time, and overshoot are obtained, respectively. It also demonstrates the d-axis and q-axis voltages. The voltage on the q-axis is zero since the reference frame can be positioned on the d-axis. Figure 4.8 depicts the simulated response of three-phase inverter voltages and currents, filter voltages and currents, and grid voltages and currents. The output responses as observed from the simulation results have good performance specifications such as rising time, overshoot, and settling time. The response of inverter, filter, and grid currents is shown in Figure 4.9.

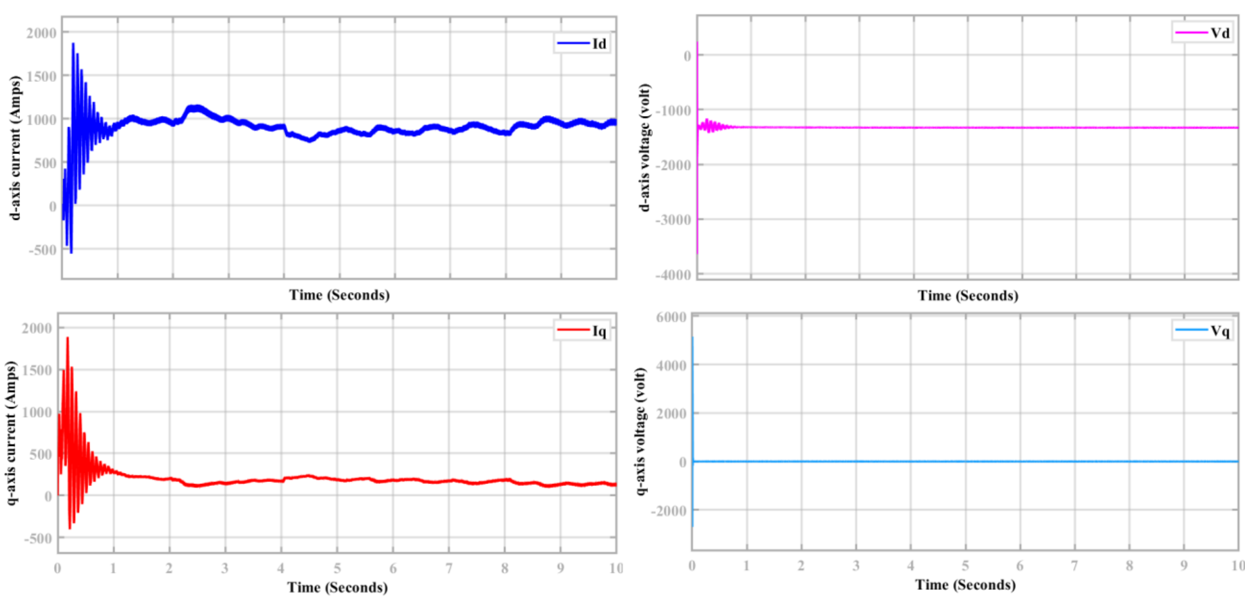

Figure 4. 7 DQ-axis current control and voltage control using a PI controller

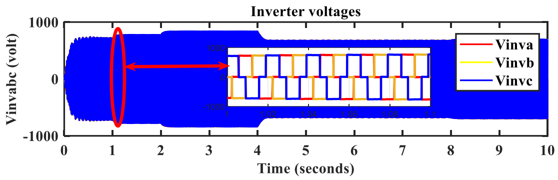

(a)

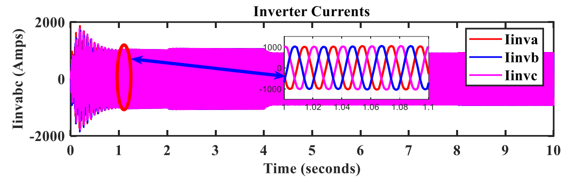

(b)

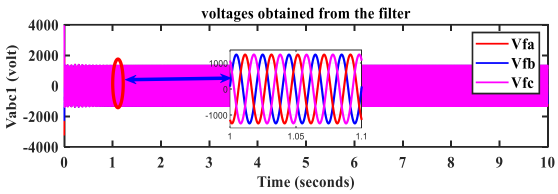

(c)

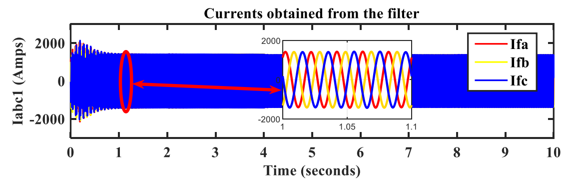

(d)

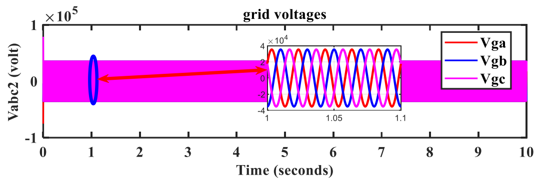

(e)

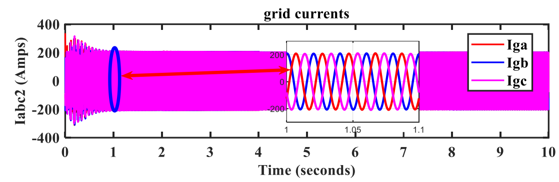

(f)

Figure 4. 8 (a) Inverter voltages (b) Inverter currents (c) Filter output voltages (d) Filter output currents (e) Grid voltages (f) Grid currents.

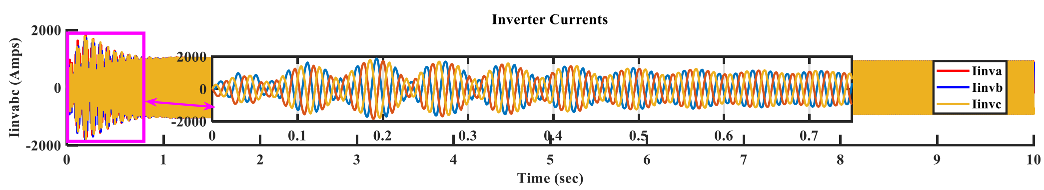

(a)

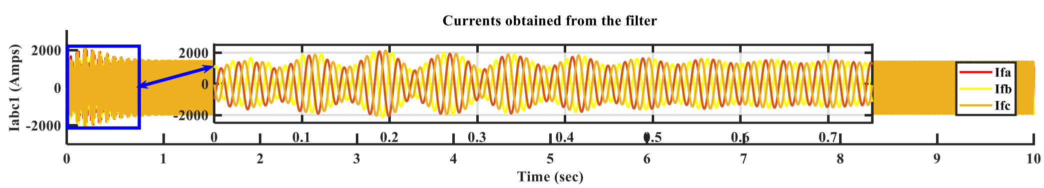

(b)

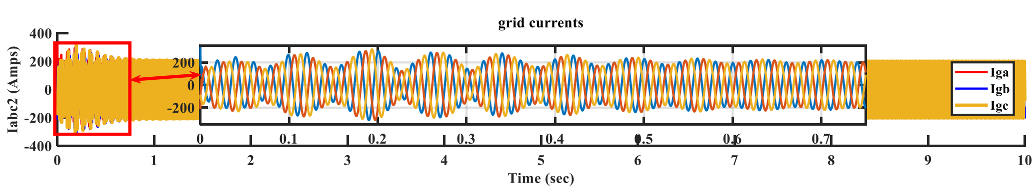

(c)

Figure 4. 9 (a) inverter currents (b) filter output currents (c) grid currents

The three-phase short-circuit capacitor defect occurs in the middle of the transmission line, as shown in Figure 4.9. Figure 4.9 (b) shows the original simulation with the line inductors, capacitors, and resistors for comparison. The same three-phase short circuit defect occurs at 0.1s and 0.2s with a duration of 0.05s. The location of the capacitor short-circuits issue is clearly shown.

4.1.3 Simulation Results for DC-Link Voltage control with Three Controllers

Figure 4.10 shows the response of DC bus voltage control for all controllers PI, FLC, and Neuro-fuzzy controllers.

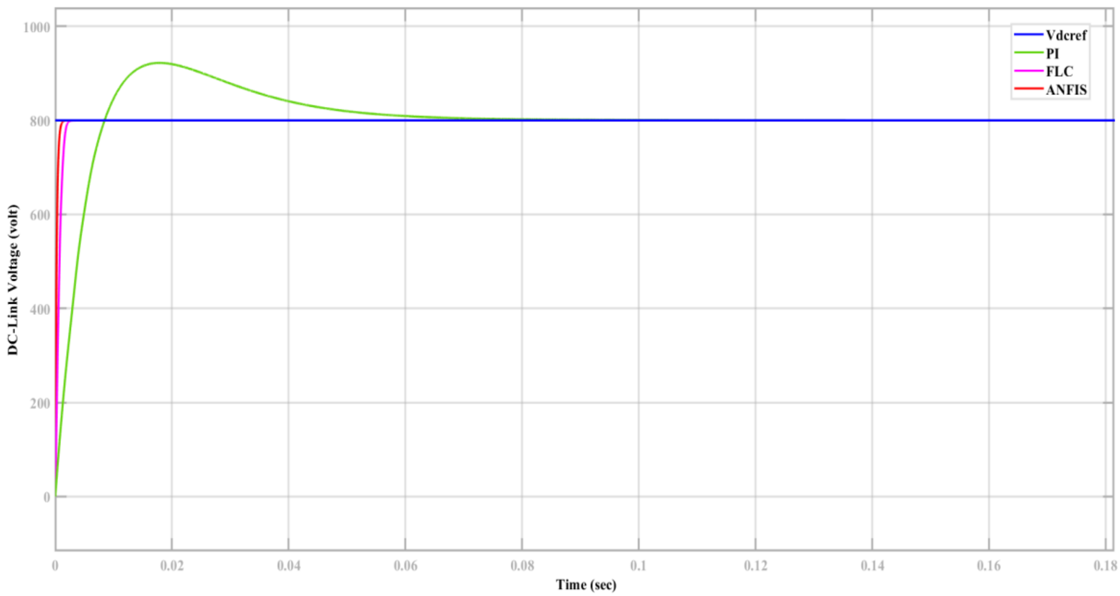

Figure 4. 10 DC bus voltage control using the three controllers

4.1.4 Simulation Results for Active Power Control with Three Controllers

Figure 4.11 shows the response of active power control for all controllers PI, FLC, and Neuro-fuzzy controllers.

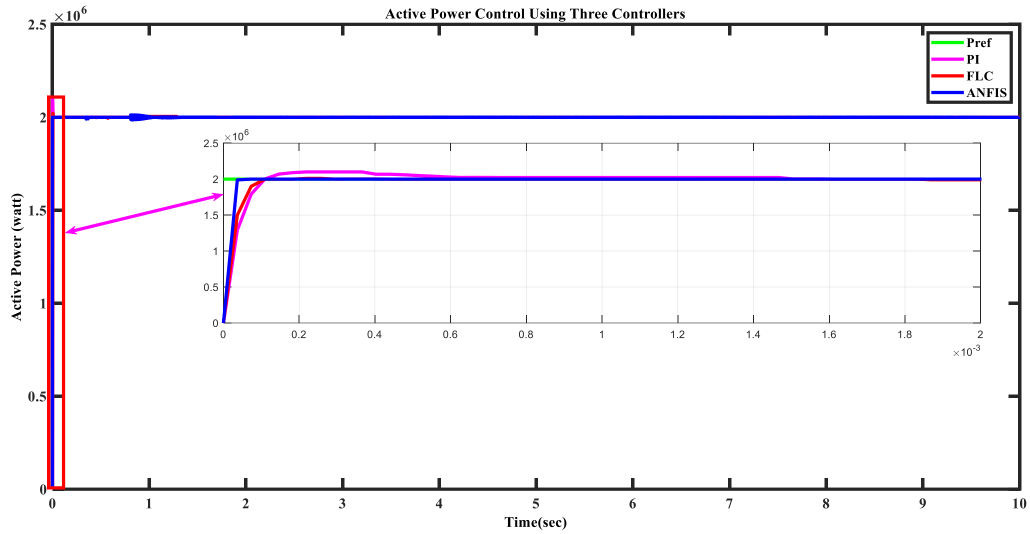

Figure 4. 11 Active power control using the three controllers

4.1.5 Simulation Results for Reactive Power Control with Three Controllers

Figure 4.12 shows the response of reactive power control for all controllers PI, FLC, and Neuro-fuzzy controllers

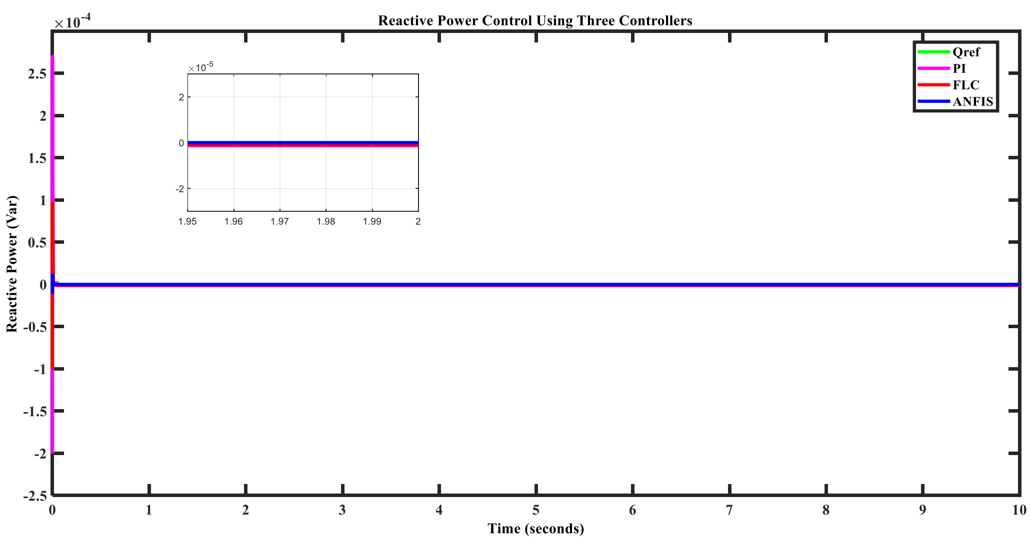

Figure 4. 12 Reactive power control using the three controllers

The reactive power is high in the transmission line means it required significantly higher voltage drop control and increased transmission network losses, lowering the power factor and system efficiency. As shown in Figure 4.12, the reactive power is controlled and is 0 VAR when PI, FL, and neuro-fuzzy controllers are used, only the differences between them are in the performance. As a result, it has a unity power factor, high transmission efficiency, and no power loss.

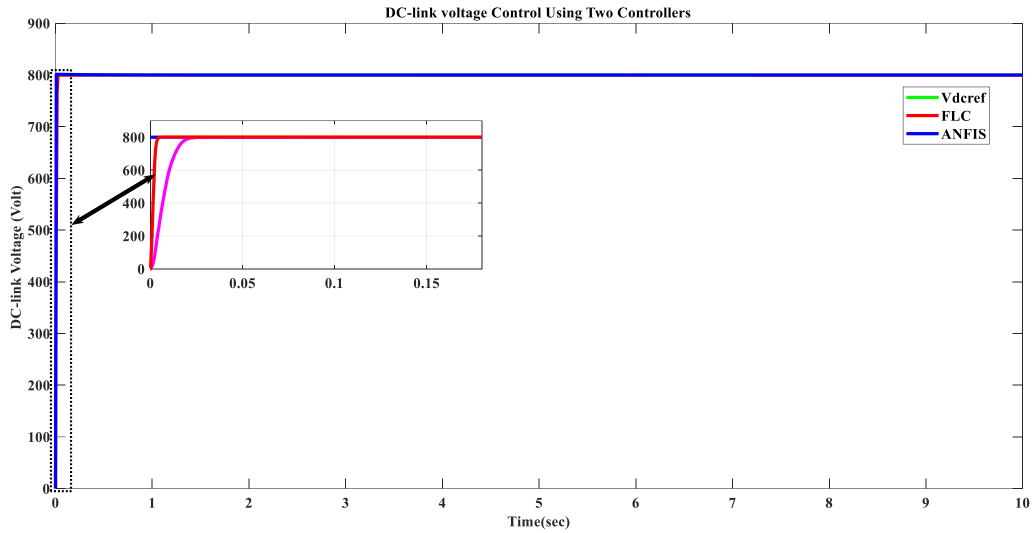

Figure 4. 13 DC bus voltage control using FLC and ANFIS

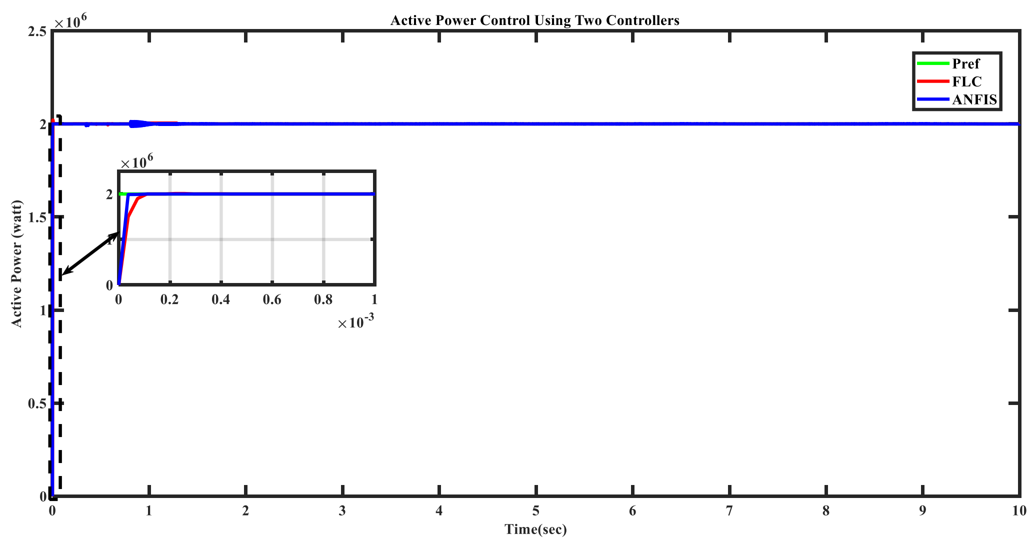

Figure 4. 14 Active power control using FLC and ANFIS

For getting the above simulation results, if the controller is fuzzy logic controller it used trial and error procedure to obtain the fuzzy rule and membership functions. The ANFIS controller does not require an accurate model of the plant. Its relative simplicity makes it easy to construct and implement. This is a fast and robust method to generate suitable initial membership functions and rule bases. High-level knowledge of system is not needed to build a set of rules for a fuzzy logic controller or for the identification needed in an artificial neural network controller. So, advantages of the ANFIS are no need of fast processors, less data storage, mathematical concepts behind fuzzy reasoning are very simple, flexible, more robust, and high efficiency. It gives faster response than FLC. It reduces design efforts.

4.2 Comparisons and Discussions

Table 4.1 illustrates the performance metrics of PI, fuzzy and neuro-fuzzy controllers. As shown in the above simulation results, the DC link voltage response to an 800 V step input signal, the active power response to a 2 MW, and the reactive power 0 Var. From them, the quick response time is observed by comparison with the desired response. Also, the settling time is 6.85e-6 sec, 0.04248e-3 sec and 0.301e-3 sec of which the reductions are sought from DC link voltage, active power, and reactive power flow, respectively. The steady-state error could also be improved. As a result, the proposed controllers produce the best performance indices. Finally, to compare the conventional PI with FLC developed using an adaptive neuro-fuzzy inference system. As seen in Figure 4.10, Figure 4.11, and Figure 4.12, the adaptive neuro-fuzzy inference system has the best output response; the least overshoot and settling time.

Despite the advantages of fuzzy logic control, the main drawbacks are the lack of a systematic design methodology and the difficulty in predicting the stability and robustness of the controlled system. A trial-and-error iterative approach is taken for the controller design due to which we get a sluggish response. Neuro-fuzzy learning incorporates the architecture of a neural network-based fuzzy inference system. A given training data set is partitioned into a set of clusters based on the subtractive clustering method. This is a fast and robust method to generate suitable initial membership functions and rule bases. A fuzzy If-Then rule is then extracted from each cluster to form a fuzzy rule base from which a fuzzy neural network is designed. Then a hybrid learning algorithm is used to refine the parameters of the fuzzy rule base.

Table 4. 1 Comparison between PI, FLC, and neuro-fuzzy controllers

Comparisons	**PI Controller**			**FLC**			**Neuro-Fuzzy Controller**		
	t_r (ms)	t_s (ms)	o_s (%)	t_r (ms)	t_s (ms)	o_s (%)	t_r (ms)	t_s (ms)	o_s (%)
DC-Link Voltage Control	6.232	7.461	14.37	1.221	1.236	0.505	0.4916	0.6858	0.50
Active Power Control	0.0585	18.485	10.404	0.0275	5.416	7.184	0.0068	0.04248	0.53
Reactive Power Control	0	5	2.75	0	2.015	1.501	0	0.301	0.1

Maximum overshoot, settling time, and rise time are used to evaluate performance. The obtained parameters show that ANFIS outperforms PI and FLC for DC bus voltage control and active and reactive power control. The neuro-fuzzy controller improves the system's performance. The simulation results show that the error is almost always zero. Successful simulations show that neuro-fuzzy controllers outperform PI and FL controllers in terms of intended performance. Table 4.1 compares the dynamic performances of DC bus voltage and power flow controllers.

5. CONCLUSIONS AND RECOMMENDATIONS

5.1 Conclusions

This thesis is intended to demonstrate the successful application of adaptive neuro-fuzzy controllers, fuzzy logic controllers, and PI controllers for power flow control of wind energy conversion systems-based permanent magnet synchronous generators. It has provided and modeled an overall perspective on wind energy conversion systems. It has shown that fuzzy logic controllers perform better than conventional PI controllers, with the neuro-fuzzy controller performing the best of the two. The dynamic performances of these controllers are compared in Table 4.1. Simulation results are presented and analyzed for all three controllers. The right term must be chosen repeatedly in the traditional PI controller design to get a good response. Design with a fuzzy logic controller gives good results, but also a trial-and-error method is needed to find the required parameters. Design with adaptive neuro-fuzzy controller reached a very good response and was very fast. The adaptive neuro-fuzzy inference system controller has the advantages of automatically determining the number of rules, reducing computing time, learning more quickly, and producing fewer errors than other methods. With proper design, the neuro-fuzzy controller can be replaced in PI and fuzzy controllers for the power flow control of WECS-based PMSG. The controllability of the converters can be tested. Although the power converter is stable with all controllers, a good transient and steady-state performance is achieved. From the active power plots, it can be observed that the overshoot given by the ANFIS controller is reduced to 0.53% from 10.404%, while the regulation time is reduced to 0.00685msec from 0.0585msec, and the settling time is reduced to 0.04248msec from 18.485msec and by fuzzy logic controllers, the overshoot is reduced to 7.184%, the regulation time is reduced to 0.0275msec and settling time is reduced to 5.416msec from the PI controllers. From the reactive power plots, it can be observed that the overshoot given by the ANFIS controller is reduced to 0.1% from 2.75%, while the settling time is reduced to 0.301msec from 5msec, and by fuzzy logic controllers, the overshoot is reduced to 1.501%, the settling time is reduced to 2.015msec from the PI controllers. From the DC-bus voltage plots, it can be observed that the overshoot given by the ANFIS controller is reduced to 0.501% from 17.461%, while the regulation time is reduced to 0.4916msec from 6.232msec, and settling time is reduced to 0.6858msec from 7.461msec from PI controllers. The use of neuro-fuzzy controllers, when compared to conventional PI controllers and fuzzy logic controllers, reduces design efforts, and produces the best results, according to simulation results.

5.2 Recommendations

In this thesis, MATLAB simulation for power flow control of a permanent magnet synchronous generator based on a wind energy system has been carried out. This simulation can be implemented in hardware to observe the actual feasibility of the proposed control strategy and to enhance the system's performance. The proposed technique might also be applied to a wind farm, which is a network of interconnected wind turbines. Due to their benefits, direct torque control and direct power control should be suggested as additional control strategies for this WECS-based PMSG. There are no current controllers or coordinate transformations. Finally, an adaptive neuro-fuzzy inference system-based model predictive controller is suggested in addition to the neuro-fuzzy controller. Because it is far more difficult and computationally demanding to obtain a practical model of a wind energy conversion system. Since these methods do not use models, knowledge of the plant is not necessary. This controller can overcome the limitation of the neuro-fuzzy controller. By using the simple use of parameter estimates, it can enhance power flow and robustness to filter parameter variations/mismatches. It can be used to improve the system response much more.

ACKNOWLEDGMENTS

This research thesis was funded by Adama Science and Technology University under the grant number ASTU/SM-R/576/22, Adama, Ethiopia.

REFERENCES

Abir, A., & Mehdi, D. (2017). Control of permanent-magnet generators applied to variable-speed wind energy. *International Conference on Green Energy and Conversion Systems, GECS 2017*.

Ali, A., Moussa, A., Abdelatif, K., Eissa, M., Wasfy, S., & Malik, O. P. (2015). ANFIS-Based Controller for Rectifier of PMSG Wind Energy Conversion System. *IEEE*, 99–103.

Apata, O., & Oyedokun, D. T. O. (2020). An overview of control techniques for wind turbine systems. *IEEE Transactions on Energy Conversion*, *4*, 929–937.

Asri, A., Mihoub, Y., Hassaine, S., Logerais, P., & Allaoui, T. (2015). Intelligent Maximum Power Tracking Control of a PMSG Wind Energy Conversion System. *Journal of Engineering Science and Technology*, 1–10.

Bayhan, S., Fidanboy, H., & Demirbas, S. (2013). Active and reactive power control of a grid-connected permanent magnet synchronous generator in a wind power conversion system. *IEEE on Renewable Energy Research and Applications, ICRERA*, *October* 1048–1052.

Berhanu, M., Mekonnen, Y., Leidhold, R., Mamo, M., Muluneh, Z., & Sarwat, A. (2018). Analysis of a Doubly Fed Induction Generator Through Modeling and Simulation. *2018 IEEE PES/IAS PowerAfrica*, 652–657.

Bipin Biharee Srivastava. (2014). Tracking of Maximum Power from Wind Using Fuzzy Logic Controller Based On PMSG. *Ijmer*, *4*(12), 43–51.

Bisoyi, S. K. (2013). Modeling and Analysis of Variable Speed Wind Turbine equipped with PMSG. *International Journal of Current Engineering and Technology*, *2*(2), 421–426.

Bisoyi, S. K., Jarial, R. K., & Gupta, R. A. (2013). Modeling and Control of Variable Speed Wind Turbine. *International Journal of Emerging Technologies in Computational and Applied Sciences (IJETCAS)*, 56–62.

Blaabjerg, F., Liserre, M., & Ma, K. (2012). Power electronics converters for wind turbine systems. *IEEE Transactions on Industry Applications*, *48*(2), 708–719.

Bunjongjit, K., & Kumsuwan, Y. (2013). Performance Enhancement of PMSG Systems with Control of Generator-side Converter Using d-axis Stator Current Controller. *IEEE*.

Chai, Z., Li, H., Xie, X., Abdeen, M., Yang, T., & Wang, K. (2021). modeling and grid-connected stability study of virtual synchronous control-based doubly-fed induction generator wind turbines in weak grids. *International Journal of Electrical Power and Energy Systems*, *126*(PA), 106601.

Chatri, C., & Ouassaid, M. (2018). Design of Fuzzy Control T-S for Wind Energy Conversion System Based PMSG Using LMI Approach. *Colloquium in Information Science and Technology, CIST*, *2018-October*(1), 466–471.

Cheng, M., & Zhu, Y. (2014). The state of the art of wind energy conversion systems and technologies: A review. *Energy Conversion and Management*, *88*, 332–347.

Chong, C. H., Rigit, A. R. H., & Ali, I. (2021). Wind turbine modeling ad simulation using Matlab / SIMULINK. *IOP Conference Series: Materials Science and Engineering*, *1101*(1), 012034.

Davidson, I., Muashekele, H., & Mukapuli, N. (2014). Benguela Community/UNAM Wind Power Demonstration Project—Experiences in Implementation. *Journal of Energy and Power Engineering 8*, *8*, 1067–1072.

Deng, F., Liu, D., Chen, Z., & Su, P. (2017). Control Strategy of Wind Turbine Based on Permanent Magnet Synchronous Generator and Energy Storage for Stand-Alone Systems. *Chinese Journal of Electrical Engineering*, *3*(1).

Errami, Y., Obbadi, A., Sahnoun, S., Benhmida, M., Ouassaid, M., & Maaroufi, M. (2016). Design of a nonlinear backstepping control strategy of grid interconnected wind power system based PMSG. *AIP Conference Proceedings*, *1758*.

Errami, Y, Ouassaid, M., & Maaroufi, M. (2013). Control of a PMSG-based wind energy generation system for power maximization and grid fault conditions. *Energy Procedia*, *42*, 220–229.

Errami, Youssef, Obbadi, A., & Sahnoun, S. (2021). Dynamic performance analysis of grid-connected PMSG based on nonlinear control. *International Journal of Ambient Energy*, 1–8.

Et. al., Eswaraiah G. (2021). Analysis and Performance of Grid Connected Straight Driven PMSG Based Wind Turbines. *Turkish Journal of Computer and Mathematics Education (TURCOMAT)*, *12*(2), 1304–1312.

Fang, H. (2012). Adaptive Neuro-fuzzy Inference System in the Application of the Financial Crisis Forecast. *International Journal of Innovation, Management, and Technology*, *3*(3), 250–254.

Giallanza, A., Porretto, M., Cannizzaro, L., & Marannano, G. (2017). Analysis of the maximization of wind turbine energy yield using a continuously variable transmission system. *Renewable Energy*, *102*, 481–486.

Hailemariam, Z. M., Leidhold, R., & Tesfamariam, G. T. (2019). Real-Time Speed Control of a

PMSM for Wind Turbine Application. *IEEE PES/IAS PowerAfrica Conference: Power Economics and Energy Innovation in Africa, PowerAfrica 2019*, 396–401.

Han, B., Wang, Y., Li, H., & Zhang, X. (2013). Supplementary power control of PMSG-based wind farms for system dynamic stability. *2013 International Conference on Electrical Machines and Systems, ICEMS 2013*, 291–295.

Hassanzadeh, F., & Hajizadeh, A. (2017). Back-to-back Converter Control of Grid-connected Wind Turbine to Mitigate Voltage Drop Caused by Faults. *IEEE Transactions on Power Systems*.

Jamali, N., Amlashi, S., & Info, A. (2012). Design and Implementation of Fuzzy Position Control System for Tracking Applications and Performance Comparison with Conventional PID. *IAES International Journal of Artificial Intelligence (IJ-AI)*, *1*(1), 31–44.

Jha, D. (2017). A Comprehensive Review on Wind Energy System for Electric Power Generation: Current Situation and Improved Technologies to Realize Future Development. *International Journal of Renewable Energy Research (IJRER)*, *7*(4), 1786–1805.

Kim, H. W., Kim, S. S., & Ko, H. S. (2010). Modeling and control of PMSG-based variable-speed wind turbine. *Electric Power Systems Research*, *80*(1), 46–52.

Kim, Y. S., Chung, I. Y., & Moon, S. Il. (2015). Tuning of the PI controller parameters of a PMSG wind turbine to improve control performance under various wind speeds. *Energies*, *8*(2), 1406–1425.

Kumar, D., & Chatterjee, K. (2016). A review of conventional and advanced MPPT algorithms for wind energy systems. *Renewable and Sustainable Energy Reviews*, *55*, 957–970.

Liserre, M., Member, S., Cárdenas, R., Member, S., Molinas, M., & Rodríguez, J. (2011). Overview of Multi-MW Wind Turbines and Wind Parks. *IEEE Transactions on Industry Applications*, *58*(4), 1081–1095.

Ma, X. H., Tian, D., Zhang, Z. H., Deng, Y., & Li, Y. W. (2015). Combined wind speed model based on real wind data. *IET Conference Publications*, *2015*(CP679), 2–5.

Marmouh, S., Boutoubat, M., & Mokrani, L. (2017). MPPT fuzzy logic controller of a wind energy conversion system based on a PMSG. *Proceedings of 2016 8th International Conference on Modelling, Identification and Control, ICMIC 2016*, 296–302.

Maroufi, O., Choucha, A., & Chaib, L. (2020). Hybrid fractional fuzzy PID design for MPPT-pitch control of wind turbine-based bat algorithm. *Electrical Engineering*, *102*(4), 2149–

2160.

Miao, D. M., & Shen, J. X. (2013). Comparative study on permanent magnet synchronous generator systems with various power conversion topologies. *International Conference on Power Engineering, Energy and Electrical Drives*, *May*, 1738–1743.

Muhammed, S., & Krishnakumari, V. (2014). Performance Analysis of a PMSG-Based Wind Energy Conversion System. *International Journal of Engineering Sciences & Research Technology*, *3*(8), 698–702.

Noman, M., Li, G., Wang, K., & Han, B. (2021). Electrical control strategy for an ocean energy conversion system. *Springer*, 1–18.

Pandya, M. M. (2020). Grid-connected PMSG Wind Energy Generation System : Active and Reactive Power Control. *International Journal of Grid and Distributed Computing*, *13*(2), 1832–1845.

Rodrigues, S., Pinto, R. T., Bauer, P., & Pierik, J. (2013). Multi-Objective Optimization of a PMSG Control System through Small-Signal Analysis. *IEEE*, 1189–1195.

Sánchez, R. T., & Rios, A. M. (2016). Modeling and control of a wind turbine. *Bond Graphs for Modeling, Control and Fault Diagnosis of Engineering Systems, Second Edition*, *2013*, 547–585.

Sekhar, V., & Babu, N. R. (2016). Modified fuzzy logic-based control strategy for grid-connected wind energy conversion system. *Journal of Green Engineering*, *6*(4), 369–384.

Shariatpanah, H., Fadaeinedjad, R., & Rashidinejad, M. (2013). A new model for PMSG-based wind turbine with yaw control. *IEEE Transactions on Energy Conversion*, *28*(4), 929–937.

Tahiri, M., Djebli, A., & Mimet, A. (2017). Drive-train Flexibility Effect on Control Performance of a Horizontal Axis Wind Turbine. *International Journal of Applied Engineering Research*, *12*(16), 5511–5519.

Thakur, A. (2020). A Comprehensive Review on Wind Energy System for Electric Power Generation : Current Situation and Improved Technologies to Realize Future Development. *International Journal of Renewable Energy Research*, *7*(4).

Tiwari, R., & Babu, N. R. (2016). MPPT control-based Fuzzy Logic Controller using Permanent Magnet Synchronous Generator in Wind Energy Conversion System. *IFAC (International Federation of Automatic Control) Hosting by Elsevier*, *49*(1), 462–467.

Tripathi, S. M., Tiwari, A. N., & Singh, D. (2015). Grid-integrated permanent magnet synchronous generator based wind energy conversion systems: A technology review. *Renewable and Sustainable Energy Reviews*, *51*, 1288–1305.

Vadi, S. (2020). Design and Simulation of a Grid Connected Wind Turbine with Permanent Magnet Synchronous Generator. *IEEE International Conference on Smart Grid*, 169–175.

Yadav, M. K., & Upadhayay, A. K. (2014). Power Flow Control of Permanent Magnet Synchronous Generator Based Wind Energy Conversion System with DC-DC Converter and Voltage Source Inverter. *International Journal of Electronic and Electrical Engineering.*, *7*(8), 803–814.

Yaramasu, V., Member, S., Wu, B., & Member, F. (2013). Predictive Control of Three-Level Boost Converter and NPC Inverter for High Power PMSG-Based Medium Voltage Wind Energy Conversion Systems. *IEEE Transactions on Industry Applications*, *c*, 1–15.

Yüksel, O. L., Güney, E., & J, H. Ç. (2013). Power Quality Control and Design of Power Converter for Variable-Speed Wind Energy Conversion System with Permanent-Magnet Synchronous Generator. *The Scientific World Journal*, *2013*.

APPENDICES A: Parameters Used

A.1 Wind Turbine Parameters

Table A. 1 Wind turbine parameters

Parameter	Symbol	Value	Units
Air density	ρ	1.225	Kg/m^3
Rated wind speed	V_{Rated}	12	m/sec
Cut-in wind speed	V_{cut-in}	3	m/sec
Maximum power coefficient	C_{p-max}	0.48	-
Optimum tip speed ratio	λ_{opt}	8.1	-
Rated mechanical power	P_{max}	2	Mw
Number of rotor blades	-	3	-
Rotor diameter	D	70.8	m
Speed range	-	19-29.1	rpm
Rated speed	ω_m	26.3	rpm
Total moment of inertia	J_t	0.2	Kg.m^2
Total damping coefficient	B_v	85.5	N*sec/rad

A.2 Permanent Magnet Synchronous Generator Parameters

Table A. 2 Electrical machine parameters

Parameter	Symbol	Value	Units
No of pole pairs	P	4	-
Rated mechanical angular speed	ω_g	152.89	Rad/sec
Armature resistance	R_s	0.48	Ω
d-axis stator inductance	L_d	1.6	mH
q-axis stator inductance	L_q	3	mH
Rated torque	τ_{eRated}	40	watt
Rated power	P_{Rated}	2	Mw
Flux induced by magnets	ψ_m	0.675	wb

A.3 Power Converters Parameters

A.3.1 Rectifier Parameters

The AC-to-DC converter parameters were obtained from the AC power generator to DC power, but it was not pure DC power, which means that it was full of ripple, so the equations used to omit these ripples were given in Chapter 3, section 2.5.1 and by using these equations can be obtained the following.

Table A.3. 1 AC-to-DC rectifier converter parameters

Parameter	**Symbol**	**Value**	**Units**
Maximum phase voltage	V_m	282.15	V
Cut-off frequency	f_c	22.54	Hz
Inductor	L	1.4	mH
Capacitor	C	35.9	mF
Load resistance of the rectifier	R_{load}	30	Ω
Ripple frequency	f_r	300	Hz
Switching frequency	f_{sw}	25000	Hz

A.3.2 DC-DC Boost Converter Parameters

The DC-to-DC converter parameters were obtained by selecting a power rating based on the generated power capacity and voltage ripple requirements for the output voltage of the converter. The equations used to obtain these values were given in Chapter 3, Section 2.5.2.

Table A.3. 2 DC-DC boost converter parameters

Parameter	**Symbol**	**Value**	**Units**
Low voltage side capacitor	C_1	8.75	F
High voltage side capacitor	C_2	5.7	mF
Inductor	L_{boost}	7.604	H
Duty cycle	D	0.455	-
Load resistance	R_{Lboost}	13	Ω

A.3.3 DC-AC Converters (Inverter), Filter Parameters, and Grid Parameters

The DC-to-AC converter (Inverter) parameters were obtained based on the output real power and voltage of the converters, the harmonic due to the power converter switches were reduced. The harmonic generated are removed through the filters. The equation used to obtain these values was given in Chapter 3, Section 2.5.3, 2.6, and 2.9.

Table A.3. 3 DC-AC converter parameters and grid parameters

Parameter	**Symbol**	**Value**	**Units**
Grid side inductance	L_2	56.83	μH
Inverter side inductance	L_1	56.83	μH
The equivalent dc capacitor	C_{dc}	0.334	mF
The sum of dc resistance	R_P	0.37	Ω
Damping resistance	R_d	0.3	Ω
The grid side resistance	R_g	0.0057	Ω
The inverter side resistance	R_i	0.0057	Ω
d-axis average switching function	s_d	0.266	-
q-axis average switching function	s_q	0	-
Modulation	m	0.95	-
Filter capacitor	C_f	0.669	mF
Transmission line reactance	x_L	2.80	Ω
Transformer reactance	x_T	7.98	Ω
The angle of the grid	δ	70.74	degree
Filter inductor	L_f	0.114	mH

A.3.4 PI Controller Parameters used

For control of power flow and DC bus voltage, the PI Controller is used as one of the controllers, so the parameter PI controller can be obtained by looking at the stability of the system. From the one of PI tuning methods, I used the manual tuning method and gained the value of constant gains. Table A.3.4 illustrates the PI controller parameters used for current control, active power control, and reactive power control.

Table A.3. 4 PI controller parameters used

PI Controller gains		
Parameter	$\boldsymbol{k_p}$	$\boldsymbol{k_i}$
DC-bus Voltage Control	10 if it is 9, it is unstable	0.35

d-axis Current Control	1.2 if it is 3.2, it is unstable	0.9
q-axis current control	0.5	1
Active Power Control	100 if it is below 100 it is unstable	0.25
Reactive Power Control	1	0.25

APPENDICES B: Related MATLAB/SIMULINK Model and Program

B.1 MATLAB/SIMULINK Related

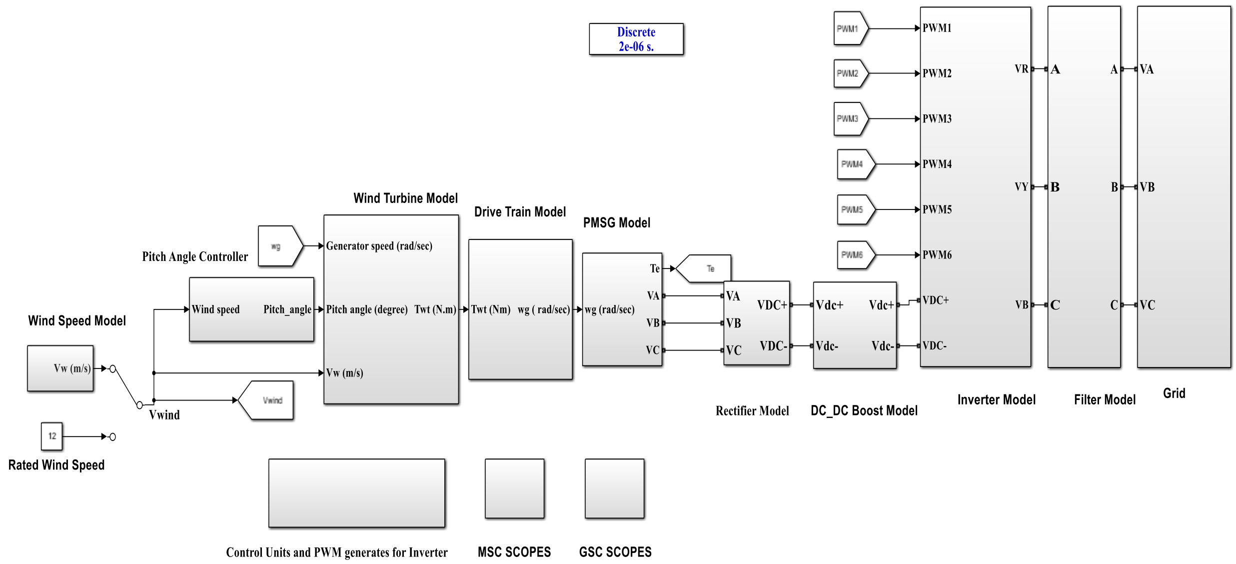

Figure B. 1 Simulation diagram of WECS-based PMSG

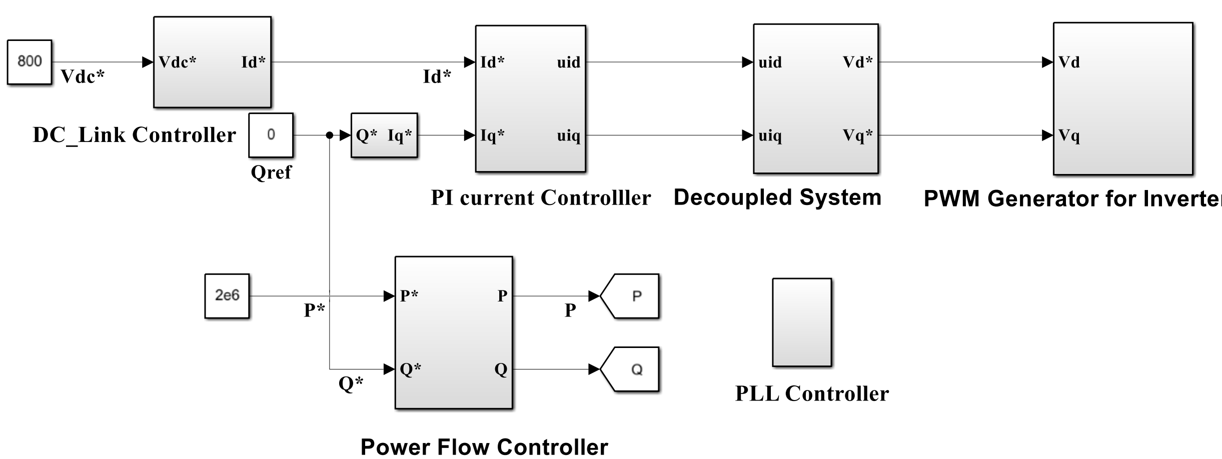

Figure B. 2 Simulation diagram for generating PWM for inverter and power flow control

B.2 MATLAB Program Related

The following are the MATLAB Code use for the design of WECS:

```
clc; clear all;

%% Wind Gust speed model
function Vwg=wind_gust(t)
Tg=20;%wind gust period
T1g=10;%starting time in sec
maxg=1.2;% maximum gust wind speed m/s
if t<=T1g
   Vwg=0;
 else if t>T1g && t<T1g+Tg
       Vwg=(maxg/2)*(1-cos(2*pi(t/Tg-Tg/T1g)));
     else t>T1g+Tg
       Vwg=0;
     end
   end
%% Wind ramp speed model
function Vwr=wind_ramp(t)
Tr=20;%wind ramp period
T1r=10;%starting time in sec
T2r=21;% end time in sec
Vwrmax=1.2;%m/s
if t<=T1r
   vwr=0;
else if t>T1r && t<T2r
       vwr=(Vwrmax)*(t-T1r)/(T2r-T1r);
else if T2r<=T2r+Tr
       vwr=Vwrmax;
else t>T2r+Tr
      vwr=0;
    end
   end
 end
%% Generating wind speed, I am creating an array for fluctuating wind speed.

y=xlsread('windspeed.xlsx', 'sheet1',  'A1:A40')

m=mean(y); %the mean of wind speed

S=std(y); %the standard deviations of wind speed

pro=1/(S*sqrt(2*pi))*exp(-(y-m).^2/(2*S^2))% probability density

% I need a time data

for i=1:length(y)

   time(i)=i;
```

```
end
plot(time,y,'r')
xlabel ('time','fontsize',14)
ylabel('wind speed','fontsize',14)
%% Rectifier filter design
VLLmax=282.15; Prated=23e3; Vdc=228;
fsw=25e3;% switching frequency
ripple_output_voltage=0.01;  ripple_inductor_current=0.3; Iorec=10; Icri=10.5;
input_current=20; diL=6;%input current variation by 1%
dv1=2.8215;%output voltage variation by 3%
dvr=500; Lmin=0.013*VLLmax/(2*pi*f*Icri)%the minimum inductance value (Lmin)
Lmax=1.25*Lmin%the maximum inductance value (Lmax) increased by 25%
fr=6*f;% ripple frequency
fc=sqrt(dv1/(dvr)*fr^2);%cutoff frequency
Crec=1/(4*pi^2*fc^2*Lmax)
Vdcrec=1.654*VLLmax;
Rload=Vdc/(Iorec)%mimimum load to be applied more of
%% Design of boost converter
Vdc=436;%minimum out voltage available at the rectifier output
V_bus=800;%DC_DC converters output
Pboost=2e6%power rating of the DC_DC converters
Vin=Vdc;%input voltage of boost converter
Vdc_boost=V_bus;%output voltage of boost converter
fsw_boost=25e3;%the switching frequency of boost converter
Ts=1/fsw_boost;
D=1-(Vin/Vdc_boost)%D is the duty cycle of the boost converter
v_boost=Vdc/(1-D);
Idc_boost=Pboost/Vdc_boost;
% input current ripple(dI)
Ioripple=0.2;% 20-40% of the output current
dIL=Ioripple*Idc_boost*(Vdc_boost/Vin);
```

```
C1=dIL/(8*0.05*262);
% output voltage ripple(dv) Here i considering 1% voltage variation in
% output voltage,standard is 0.5%-1%.
dv=Vdc_boost*1/100;
Rboost=(Vdc_boost/Idc_boost);%minimum load to be applied more than of
Lboost=(Vdc_boost-Vin/(2*Pboost))*(Vin^2/Vdc_boost)*Ts;
C2=Vdc_boost*D/(Rboost*dv*fsw_boost);%the capacitance value (C_boost)
%% Inverter filter calculation
Ts=100e-6;%sampling time
Pmin=2e6;%minimum active power
U=690;%inverter phase 2 phase voltage
fsw=1/Ts;%switching frequency
Vdc=800;%dc-bus voltage
w=2*pi*f;%angular frequency
wsw=2*pi*fsw;%angular switching frequency
%base value
zb=[U^2]/Pmin;%impedance base
cb=1/(w*zb);%capacitor base
% filter parameters
delta_ILmax=0.1*((Pmin*sqrt(2))/U);
L1=Vdc/(16*fsw*delta_Ilmax);%inverter side inductance
Rf=L1*100;%resistance of inductor inverter side
x=0.15; cf=x*cb;% filter capacitor
% Calculation of the factor 'r' between Linv and Lg
r=0.6;
L2=r*L1 ;%grid side inductance
wres=sqrt((L1+L2)/(L1*L2*cf));%calculation of wres
fres=wres/(2*pi);%resonant frequency of the filter
Rd=1/(3*wres*cf);%damping resistance or parallel resistance Rp
cfmax=(0.15*Pmin)/(2*pi*f*U^2);%maximum filter capacitor
Lf=(0.1*U^2)/(2*pi*f*Pmin);%filter inductor
```

```
Rg=L2*100;%resistance of inductor side of the grid
cd=cf/2;%The DC-equivalent capacitor
%% The Value of PI controller gains for current control, DC-link voltage control
 and power flow control, respectively.
Kp1=10;% Proportional gain ti1=40;% Integral time constant for dc-link
Kp2=1.2;%Proportional gain for current control Ki2=1;%Integral gain for current control
Kp3=100;%Proportional gain  Ki3=0.5;%Integral gain for active power control
Kp4=0.25;%Proportional gain Ki4=1;%Integral gain for reactive power control
%%Controllability test for dc-dc boost converter
%% initial value
A12=(1-D)/Lboost; A21=(1-D)/C2; A22=1/(Rboost*C2); B11=1/Lboost; B22=1/C2;
A1=[0 -A12;A21 -A22]; B1=[B11 0;0 -B22]
CharPoly=poly(A1)%Find the characteristic polynomial
poles=roots(CharPoly)%Find the s/m poles
% eigenvalues (just for checking the stability)
E=eig(A1)
damp(A1);%Calculate eigenvalues, zeta, wn, and time constant
% Controllability test, Kalman's test: method1
%Controllability matrix
Uc=[B1 A1*B1]
%Co=ctrb(A,B)
if rank(Uc)==size(A1,1)
   'It is controllable'
else
   'It is not controllable'
end
R1=rank(Uc)% finding the rank
d1=det(A1)%finding the determinant
%checked!!
%% stability test using the eigenvalue analysis
if (real(E(1))==0||real(E(2))==0)%lya will fail
```

```
    if (real(E(1))<=0||real(E(2))<=0)
        disp('system is marginally stable')
    else
        disp('system is unstable')
    end
else
    Q=eye(2);%lyap will succeed given a positive definite matrix
    R=lyap(A1,Q);%solve for P
    pm1=det(R(1,1))% Sylvester's method to see if p is PD
    pm2=det(R(1:2,1:2))
    if (pm1>0&&pm2>0) %logic to assess stability condition
        disp('system is asymptotically stable')
    else
        disp('system is unstable')
    end
end
%% Controllability test for dc-ac converter
m=0.95;%modulation index
dd=0.2996;% average duty cycle of d-axis
dq=0.0662;% average duty cycle of q-axis
Rf=0.76;% inverter resistance
Rp=1.59; %the sum of DC resistance
A11=Rf/Lf; A12=w; A13=dd/(2*Lf); A21=w; A22=Rf/Lf; A23=dq/(2*Lf);
A31=1.5*dd/Cd; A32=1.5*dq/Cd; A33=-2/(Rp*Cd); B11=1/Lf;
A2=[-A11 A12 A13;-A21 -A22 A23;-A31 -A32 A33]
B2=[B11;0;0]
CharPoly=poly(A2) %Find characteristic polynomial from A2
poles=roots(CharPoly)%Find the s/m poles
% eigenvalues (just for checking the stability)
E=eig(A2)
% Controllability test, Kalman's test: method1 %controllability matrix
```

```
%Uc=[B2 A2*B2 A2^2*B2]
Uc=ctrb(A2,B2)
damp(A2);% Calculate eigenvalues, zeta, wn, and time constant
if rank(Uc)==size(A2,1)
   'It is controllable';
else
   'It is not controllable';
end
R2=rank(Uc)
D2=det(Uc)
%%checked!!
%% stability test using the eigenvalue analysis
if (real(E(1))==0||real(E(2))==0||real(E(3))==0)%lya will fail
   if (real(E(1))<=0||real(E(2))<=0||real(E(3))<=0)
      disp('system is marginally stable')
   else
      disp('system is unstable')
   end
else
   Q=eye(3);%lyap will succeed given a positive definite matrix
   R=lyap(A2,Q);%solve for P
   pm1=det(R(1,1))% Sylvester's method to see if p is PD
   pm2=det(R (1:2,1:2))
   pm3=det(R (1:2:3,1:2:3))
   if (pm1>0&&pm2>0&&pm3>0) %logic to assess stability condition
      disp('system is asymptotically stable')
   else
      disp('system is unstable')
   end
end
%Stability checked!!!
```